Vibration Enhanced Flooded Bed Dust Scrubber with Liquid-Coated Mesh Screen

Mahmud Esad Uluer

Dissertation submitted to the faculty of the Virginia Polytechnic Institute and State University in partial fulfillment of the requirements for the degree of

Doctor of Philosophy

In

Mining Engineering

Christopher A. Noble, Chair

Seyed H. Amini

Shima Shahab

Serhat Keles

Mario Karfakis

September 19, 2023

Blacksburg, Virginia

Keywords: Respirable coal mine dust, Flooded bed dust scrubber, Vibrating mesh filter, Filter surface modification

Vibration Enhanced Flooded Bed Dust Scrubber with Liquid-Coated Mesh Screen

Mahmud Esad Uluer

ABSTRACT

Respirable coal mine dust (RCMD) is one of the biggest occupational health hazards. Dusty mining environments can cause life-threatening respiratory health problems for coal miners known as black lung. Over the last 20 years, the flooded bed dust scrubber (FBS) has been employed as an integral component of dust control strategies for underground continuous mining operations. These units have been shown to be effective and robust in mining environments; however, several technical challenges and knowledge gaps limit their performance and efficiency. Despite the capability of the FBS, there are numerous technical challenges that limit its performance and efficiency. In particular, the static panel filter, instrumental in most scrubber designs, is fundamentally limited in collection efficiency and causes numerous operational challenges including rapid clogging. Furthermore, the current design of the filter panel is not capable of evenly wetting the entire surface area. This allows dust-laden air to pass through the filter media and decreases the cleaning capability of the FBS. In this research, both a lab-scale and a full-scale vibration-enhanced FBS with a liquid-coated filter panel were designed, manufactured, and tested. The results confirmed that a vibration-induced filter panel enhances dust collection performance and reduces mesh clogging. In addition, laboratory-scale mesh clogging tests showed that a hydrophilic mesh provided superior clogging mitigation and better performance. Typical results from bench-scale tests showed notable improvements in dust collection efficiencies by over 6% in wet condition and over 7% in dry condition while reducing mass accumulation in the filter by almost 10% in wet condition and over 40% in dry condition. The prototype testing was less conclusive, with deviations between the static

mesh and vibrating mesh depending on the mesh density and operating conditions. Nevertheless, with the highest mesh density tested (30-layer), the vibrating mesh notably outperformed the static mesh with superior collection efficiency and reduced airflow loss. The system was further analyzed to investigate the size-by-size recovery of dust particles to various endpoints in the scrubber, under both vibrating and static conditions. Results show that while a majority of the particles are recovered into the demister sump, nearly a quarter of the dust mass is recovered upstream of the screen. In addition, the data confirm that vibration prompts notable improvements to collection efficiency, particularly in the finest size class (- 2.5 micron).

Vibration Enhanced Flooded Bed Dust Scrubber with Liquid-Coated Mesh Screen

Mahmud Esad Uluer

GENERAL AUDIENCE ABSTRACT

Coal mine dust is an unintended and unavoidable consequence of coal extraction operations that poses significant health and safety risks. The inhalation of small, respirable dust particles can cause incurable lung diseases, including silicosis and coal workers' pneumoconiosis known as black lung. To minimize occupational hazards of underground coal mine dust, the Mine Safety and Health Administration (MSHA) periodically brings legislation to the industry. The recent respirable dust rule mandates reducing the maximum allowable respirable dust concentrations in the mine environment to below 1.5 mg/m3 at the working face and below 0.5 mg/m3 at intake entries. In order to comply with these regulations, modern mining techniques utilize several dust mitigation strategies, and the flooded-bed dust scrubber (FBS) is one such technology used extensively on continuous miners. The conventional static panel filter, instrumental in most scrubber designs, however, is fundamentally limited in collection efficiencies due to a high clogging rate and a tradeoff between mesh density and airflow rate. Moreover, poorly wetted areas allow dust-laden air to pass through the filter media. To overcome these deficiencies, a novel liquid-coated vibrating mesh panel is introduced in this research. A laboratory-scale dust scrubber unit and a full-scale unit with a vibration-enhanced mesh screen panel were manufactured and employed to investigate the efficacy of the concept as compared to that of a static mesh. A series of experimental design studies were employed to determine the effective vibrational parameters, scrubber operational parameters, and the impact of mesh variations on dust collection and clogging mitigation. Optimized results from this research were also evaluated against those of a static mesh to determine performance improvement while investigating the mechanisms controlling dust collection and particle department

through the scrubber system. Results from the laboratory study show that vibrating mesh conditions, higher water flow rates, and a hydrophilic mesh screen panel led to an improvement in the cleaning efficiency of the scrubber system. Compared to a static-mesh to FBS, the vibrating-mesh FBS showed a significant reduction in pressure drop across the mesh screen indicating lower air loss through the test duration. Overall, the findings confirm that vibrating mesh conditions have the ability to improve filter clogging issues while maintaining high collection efficiencies which can lead to better and healthier working conditions and prolonged operational time with less frequent maintenance. This research supports further technological advancement in mine dust mitigation technologies.

Acknowledgements

I would like to thank Allah first and foremost for all the blessings bestowed upon me throughout my Ph.D. and my entire life.

I would like to thank the commission members for the time they devoted to me and for their wonderful guidance. I would like to thank our project team for patiently listening to my work in our regular meetings and constantly guiding me.

I would like to acknowledge Matt Shigo's assistance in designing and manufacturing the test setup, Brian Arnold’s help in testing, John Sczap's assistance in providing the laboratory procedure for surface preparation and contact angle measurements as well as Tim Beckley (NIOSH), and his team's assistance in testing at their Pittsburg, PA facility. I express gratitude to the Improvement of Mine Safety and Health, Inc. (Alpha Foundation) for the continued funding throughout this project. I am very grateful to the Turkish Ministry of National Education, whose financial support allowed me to complete my graduate study.

I would like to acknowledge Kris Strickland, Dr. Serhat Keleş, and Dr. Chad Sechrist for their never-ending help when I needed it in the laboratory. I would like to especially thank Dr. Aaron Noble, who did everything he could for my academic progress throughout the entire doctoral program. I would like to thank Kris Strickland, Maggie Noonan, Nathan Youmans, and Dr. Aaron Noble who never spared their help in improving my research with their constructive critiques.

I would like to thank my parents who helped me to reach this point by providing the vision for me, my siblings who always made me feel confident with the moral support they gave me, and my friends in North America and in Turkey.

Finally, I would like to thank my wife, Cansu Uluer, who has always been by my side with her extraordinary support since the day I first decided to pursue a Ph.D., and has always compensated for my shortcomings by being a wonderful mother to our children. I could not have accomplished this without her unconditional support. I would like to thank my children Muhammed Emir and Ahmed Selim for being one of my greatest sources of motivation during my Ph.D., as in every moment of my life.

Contents

List of Figures

List of Tables

Chapter 1

1. Introduction

1.1. Overview

Mining activities are highly mechanized and require continuous operation. This presents a number of challenges, including dust-related issues. As a result of coal extraction and transportation operations, dust production is an unavoidable consequence of the operation. If there are no efficient dust control systems in place, dust blends easily into the air ventilating the mine. There has been considerable research showing that inhaling ultrafine coal mine particles which remain in the lungs for years after exposure causes permanent disability and fatalities in coal miners. These illnesses include pneumoconiosis, silicosis, emphysema, and chronic bronchitis, collectively referred to as black lung or coal workers' pneumoconiosis (CWP) [1,2]. The extraction of rock within or adjacent to the coal seam can also release respirable silica (quartz) dust into the ventilation system, causing silicosis if excessive amounts are inhaled. As disabling and potentially fatal lung diseases, coal workers' pneumoconiosis (CWP) and silicosis cannot be cured [3], so it is crucial that mine workers do not work under dusty conditions.

Between 1995-2004, the National Institute for Occupational Safety and Health (NIOSH) reported that CWP caused more than 10,000 miners' deaths [4]. In addition to the health problems, generated coal dust, if allowed to travel freely through the mining environment, triggers a devastating secondary explosion when a methane explosion occurs [5]. This causes a significant amount of damage to both life and property in the mining environment. As such, it is also a safety issue for coal mines. Regulatory bodies regularly introduce legislation to the industry to minimize the possibility of hazardous results.

1.2. Motivation

In underground coal mines, operators employ preventative particle-collecting equipment and dust control techniques to reduce airborne dust and comply with regulations to minimize airborne dust emissions. Onboard dust scrubber units are usually equipped with continuous mining machines. These machines are most commonly used in room and pillar mining operations with blind headings. These units help eliminate coal dust close to the face before it pollutes the air in other sections. In addition to coal dust, these mining machines also produce aerosols and other gases. Dust scrubbers are installed on continuous miners to capture and minimize particulates generated from cutting. This is to eliminate dust-laden air close to the mining face. As a preventative dust removal system, flood bed dust scrubbers have been widely used in continuous mining operations for several decades [6-8]. It is imperative to note that flooded-bed scrubber units (FBS) are capable of many types of dust removal tasks, but they face a variety of technical challenges that limit their performance and efficiency. The static panel filter, which is an integral part of most scrubber designs, is fundamentally limited in its collection efficiency. Over a period of operation, some coal particles lodge in the filter panel. Airflow loss through the scrubber is most commonly caused by clogged filter panels. A FBS can lose up to a third of their airflow in just one cut. Particles will also build up on the screen when the spray does not completely wet the filter panel. It will also cause poor liquid-particle agglomeration. These technical challenges affect continuous miner operational capacity and require frequent maintenance to be performed. As a means of maintaining and improving mining operations efficiency, it is necessary to minimize operational challenges associated with FBS by improving their cleaning efficiency. This study is directed toward achieving this goal.

1.3. Research Objectives

This research aims to introduce an improved FBS that eliminates existing operational challenges, thus reducing dust concentrations in underground coal mines. As a result of the vibrational component embedded in the investigated design, it will enhance dust collection efficiency while

minimizing filter panel clogging and other operational issues associated with dust collection. The key element of the novel design is a vibrating mesh panel. This is mainly intended to improve dust collection system efficiency. As well as providing stable performance for a prolonged period of time without frequent maintenance, it can also assist in improving health, safety, and productivity outcomes through increased dust capture and reduced mesh clogging, as compared to traditional FBS with static mesh filters. To evaluate the FBS unit's performance under a number of operational parameters, including the vibrational frequency and amplitude of the filter panel and the water spray system, bench-scale, and full-scale FBSs have been designed and manufactured. In order to optimize the design and use of FBS in real applications, this study identifies and evaluates test parameters, filter panel design, and surface variations. These parameters have a major influence on system efficiency. Following the lab-scale study, a detailed technical design for a mine-worthy unit was developed and tested. Testing the full-scale prototype will provide evidence of how the investigated method improves dust collection efficiency in a high-fidelity environment.

1.4. Organization of Tasks

"Collecting Mine Dust Particles with Liquid-Coated Vibrating Meshes" project, sponsored by Alpha Foundation, and the project team contributed greatly to the formation and development of the theoretical approach of the novel design proposed in this dissertation. The multidisciplinary project has multiple principal investigators from various disciplines.

- Dr. Lei Pan and his group (Michigan Technological University, Chemical Engineering) investigated macroscopic and microscopic collisions between particles and a vibrating mesh and developed a model for explaining filter clogging.

- Dr. Sunghwan Jung and his group (Cornell University, Department of Biological and Environmental Engineering) studied microscopic adhesion between particles and a liquid-air interface using high-speed video recording.

- Dr. Shima Shahab and her group (Virginia Tech, Mechanical Engineering) mainly studied multiphase flow simulations and revealed an energy harvesting approach to applying the proposed technique in underground coal mines. Her group investigated translating the vibration into the mesh screen optimally in their simulations.

- Dr. Hassan Amini and his group (West Virginia University, Mining Engineering) measured and analyzed in-mine vibrations and post-processed them to effectively harvest machine-generated vibrational energy. Dr. Amini also did the initial proof-of-concept scrubber unit when he worked with Dr. Noble at Virginia Tech, Mining Engineering between 2018 and 2019.

- Dr. Aaron Noble and his group (Virginia Tech, Mining Engineering) designed and fabricated the bench-scale and full-scale prototypes, studied the proposed design experimentally using these prototypes, and analyzed/discussed the study results.

The author of this dissertation has worked with Dr. Aaron Noble's group since 2020. His contribution to the project since then has been designing and producing small and full-scale prototypes with the help of Matt Shigo in accordance with operational parameters. He performed validation tests on the models, obtained experimental results, and analyzed/transformed them into statistically meaningful outcomes. In this dissertation, the author has also established the relevance of his research and the work of other members of the project team.

1.5. Organization

This study aims to demonstrate the enhancement of utilizing vibration to improve the capture efficiency of an FBS. A novel dust-capturing technique, design parameters, and their individual and combined impacts on the system, particle department through the system, the impact of various mesh screen designs and surface modifications, and full-scale prototype construction and testing efforts will be included in the dissertation. This dissertation has seven chapters. Each chapter of the dissertation discusses the following objectives:

- Chapter 2 contains an extensive literature review on coal dust in underground coal mines, as well as dust control techniques for suppressing coal dust. The chapter also reviews the mesh screen clogging issue with alternative suggestions to combat the operational deficiencies of the traditional FBS design. Furthermore, vibrations on the continuous miner are discussed along with the energy harvesting approach.

- Chapter 3 introduces a bench-scale scrubber system tested and validated in the laboratory.

- Chapters 4 and 5 characterize the parameters that influence system efficiency and evaluate the impact of vibration, mesh designs, and filter panel surface modifications. The proposed design is validated experimentally, and experimental results are presented.

- Chapter 6 describes the design and manufacture of a full-scale prototype. This chapter also discusses the results of a series of tests with the full-scale prototype in a simulated mine environment.

- Chapter 7 summarizes the results of this novel method and contains the author's recommendations.

1.6. References

1. U.S. Department of Labor (2014) Lowering miners' exposure to respirable coal mine dust, including continuous personal dust monitors. Fed Regist Vol 79, Number 84. http://arlweb.msha.gov/regs/fedreg/final/2014finl/2014-09084.asp. Accessed June 5, 2022.

2. Sinclair J (1958) Environmental conditions in coal mines: including fires, explosions, rescue and recovery work. Pitman, 1958.

3. CDC (2019) Centers for Disease Control and Prevention, National Institute for Occupational Safety and Health, Occupational Respiratory Disease Surveillance, National Occupational Respiratory Mortality System (NORMS) National Database.

4. U.S. Department of Labor (2014) Final rule.

http://arlweb.msha. gov/regs/fedreg/final/2014finl/2014-09084.asp. Accessed June 5, 2022.

5. Cashdollar KL, Sapko MJ (2006) Explosion hazards of coal dust in the presence of methane. Handbook for methane control in mining, pp 147–150

6. Wang W, Peng FF (1991) Analyses of respirable dust distributions with multiple dust sources on longwall faces. Proc. of Soc. for Mining, Metallurgy & Exploration. pp 367–375

7. Colinet JF, Spencer ER, Jankowski RA (1997) Status of dust control technology on U.S. longwalls. Proceedings of 6th International Mine Ventilation Congress. pp 345–351

8. Arya S, Sottile J, Novak T (2018) Development of a flooded-bed scrubber for removing coal dust at a longwall mining section. Saf Sci 110:204–213.

Chapter 2

2. Literature Review

2.1. Preface

The coal industry will continue to play a significant role as an energy source for the foreseeable future despite recent declines in the number of active coal mines and the number of miners employed by them. Through 2050, coal is estimated to produce 29 percent of all electricity worldwide [1]. In addition, metallurgical coal continues to be a significant commodity.

On a global scale, coal still has a prominent place in the energy portfolio. However, coal dust, which is inevitably generated during coal production, has very serious consequences that may threaten employee health and mine field safety. In order to minimize these hazards, the coal industry and regulatory bodies must work in harmony. Recently, studies ongoing for decades have gained traction for this purpose.

Underground coal mine ventilation projects are continuously monitored and improved as necessary. Moreover, the prevention of coal dust spreading to the mine and the minimization of coal dust, while it is still at its source, are of critical importance. For this reason, it is necessary to make significant improvements to the equipment used to minimize dust released during coal production.

In this research, the characteristics of coal dust, its adverse effects on people and the environment, its removal methods, and the development of these techniques are discussed. The critical components of the FBS system's vibration-enhanced and modified filter panel surface are introduced in this dissertation.

2.2. Dust Hazards in Underground Coal Mining

2.2.1. Overview

Underground mining is a form of coal extraction that involves removing rock and soil from a coal seam. Underground mines are accessed through shafts, slopes, or drifts, which are opened from the surface. Portals (entrances and exits to the mine), mains, submains, panels, and working faces are the elements of the underground mine. Panels are the working sections of the production operation. A room-and-pillar method and a longwall method are the two major methods used in underground coal mines. Both methods involve driving entries into the seams of coal. Room-and-pillar mining employs a continuous miner who mechanically cuts and loads coal onto a shuttle car, which is typically a face transport vehicle [2].

Room-and-pillar mining can be done in several ways. Room-and-pillar continuous mining has gained traction over conventional room-and-pillar mining methods since continuous miners were introduced in the late 1940s. Over 38 percent of underground coal production has been carried out by room-and-pillar continuous mining in recent years [3].

2.2.2. Continuous Mining

Underground mining is divided into two main methods: room-and-pillar mining and longwall mining. Room-and-pillar mining uses pillars of coal to support the roof strata and roof bolts to prevent rock from falling from the strata. Continuous miners (a machine with rotating cutters on booms) cut coal [2]. The operator chooses this method for its high productivity (65–70% extraction [4]), its high safety, the elimination of noxious gases generated after blasting, and the restriction of workers working directly under the exposed roof.

With the introduction of continuous miners in late 1940, coal extraction has made a quantum leap forward. Continuous miners (Figure 2.1) use tungsten carbide steel ‘teeth’ to scrape coal from seams or cut coal in situ with a large rotating steel drum. A conveyor transports the coal to the

shuttle car after collecting the coal with two gathering arms. Next, the coal is transported to the shuttle car with the help of the conveyor. In addition to the scrubbing unit, the methane sensor, and the water spray arrangement, the continuous miner has a number of other features that are very useful in regard to health and safety.

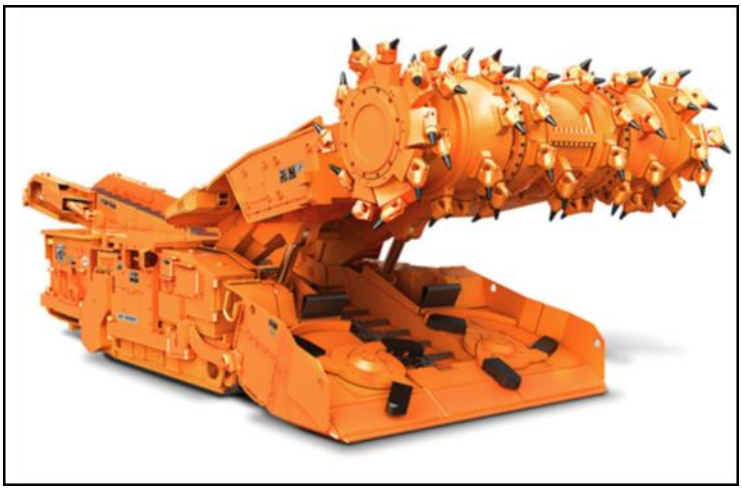

Figure 2.1: Continuous miner Joy 12CN27 (Source: Joy Global).

In general, continuous miners are combined with shuttle cars to transport coal from the face to feeder breakers. In the underground conveyor system, coal is transported to the surface and taken to the surface by the underground conveyor system. A quad bolter can be used to bolt vertically and sideways in a sidewall to a height of 90 degrees. As soon as the coal is received from the shuttle car, a feeder breaker crushes it to the desired size and sends it to the central belt. There is a belt conveyor in the middle of this crawler-mounted machine [5].

2.2.3. Respirable Coal Mine Dust (RCMD)

Coal production creates dust in the face, as do all conventional mining activities. Airborne particles in underground mines that can be inhaled by miners and deposited in the gas exchange region of the lungs are known as respirable coal mine dust (RCMD) [6].

There are many sources of RCMD, including coal extraction (coal and minerals associated with the coal being mined), rock adjacent to the coal seam being mined, rock dust products used in mines to control explosions, and other mining activities (for example, diesel fuel burning and belt abrasion). In addition to coal particles, RCMD contains crystalline silica, silicate minerals, carbonates (mostly from rock dusting), and particulates from diesel engines [7].

Respiratory dust, defined as minus 10 micrometers of size [8], can be inhaled into the lungs' gas exchange region and is known to pose a serious health threat to many workers. A coal worker's pneumoconiosis (CWP), or black lung, is caused by overexposure to respirable coal mine dust in coal mining. Progressive Massive Fibrosis (PMF), a severe form of CWP, can be fatal and disabling. CWP and silicosis are both disabling and/or fatal lung diseases caused by high exposure to respirable silica dust. Once contracted, CWP or silicosis cannot be cured. To prevent these diseases from developing, it is important to limit worker exposure to respirable dust.

Furthermore, float dust generation generated during coal mining can also pose a safety hazard. As coal dust settles from ventilated air onto mine entrance floors, roofs, and ribs, it is known as float coal dust [9]. In many mines, coal dust explosions are triggered by methane gas explosions that lift the dust back into the air. According to MSHA regulations, rock dust is required to inert coal dust that has been deposited.

2.2.4. Dust Standard in the US

Before the Federal Coal Mine Health and Safety Act of 1969 (Public Law 91-173), no respirable dust exposure limits were imposed in the U.S. coal mining industry. Mine workers' dust exposure was not monitored by personal dust sampling either. The U.S. Bureau of Mines (USBM) conducted personal dust sampling at a few mines in 1968 to assess worker exposure. Two of the sampled occupations had maximum exposure levels approaching 40 milligrams per cubic meter of air (mg/m3) due to high respirable dust concentrations at these mines.

As a result of the 1969 Act, the National Institute of Occupational Safety and Health (NIOSH) [10] established the Coal Workers' Health Surveillance Program (CWHSP). The CWHSP data

indicated that one in three miners with 25 or more years of experience had CWP [11]. Over the next 30 years, the prevalence of lung diseases decreased substantially. There has been an increase in the prevalence of CWP since 2000, particularly among longest-tenured mine workers. CWP cases have also rapidly developed in recent years [12, 13], and PMF cases have increased significantly. In order to reduce coal mine worker exposure to respirable dust, MSHA promulgated a revised dust regulation in 2014 [14]. New dust standards for respirable coal mine dust were set at 1.5 mg/m3 silica limits were set at 100 g/m3, mine operators were required to use new dust sampling instruments with real-time feedback, mine operators had to collect more compliance samples, the CWP surveillance program included spirometry testing, and additional dust sampling requirements were changed.

2.2.5. RCMD in Room and Pillar Mining

Coal mining processes and mine locations affect RCMD composition and concentration. Mining companies need a large coal seam to operate the mine economically. Compared to surface mining, underground coal mining generally has higher dust concentrations. To extract coal from underground mines, cutting through rock might be necessary because of geological features such as faults and seam splits.

In addition to mining methods, job titles and duties are associated with different RCMD exposures. The highest exposure rates are for miners working near the coal face, where continuous miners or longwall machines liberate coal from rock [15]. Operators of continuous miners, roof bolters, headgate and tailgate shearers, and jack setters (shield operators) are among them. A room-and-pillar mine (Figure 2.2) has parallel entries driven to a predetermined boundary. To transport coal from the miner to intermediate haulage, a continuous miner cuts and loads coal. Shuttle cars transport coal. Using cross-cuts, entries are connected, creating pillars. As shown in Figure 2.2, a room-and-pillar continuous miner section is a typical five-entry development in which the continuous miner cuts and loads a shuttle car from entry 2 to entry 5. Dual-split ventilation systems provide intake air through entries two and four and return it through entries one and five [16]. Continuous miners advance the entry by 18 feet or more with every cut.

The continuous miner, which generates dust during cutting and loading processes, is the primary source of respirable coal mine dust in a continuous-mining section. This dust can become airborne and can be harmful to human health. Airborne RCMD can affect both operators and those working downwind of them. A variety of other sources of RCMD can be found, including dust from conveyors, dust from intake airways (due to re-entrainment of settled dust from floors and sides), and dust from rock dusting [2]. An operator in a continuous-miner section is the designated occupation, the occupation with the highest level of exposure to RCMD. A survey of MSHA (RCMD sample data from 2001 to 2004 – 17,000 samples) indicated that around 11 percent of continuous miners and roof bolters exceeded the 2 mg/m3 standard, and about 20 percent exceeded 100 mg/m3 for silica [17].

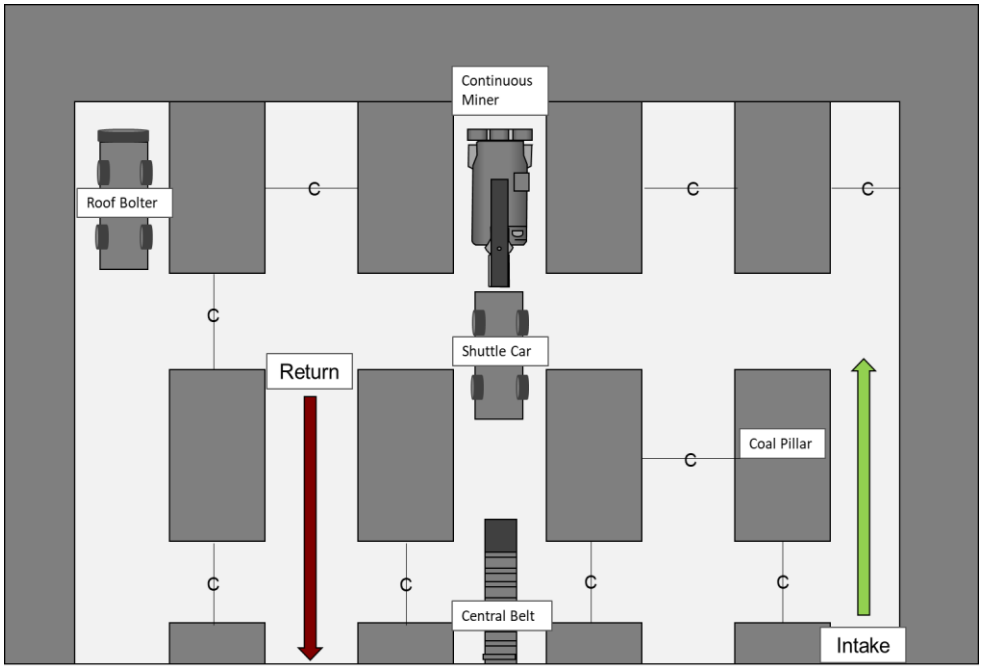

Figure 2.2: An illustration of a room-and-pillar coal mining method.

2.3. Underground Continuous Mining Dust Mitigation Technologies

To control dust generation and worker exposure, the first step should be to minimize respirable dust generated by efficient cutting. Dust does not have to be controlled if it is not generated. To prevent respirable dust from becoming airborne, to prevent any remaining airborne respirable dust from reaching workers' breathing zones, and to remove dust incorporated into ventilated air, dust collectors and various ventilation methods are employed. As long as dust is not inhaled by workers, it cannot cause lung diseases. The final step is to maintain the controls implemented so that they remain effective [18]. The most effective dust control measures are those applied close to dust sources and maintained regularly. There is an emphasis on worker education and training as important components of these measures as well [19].

Continuous mining machines are the largest source of respirable dust in continuous mining operations. Continuous mining operations can expose the miner operator and anyone downwind to dust generated by continuous miners. Dust is diluted, suppressed, directed, or captured with air and water, as is the case with dust sources in general. The primary method of protecting workers against overexposure to respirable dust is to ventilate a continuous mining section, whether by blowing air or exhausting it. In order to control respirable dust efficiently, water spray systems, ventilation, and mechanical equipment (scrubbers) need to be correctly applied [15]. Any effective dust control strategy begins with routine maintenance of scrubbers, water sprays, and bits. Dust suppression is the most effective dust control method. Once dust becomes airborne, other control methods must be applied to dilute it, direct it away from workers, or remove it from the work environment. The dust-laden air is directed away from the operator by water sprays that move it into the return entry or behind the return curtain, which redirects dust. The dust can be captured by water sprays or mechanical means (e.g., fan-powered dust collectors) that interact with the dust in the air. Respirable dust concentrations can also be adversely affected by bit type and bit wear. Regular inspection and replacement of dull, broken, or missing bits can increase cutting efficiency and reduce dust production. [20]. A continuous mining section uses either blowing or exhausting ventilation to dilute and direct dust away from workers. Each method has advantages and disadvantages.

2.3.1. Face Ventilation

In order to control respirable dust exposure, coal mine operators need to be able to control the velocity and quantity of ventilated air. MSHA requires active face ventilation at 3,000 cfm [21]. However, when using scrubbers, MSHA generally recommends that the face airflow be at or slightly above the scrubber's airflow capacity. When designing a ventilation system, it is imperative to have sufficient mean entry air velocity to confine dust near the face. In addition, it is also critical to direct it toward return entry in sufficient quantities to dilute the respirable dust generated. Underground coal mining uses blowing and exhausting ventilation systems. Both systems have advantages and disadvantages regarding worker dust exposure [15].

By blowing air behind a line brattice or tubing, this type of ventilation delivers intake air to the working entry. This system allows the continuous miner operator to be positioned in clean discharge air at the end of the blowing curtain or tubing while the dust-laden air is swept toward the return entryway. As clean air blows toward the face, dust-laden air sweeps toward the return entryway. In addition to effectively sweeping dust and methane from the face, the method also places mobile equipment operators (e.g., shuttle car operators) and roof bolter operators in return air so they can work downwind [15].

A working entry is supplied with intake air for exhaust ventilation. The clean air sweeps the face, and the dust-laden air is then drawn behind the return curtain or through the exhaust tubing to the return entries behind the return curtain or exhaust tubing. In addition to providing fresh air to mobile equipment, this system allows continuous miners more freedom of movement than blowing ventilation systems [15]. Also, exhausting ventilation allows shuttle car operators to easily determine where continuous miner operators are located when entering the face area since it provides superior visibility around the loading area. Miners will be exposed to dust-laden return air at the end of the line curtain when using this method [22].

2.3.2. Water Spray Systems

In order to control dust on continuous miners, a variety of sprays are available. A spray system must take into account a number of factors, such as the type of spray nozzle, location, pattern, flow, and pressure. Each spray is designed according to its intended application. While higher

water pressure improves water spray effectiveness, it also entrains large quantities of air and dust, resulting in dust rollback [15].

Water sprays were first used to lubricate bits, cool bits, and control dust on continuous miner machines. Despite restricting respirable dust exposure to a limited extent, these sprays cause large amounts of dust rollback and turbulence. During continuous miner operation, dust rollback invades the operator's position, resulting in dust overexposure. The researchers relocated sprays beneath and atop the cutting drum to control dust rollback. Miner operator dust exposures are reduced by 40% when using these boom sprays compared with a factory-installed spray system [23].

2.3.3. Flooded Bed Dust Scrubber (FBS)

Most continuous mining machines in underground coal mines today use FBS, which are fan-powered dust collectors [24]. Scrubber inlets located near the cutter head move air toward the face and capture dust. As shown in Figure 2.3, dust-laden air is captured from the cutting face by FBS, which carries it through ductwork on the miner and then passes this air through a water spray-sprayed filter panel. In the process of impacting and traveling through the filter panel, dust particles mix with water droplets. These droplets are then removed from the airstream by the mist eliminator. Lastly, the fan discharges the cleaned air back into the mine [25].

FBS can remove over 90% of respirable dust pulled into the unit. Although MSHA does not consider the scrubber a ventilation device, it can help direct ventilated air to the face [26]. It is critical that the brattice curtain mouth is outside the scrubber's discharge point to direct the scrubber exhaust into the return airway to optimize scrubber performance in mines using exhausting face ventilation. To achieve this, the curtain would have to be approximately 40 feet away from the face [27].

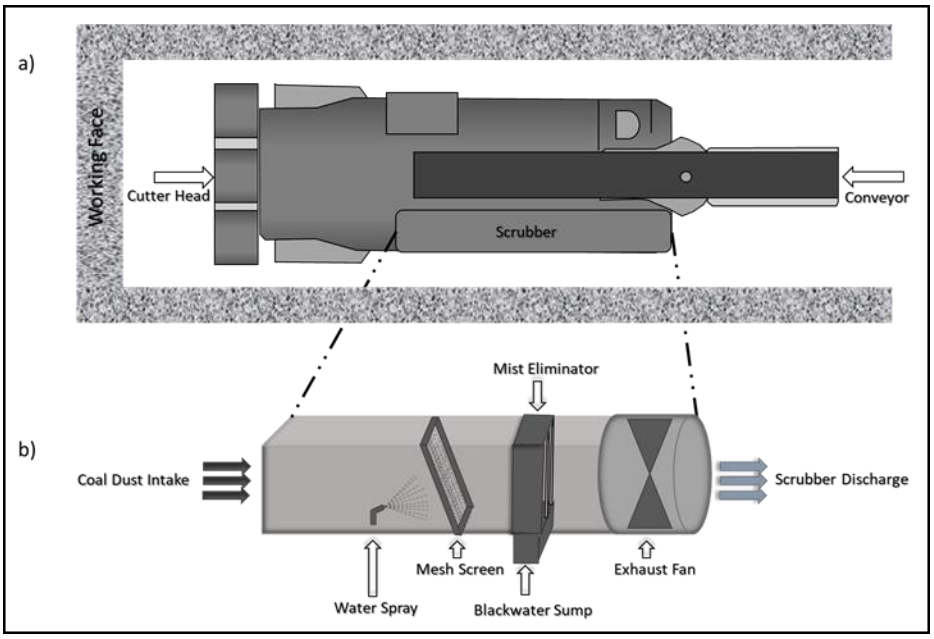

Figure 2.3: a) Continuous miner top view b) Flooded bed scrubber side view

In FBS, dust reduction is determined by two factors: capture efficiency and collection efficiency.

i. By determining the amount of air drawn into or "captured" by the scrubber and the amount of air supplied to the face, the capture efficiency is determined. It is ideal for the scrubber to capture almost 94% of the ventilating air if it has a capacity of 7,500 cfm and is supplied with 8,000 cfm of air. This means that increasing FBS airflow capacity can be beneficial. Maximum scrubber airflow capacity has been increased to 20,000 cfm [28].

ii. As a measure of collection efficiency, the scrubber removes a percentage of respirable dust that enters it before it is discharged back into the mine atmosphere. Air entering a scrubber with a dust concentration of 10 mg/m3 and air discharged by the scrubber with a dust concentration of 1 mg/m3 would result in a collection efficiency of 90% [28].

In continuous mining, scrubber performance is determined by capture and collection efficiency. According to previous research, when face air flow and scrubber air flow were equal, the lowest dust levels were observed [29]. It is assumed that all air supplied to the face will be drawn into the scrubber and cleaned before being discharged at a 1:1 ratio. When the face ventilation air is greater than the scrubber, a portion of the air can bypass the scrubber and expose the mine workers to dust clouds in full concentrations. A portion of the face air will be recirculated if the face ventilation

air falls below scrubber capacity, which releases methane. It is therefore imperative to ensure that the scrubber captures 100% of the dust-laden ventilating air at the face, as well as removing more than 90% of the dust from the captured airstream if optimum scrubber performance is achieved [28].

A scrubber's dust collection efficiency and air-moving capacity are affected by the density and type of media used in the filter panel. It is safe to say that optimal performance is achieved if FBS are capable of drawing dust-laden air from the cutting face and removing a high percentage of respirable dust (>90%) [30].

It has been evaluated whether FBS can collect respirable dust efficiently when supplemental controls are implemented within the scrubber, whether different filter media are used, and whether different filter densities are used [28, 31]. Additional dust collection controls (surfactant or oil emulsion added to scrubber spray water or atomizing or fogging sprays added upwind of the normal sprays) had minimal effect. The use of different filter materials (bottle brush and synthetic materials) could benefit dust collection [32].

A scrubber's relative overall performance was determined by its dust collection efficiency and air-moving capacity. Increasing the filter density improved dust collection, but decreased airflow through the scrubber. Based on these findings, NIOSH recommends dust collection improvement with 30-layer stainless steel wire mesh or synthetic filter panels in FBS. As a result of higher air velocity in the scrubber, collection efficiency also increased [33], regardless of the filter panel tested.

Another recent study examined the mass accumulation of clogged dust particles within the FBS filter using experimental and theoretical methods in a laboratory test setup [34]. According to the research, the pressure drop was higher when dust accumulated in the filter. Pressure drops through porous materials are directly related to airflow rates. Despite improving collection activity, densely packed filter mesh reduces the airflow rate. It is critical to use fine filter media to maintain high airflow rates. Conversely, fine filter media cannot effectively trap dust particles, allowing dusty air to travel back into the mine. NIOSH found that 20-layer and 10-layer stainless-steel wire mesh filters are less effective at collecting RCMD particles than denser stainless-steel wire mesh in a traditional FBS [28].

As water is sprayed on a screen, dust-laden air is forced through droplets. The FBS works by spraying water on a screen. With increasing water influx onto the screen surface, fibrous filters perform better with increased water inflow, improving particle cleaning [35].

To investigate the impact of airflow and water rates on cleaning performance, Gupta et al. altered the airflow and water rate systematically [36]. According to the researchers, higher water flow results in more pronounced flooding of the filter surface and alleviates clogging.

Coal dust often floats on top of puddled water in underground mines due to its hydrophobic nature. Adding a wetting agent to spray water increases the coal's wetting ability and captures more airborne dust by the reduced surface tension of the water. Coal mining has been subjected to multiple wetting agent tests over the years with mixed results. Some studies have shown negligible improvements in dust control [37,38], others show a 25% improvement in dust capture [39], and others show a 40% improvement at one mine but inconclusive results at a second mine [40]. Wetting agent concentration was found to enhance wetting in all of these studies and others [41]. Additionally, prior to the use of chemical additives, it is worthwhile to consider how these additives might impact miners' health.

As part of this study, the surface of the vibrating filter media is modified, instead of adding additional substances to the spray water to increase filtering efficiency. In addition to improving adhesion between mine dust particles and liquid interfaces, the surface modifications increase the uniform wetting of the mesh screen surface with liquid. When the mesh has a hydrophilic surface, water droplets will stay on the mesh for a longer period of time. This allows more dust particles to be captured. Surfaces with hydrophobic properties will, however, allow droplets to drain more rapidly, enabling them to continue to the mist eliminator. To examine the combined effect of mesh design and surface modification on dust collection, vibration-enhanced and surface-modified stainless-steel mesh panels of varying thicknesses were used in this study.

For several decades, FBSs have been widely used to remove dust from continuous mining operations [42-44]. There are numerous operational challenges associated with the static panel filter, which forms the basis of most scrubber designs. It is fundamentally limited in collection efficiency and prone to rapid clogging. Consequently, continuous miner operation capacity is affected and frequent maintenance becomes necessary.

The mesh screen of the scrubber is periodically removed from the scrubber by a miner and thoroughly washed. While previously recommended cleaning the filter after every 40 feet of advance [45], a recent study found that a 20-foot advance could reduce scrubber airflow by up to 35%. Therefore, NIOSH recommends cleaning the filter after every 20 feet of advancement. The detailed cleaning process causes operation downtime that slows production. There is also a problem with insufficient wetted area on the screen throughout the process. Adhesion between water and dust particles is one of the main mechanisms of dust collection on the mesh screen. Dusty air can easily pass through a mesh screen with insufficient wetted areas. As a result, dust-laden air enters the mine's atmosphere and lowers air quality.

To improve mining operations efficiency, it is necessary to enhance FBS cleaning efficiency and minimize these operational challenges. In order to achieve this, several research projects are currently underway. Researchers generally test different filter types and use different water and airflow rates. The vortecone filter, first developed by Salazar et al. [46], is widely used in the automobile industry as an oversprayed paint particle collector. That design was used to replace the mesh filter in a recent study. The FBS was found to improve cleaning efficiency while increasing pressure drop, resulting in undesirable results. Significant modifications were also required to the scrubber main structure [47-49].

Another study investigated the use of a three-slit impingement-type filter mounted on three metallic surfaces to prevent interruptions during continuous mining operations. The first and third screens are identical, whereas the slits in the second screen are displaced laterally by 6.0 mm to allow dust to hit metallic surfaces and be captured [50]. Additionally, the solid impermeable surface of the filter ensures water spreads more evenly across the surface. As the filter surface is responsible for dust capturing and water is responsible for surface cleaning, the system requires minimal water inflow to keep the surface wet. In contrast, clogging of the impingement filter may cause pressure drops to reach undesirable values rapidly.

Using a vibrating mesh screen instead of a static mesh screen as an alternative to the static mesh screen used in conventional FBS, Lu et al. and Janjua et al. conducted computational fluid dynamics (CFD) simulations to determine how vibration conditions affect dust particle-mesh interaction and mesh wetting. The simulations included airflow, coal particulates, and water spray. Furthermore, the researchers examined the effect of mesh screen aperture, dust concentration, and

water spray flow rate on filter efficiency. Based on CFD simulations, dynamic mesh screens are significantly better at capturing dust particles on their surfaces. In addition, they increase the mesh panel wetted area, thereby improving screening efficiency. Researchers found that vibrating meshes achieve an equivalent level of interaction with static meshes with a larger aperture, with low maintenance [51, 52].

2.4. Vibration on Continuous Miner

Researchers conducted a series of experimental and numerical studies and shared results proving large vibrations occur and persist throughout the operation, forming immediately after the machine is operated – not even necessarily after the machine comes into contact with the coal face [53-56]. The main reasons for vibration include the motor gearbox, the dust collection unit exhaust fan, the conveyor system motion, the cutter head/cutting arm motion, and the machine's interaction with dynamic forces during cutting cycles [57-60].

A technical report provided by Fuchs (1969) provides detailed raw vibrational characteristics data of different underground mining machines, including four types of continuous miners, despite very few studies including the vibrational energy of continuous miners in the literature [53]. Raw data was digitized and assessed to develop a demonstrable figure that illustrates average acceleration levels within the range of frequencies up to 5 kHz at the closest locations to the filter. As shown in Figure 2.4, the average acceleration at different positions for the four continuous miners under all functional modes and all operating conditions is shown at various positions, based on the results of the Fuchs report. Based on the graph, peak acceleration levels can be observed around 100 Hz.

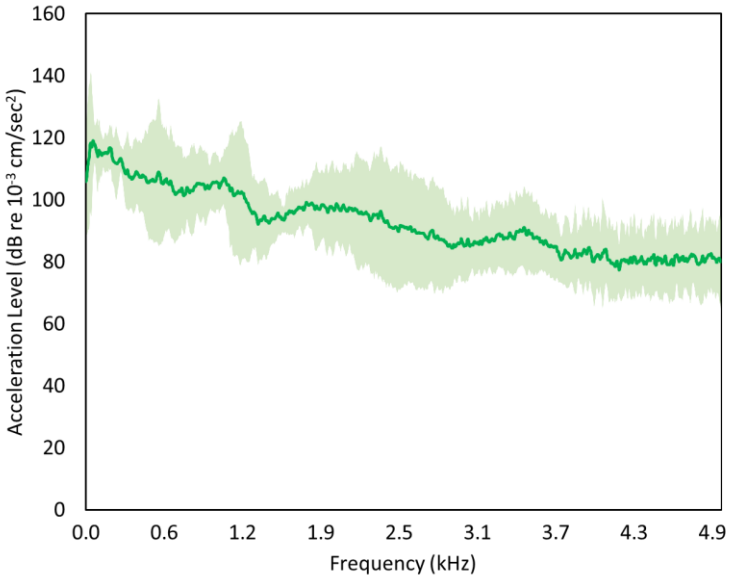

Figure 2.4: Continuous miners' acceleration levels in various positions and working environments

Using vibration levels and surface areas, the most significant noise-radiating surfaces on the continuous miner tail section were also determined using their sound power levels. Approximately 80% of the sound energy emitted by the conveyor system located in the center of the continuous miner is at frequencies between 500 and 2500 Hz [51, 53, 54, 61].

In separate studies, vibration characteristics and dynamic loads of continuous miner cutting arms were evaluated. Compared to other locations on the cutting arm, the vibration amplitude was greater at the engine location. Results indicate that higher vibration amplitudes are usually observed between 1 and 100 Hz [56, 58].

2.5. Vibrating Filter Elements

Coal dust buildup on filters can cause frequent production interruptions and poor air quality. A shaking mechanism helps the filters shed coal dust periodically. It has been used for a long time in industrial applications such as size classification, filtering, dust removal, and dust collection to vibrate the filter media and screen to achieve more sustainable particle filtering [62-64]. By

inducing vibration directly to the fibrous filter, researchers have demonstrated that the filter's efficiency can be enhanced [65-66]. Moreover, it has been shown that once vibration is applied to the membrane filter's surface area clogging can be reduced [67-73].

As demonstrated by the aforementioned studies, vibrating the filter enhances particle shedding, reduces clogging, and enhances the chance of dust particle-water droplet interaction by intensifying surface wetness. Due to the advantages described above, vibrating filters do not require frequent maintenance. Using computational fluid dynamics (CFD), Lu et al. conducted simulations to examine how vibrations affect dust particle-mesh interactions and mesh wetting conditions [51]. It has been shown that capturing dust particles on the mesh screen surface can be significantly improved with a dynamic mesh screen. In addition, it increases the wetted surface of the screen, increasing the screening efficiency.

A vibrating object moves a certain distance from its stationary position. The amplitude measures the distance between a stationary point and the extreme position on either side of it, which describes vibration intensity. At the maximum acceleration level, the mesh filter can produce the maximum oscillation amplitude. An experimental study was conducted to determine the peak acceleration of the mesh filter [74]. Figure 2.5 shows how the mesh screen responds to a predetermined frequency range. As shown in figure, peak acceleration levels are recorded between 10 and 200 Hz.

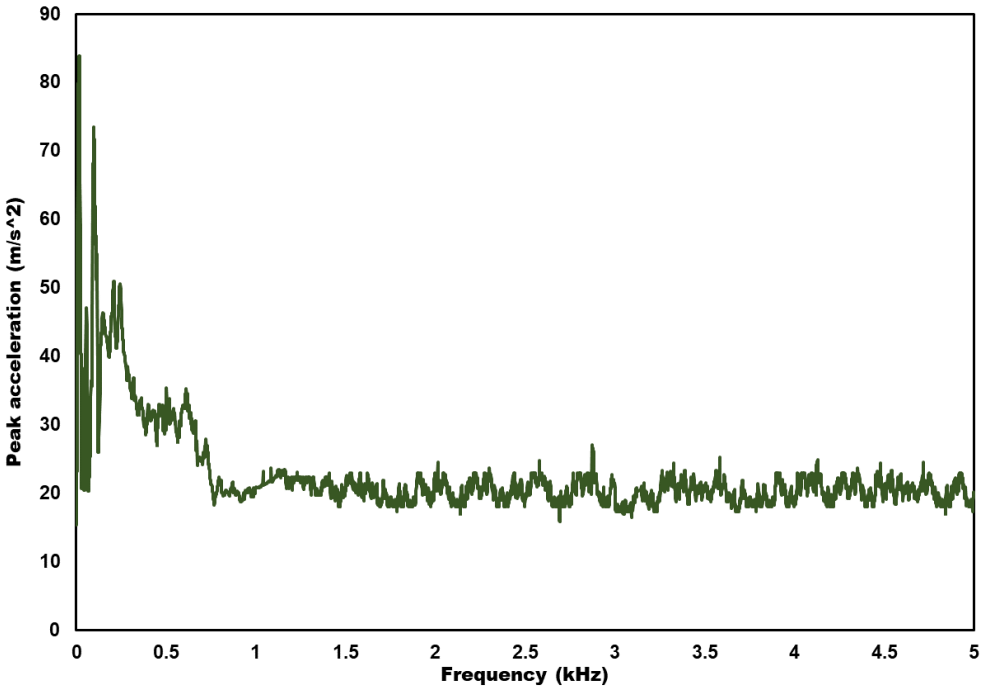

Figure 2.5: Frequency-Peak Acceleration in the bench scale FBS

2.6. Vibrational Energy Transmission

Research into energy harvesting (EH) has been a significant aspect of research in the past few years. EH converts the energy present on Earth into electrical energy to operate autonomous electronic devices [75, 76]. Energy can be harnessed from solar power, thermal energy, and kinetic energy, particularly from vibrational motion [77]. Devices like sensors and wireless electronics can be powered by EH using vibrations. Its mechanism depends on electromagnetic, piezoelectric, and hybrid electromagnetic sources [78-82].

The vibration-based energy harvester is typically made up of a spring-mass-damper system, which generates maximum power when its resonant frequency matches that of the vibrations in the environment [82]. Using softening springs in vibration energy harvesters may have advantages over linear springs and hardening springs, according to the researchers. Calculations showed that stiffness nonlinearities can improve energy harvester performance. A softening spring yields more

power than a linear or a hardening spring. The bandwidth and harvested power will also increase as the stiffness decreases.

By using the energy harvesting approach, the natural vibration generated throughout the continuous miner operation can be translated into frequencies and amplitudes most suitable for dust particle capture and minimum particle clogging. In this way, the output vibration will be able to pass through the mesh screen.

2.7. Summary

2.7.1. Literature Highlights

Background research and developments in dust-scrubbing technologies relevant to mining operations are summarized in this chapter. There has been a discussion of relevant legislation and methods adopted to combat dust and comply with these rules, as well as some health and safety issues associated with dust accumulation underground. It covers many notable developments in dust scrubbing systems, as well as some of the most recent efforts towards dust control in underground coal mines. As a major part of this dissertation, vibrating the filter panel to improve the equipment's overall efficiency has been discussed towards the end of the chapter.

Studies conducted by health and safety institutions and regulatory authorities in the mining industry have concluded that prolonged exposure to airborne respirable coal dust can cause permanent disability and death. Consequently, many mine operators are working to improve dust control methods. Mine operators typically employ preventative particle-collecting devices and dust control techniques to suppress airborne dust.

To maintain and improve mining operations efficiency, FBS needs to be improved. Researchers are currently focusing on different filter types to achieve this. Various upgraded FBS filtering systems have been proposed and efforts have been made to develop them. However, none of the technologies is mature enough to be commercially viable.

The CFD simulation study showed that shaking the mesh screen of an FBS may improve the efficiency of this equipment by enhancing dust particle-mesh interaction and mesh wetting [51]. It is also concluded in the study that the vibrating mesh has an equal degree of interaction with the static mesh with a larger aperture, providing low-maintenance operation.

2.7.2. Technical and Knowledge Gaps

Due to the lack of empirical studies regarding vibration effects on FBS mesh screens, this research is an original study. An innovative filter design that minimizes filter clogging, achieves uniform wetting, and maintains high air flow rates is investigated in this study. Laboratory experiments confirmed the simulation results. Another originality of this work is the application of coatings to the filter screen to improve its wettability. As a result of this study, the proposed design can be used as one of the strongest tools to protect coal miners' lung health during continuous mining operations. It is expected that all the studies being conducted will make significant contributions to the field of research regarding FBS improvement.

Results will also provide an additional perspective on the industrial applications of the FBS and reveal how vibrations can enhance the FBS's efficiency. This study is an original study as no empirical studies have been performed regarding vibration's effect on FBS mesh screens. Further, by publishing the findings of the research in journals scanned in SCI, this study fills this knowledge gap by developing a design that can be used in continuous mining environments to improve air quality to protect coal miners' respiratory health and provide a safer workplace in underground coal mines. In addition, it serves as a valuable resource for health and safety authorities around the world and sector operators interested in this topic.

2.8. References

1. International Energy Outlook (2017). Data Available online at https://www.eia.gov/outlooks/aeo/data/ (accessed October 1, 2022).

2. National Academies of Sciences, Engineering, and Medicine. (2018). Monitoring and Sampling Approaches to Assess Underground Coal Mine Dust Exposures. Washington, DC: The National Academies Press. Doi: https:/doi.org/10.17226/25111.

3. Coal Data Browser. Aggregate Coal Mine Production: All Coal: Underground (2016). Available online at https://www.eia.gov/beta/coal/data/browser/ (accessed October 2, 2022).

4. A.J. Das, P.K. Mandal, P.S. Paul, R.K. Sinha, (2018) Strategies for underground extraction of the inclined coal seams by continuous miner. MGMI 114, 1–12

5. Subrata Samant (2021) Deployment of Continuous Miner in under Ground Coal Mine: A Case Study of Sarpi Mine

6. Almberg KS, Halldin CN, Blackley DJ, Laney AS, Storey E, Rose CS, Go LHT, Cohen RA [2018]. Progressive massive fibrosis resurgence identified in U.S. coal miners filing for black lung benefits, 1970−2016. Ann Am Thorac Soc 15(12):1420−1426.

7. Castranova, V., & Vallyathan, V. (2000). Silicosis and coal workers' pneumoconiosis. Environmental Health Perspectives. http://doi.org/10.1016/B978-1-4557-0792-8.00051-9.

8. ACGIH [2007]. Appendix C: Particle size-selective sampling criteria for airborne particulate matter. In: 2007 TLVs and BEIs. Cincinnati, OH: American Conference of Governmental Industrial Hygienists.

9. Harris ML, Cashdollar KL, Man CK, Thimons ED [2009]. Mitigating coal dust explosions in modern underground coal mines. In: Panigrahi DC, ed. Proceedings of the Ninth International Mine Ventilation Congress, New Delhi, India, pp. 143−149.

10. NIOSH (2019a). Coal Workers' Health Surveillance Program. U.S. Department of Health and Human Services, Centers for Disease Control and Prevention, National Institute for Occupational Safety and Health, https://www.cdc.gov/niosh/topics/cwhsp/default.html (accessed October 3, 2022).

11. NIOSH (2019b). Coal Workers' Health Surveillance Program (CWHSP) Data Query System. Centers for Disease Control and Prevention, National Institute for Occupational Safety and Health, Respiratory Health Division, Surveillance Branch, https://webappa.cdc.gov/ords/cwhsp-database.html (accessed October 5, 2022).

12. Antao VC, Petsonk EL, Sokolow LZ, Wolfe AL, Pinheiro GA, Hale JM, Attfield MD (2005) Rapidly progressive coal workers' pneumoconiosis in the United States: geographic clustering and other factors. Occup Environ Med 62(10):670−674.

13. Cohen RA, Petsonk EL, Rose C, Young B, Regier M, Najmuddin A, Abraham JL, Churg A, Green FHY (2016) Lung pathology in U.S. coal workers with rapidly progressive pneumoconiosis implicates silica and silicates. Am J Respir Crit Care Med 193(6):673−680.

14. 79 Fed. Reg. 24814 [2014]. Mine Safety and Health Administration: Lowering miners' exposure to respirable coal mine dust, including continuous personal dust monitors; final rule. To be codified at 30 CFR Parts 70, 71, 72, 75, and 90.

15. Colinet, J. F., J. P. Rider, J. M. Listak, J. A. Organiscak, and A. L. Wolfe, (2010) Best Practices for Dust Control in Coal Mining. Pittsburgh, PA: NIOSH.

16. Bise, C. J., (2013) Modern American Coal Mining: Methods and Applications. Englewood, CO: Society for Mining, Metallurgy and Exploration, Inc. p. 563.

17. Colinet, J. F., and J. M. Listak., (2007) Reducing Dust Generation and Optimum Suppression Techniques. Presentation to Controlling Respirable Coal Mine Dust in Underground Mines National Mine Health and Safety Academy, Beckley, WV Available at https://arlweb.msha.gov/s&hinfo/blacklung/ControlDust2007/NIOSH%20PRL%201-97.pdf (accessed October 3, 2022).

18. Colinet JF (2020) The impact of black lung and a methodology for controlling respirable dust. Min Metal Expl 37(6):1847−1856.

19. Ramani, R. V., M. C. Radomsky, J. P. Flick. 2003. Control of Airborne Respirable Dust Hazards: A Training Program for Underground Coal Miners, Available at http://miningquiz.com/powerpoints/dust_and_silica.htm (accessed October 4, 2022).

20. Organiscak JA, Khair AW, Ahmad M (1996). Studies of bit wear and respirable dust generation. Transactions of Society for Mining, Metallurgy, and Exploration, Inc. Vol. 298. Littleton, CO: Society for Mining, Metallurgy, and Exploration, Inc., pp. 1932–1935.

21. CFR. Code of Federal Regulations. Washington, DC: U.S. Government Printing Office, Office of the Federal Register.

22. Kissell FN, Goodman GVR (2003) Continuous miner and roof bolter dust control. In: Kissell FN, ed. Handbook for dust control in mining. Pittsburgh, PA: U.S. Department of Health and Human Services, Centers for Disease Control and Prevention, National Institute for Occupational Safety and Health, DHHS (NIOSH) Publication No. 2003-147, IC 9465, pp. 23– 38.

23. Schroeder WE, Babbitt C, Muldoon TL (1986) Development of optimal water spray systems for dust control in underground mines. Foster-Miller, Inc. U.S. Bureau of Mines contract H0199070. NTIS No. PB 87-141537.

24. Colinet JF, Reed WR, Potts JD. (2013) Impact on Respirable Dust Levels When Operating a Flooded-bed Scrubber in 20-foot Cuts. Pittsburgh, PA: U.S. Department of Health and Human Services, Centers for Disease Control and Prevention, National Institute for Occupational Safety and Health, DHHS (NIOSH) Publication 2014–105, RI 9693.

25. Colinet, J., Halldin, C. N., & Schall, J. (2021) Best Practices for Dust Control in Coal Mining, Second Edition. National Institute of Occupational Safety and Health, Pittsburgh. PA; Spokane, WA.

26. Taylor CD, Rider JP, Thimons ED (1996) Changes in face methane concentrations using high capacity scrubbers with exhausting and blowing ventilation. Littleton, CO: Society for Mining, Metallurgy, and Exploration, Pre-print 96-167.

27. Jayaraman NI, Volkwein JC, Kissell FN (1990) Update on continuous miner dust scrubber applications. Mining Engineering 42(3):281–284.

28. Colinet, J. F., & Jankowski, R. A. (2000). Silica collection concerns when using flooded-bed scrubbers. Mining Engineering (Littleton, Colorado), 52.

29. Jayaraman, N.I., Jankowski, R.A., and Whitehead, K.L., (1992) Optimizing continuous miner scrubbers for dust control in high coal seams, Proceedings of New Technology in Mine Health and Safety Symposium, SME Annual Meeting, Feb. 24-27, Phoenix, AZ, Chapter 20, pp. 193-205.

30. NIOSH (1997) Hazard identification 1: Exposure to silica dust on continuous mining operations using flooded-bed scrubbers. Cincinnati, OH: U.S. Department of Health and Human Services, Centers for Disease Control and Prevention, National Institute for Occupational Safety and Health, HID1, DHHS (NIOSH) Publication No. 97–147.

31. Colinet JF, McClelland JJ, Erhard LA, Jankowski RA. (1990) Laboratory evaluation of quartz dust capture of irrigated-filter collection systems for continuous miners Pittsburgh, PA: U.S. Department of the Interior, Bureau of Mines, RI 9313.

32. McClelland JJ, Colinet JF, Bringhurst B (1991) Performance evaluation of irrigated filters. Society for Mining, Metallurgy, and Exploration, Transactions Vol. 290, pp. 1828–1831.

33. NIOSH (2002) Exposure to Silica Dust on Continuous Mining Operations Using Flooded-Bed Scrubbers, Applied Occupational and Environmental Hygiene, 17:5, 322-323, DOI: 10.1080/10473220252864888.

34. Szczap, J,Pan . "Understanding Interfacial Interactions in Filter Clogging of Flooded bed Scrubbers using Experimental Approach and Modelling" {Submitting to Powder Technology}

35. Kumar, A. R., Schafrik, S., & Velasquez, O. (2020) Designing, modeling, and laboratory testing of a non-clogging impingement type filter for mining dust scrubbers. Mining, Metallurgy & Exploration, 37(6), 1911-1918.

36.Gupta, Neeraj, Ashish Ranjan Kumar, and Steven Schafrik. (2021) Laboratory Determination of Coal Dust Cleaning Efficacy of a Fibrous Filter for Flooded-Bed Dust Scrubber" Minerals 11, no. 3: 295. https://doi.org/10.3390/min11030295

37. Chander S, Alaboyun AR, Aplan FF (1991) On the mechanism of capture of coal dust particles by sprays. Proceedings of the 3rd Symposium on Respirable Dust in the Mineral Industries, Pittsburgh, PA, October 17–19, pp.193–202.

38. Tessum MW, Raynor PC (2017) Effects of spray surfactant and particle charge on respirable coal dust capture. Safety and Health at Work 8(3):296–305. https://doi.org/10.1016/j.shaw.2016.12.006

39. Kost JA, Shirey GA, Ford CT (1980) In-mine tests for wetting agent effectiveness. U.S. Department of the Interior, Bureau of Mines Open File Report 30-82, NTIS No. PB82-183344.

40. Kilau HW, Lantto OL, Olson KS, Myren TA, Voltz JI. (1996) Suppression of longwall respirable dust using conventional water sprays inoculated with surfactants and polymers Minneapolis, MN: U.S. Department of the Interior, Bureau of Mines, Report of Investigations 9591.

41. Tien JC, Kim J (1997) Respirable coal dust control using surfactants. Appl Occup Env Hyg 12(12):957–963.

42. Arya S, Novak T, Saito K et al (2019) Empirical formulae for determining pressure drop across a 20-layer flooded-bed scrubber screen. Mining, Metallurgy & Exploration, 36(6), 1169-1177. https://doi.org/10.1007/s42461-019-0091-5

43. Arya S (2018) Investigation of the effectiveness of an integrated flooded-bed dust scrubber on a longwall shearer through laboratory testing and CFD simulation. Doctoral Dissertation, Mining Engineering, University of Kentucky. https://doi.org/10.13023/ETD.2018.074

44. S. R. Cowley, B.S. McCoy (1993) "Wet scrubber apparatus," U. S. Patent 5,178,654.

45. Campbell, J. A., Moynihan, D. J., Roper, W. D., & Willis, E. C. (1983). U.S. Patent No. 4,380,353. Washington, DC: U.S. Patent and Trademark Office.

46. Salazar, A. J., Saito, K., Alloo, R. P., & Tanaka, N. (2000) U.S. Patent No. 6,093,250. Washington, DC: U.S. Patent and Trademark Office.

47. Kumar, A. R., Levy, A., Kumar, A., Schafrik, S., & Novak, T. (2020) Computational fluid dynamics modeling and laboratory analysis of aerosol particles' capture on thin swirling water film in a Vortecone. Powder Technology, 361, 499-506.

48. Kumar, A. R., & Schafrik, S. (2020) Multiphase CFD modeling and laboratory testing of a Vortecone for mining and industrial dust scrubbing applications. Process Safety and Environmental Protection, 144, 330-336.

49. Kumar, A. R., Schafrik, S., & Novak, T. (2020) Multi-phase computer modeling and laboratory study of dust capture by an inertial Vortecone scrubber. International Journal of Mining Science and Technology, 30(3), 287-291.

50. Kumar, A. R., Schafrik, S., & Velasquez, O. (2020) Designing, modeling, and laboratory testing of a non-clogging impingement type filter for mining dust scrubbers. Mining, Metallurgy & Exploration, 37(6), 1911-1918.

51. Lu, Z., Rath, A., Amini, S. H., Noble, A., & Shahab, S. (2022) A computational fluid dynamics investigation of a novel flooded-bed dust scrubber with vibrating mesh. International Journal of Mining Science and Technology, 32/3, 525-537, https://doi.org/10.1016/j.ijmst.2022.03.002.

52. Janjua, A.N., Shaefer M., Amini, S.H., Noble, C.A., Shahab, S. (under review). Vibration Energy Harvesting in Underground Continuous Mining: Dynamic Characteristics and Experimental Research of Field Data. Applied Energy. (Manuscript submitted for publication.)

53. Fuchs, E.P (1979) Coal Mining Equipment Vibration Data Report, Donaldson Company, Inc.

54. Smith, A. K., Peterson, J. S., & Kovalchik, P. G. (2008) Continuous mining machine conveyor system sound power levels.

55. Mężyk, A., Klein, W., Pawlak, M., & Kania, J. (2015) Numerical simulation of the vibration control system designed for Continuous Miner machines. Mathematical and Numerical Approaches, 363.

56. Mężyk, A., Klein, W., Pawlak, M., & Kania, J. (2017) The identification of the vibration control system parameters designed for continuous miner machines. International Journal of Non-Linear Mechanics, 91, 181-188.

57. Yantek, D. S. (2003) Estimated sound power radiated by surfaces on a continuous miner tail section using vibration measurements. National Institute for Occupational Safety and Health, Pittsburgh, PA

58. Stander, C. J., & Heyns, P. S. (2005) Instantaneous angular speed monitoring of gearboxes under non-cyclic stationary load conditions. Mechanical systems and signal processing, 19(4), 817-835.

59. Wang, J., Zhang, Y., & Dong, L. (2016) Analysis of vibration characteristics and dynamic load identification in continuous miner cutting arm. Int J Simul Syst Sci Technol, 17(13), 20-1.

60. Mężyk, A., Pawlak, M., Klein, W., & Kania, J. (2013) Methodology for optimization modal parameters in the engineering design process on the example on the example of continuous miner cutter boom.

61. Niţoi, D., & Amza, G. (2019). Industrial Air Purification System Using Ultrasonic Vibration. Current Trends in Natural Sciences Vol, 8(15), 17-22.

62. King, R. P. (2001) Classification based on sieving–vibrating screens. Modeling and simulation of mineral processing systems. Elsevier. 81-86.

63. Chen, Z., Zhou, Z., & Peng, J. (2022) Dust Removal Mechanism of the Vibrating String Filter with Charged Water Mist. International Journal of Rotating Machinery, 2022.

64. Mishin, I. F., El'bert, E. I., Belikov, V. I., Tumanov, A. N., & Kachaev, V. K. (1975) Cleaning coal tar by vibrating-screen filtration, surfactant treatment, and short-term clarification. Coke Chem., USSR (Engl. Transl.);(United Kingdom), 4.

65. Yang, X., Wang, H., & Chase, G. G. (2015) Performance of hydrophilic glass fiber media to separate dispersed water drops from ultra low sulfur diesel supplemented by vibrations. Separation and Purification Technology, 156, 665-672.

66. Kim, S. C., Wang, H., Imagawa, M., Chen, D. R., & Pui, D. Y. (2006) Experimental and modeling studies of the stream-wise filter vibration effect on the filtration efficiency. Aerosol science and technology, 40(6), 389-395.

67. Genkin, G., Waite, T. D., Fane, A. G., & Chang, S. (2006) The effect of vibration and coagulant addition on the filtration performance of submerged hollow fibre membranes. Journal of membrane science, 281(1-2), 726-734.

68. Coster, H. G. L., Farahani, T. D., & Chilcott, T. C. (2011) Production and characterization of piezo-electric membranes. Desalination, 283, 52-57.

69. Bilad, M. R., Discart, V., Vandamme, D., Foubert, I., Muylaert, K., & Vankelecom, I. F. (2013) Harvesting microalgal biomass using a magnetically induced membrane vibration (MMV) system: filtration performance and energy consumption. Bioresource technology, 138, 329-338.

70. Kuscer, D., Rojac, T., Belavič, D., Santo Zarnik, M., Bradeško, A., Kos, T. & Faccini, M. (2017) Integrated piezoelectric vibration system for fouling mitigation in ceramic filtration membranes. Journal of membrane science, 540, 277-284.

71. Khairuddin, N. F. M., Idris, A., & Irfan, M. (2019) Towards efficient membrane filtration for microalgae harvesting: a review. J Kejuruteraan, 2, 103-112.

72. Nurra, C., Clavero, E., Salvadó, J., & Torras, C. (2014) Vibrating membrane filtration as improved technology for microalgae dewatering. Bioresource technology, 157, 247-253.

73. Niţoi, D., Amza, G., Amza, Z., Radu, C., & Teodorescu, M. (2018) Practical Realisation And Finite Element Modeling Of Ultrasonic Filters Design For Air Filtration. International Multidisciplinary Scientific Geo Conference: SGEM, 18(4.2), 555-562.

74. Uluer, M.E., Shigo, M., Amini, S. H., Noble, A., (under review). “An Exploratory Investigation on the Effectiveness of a Novel Vibration-Enhanced Flooded Bed Dust Scrubber”, Mining& Metallurgy and Exploration. (Manuscript submitted for publication.)

75. Priya, S.; Inman, D.J. (2008) Energy Harvesting Technologies; Springer: New York, NY, USA.

76. Anton, S.; Sodano, H. (2007) A review of power harvesting using piezoelectric materials Smart Mater. Struct.,16, R1.

77. Harne, R.L.; Wang, K.W. (2013) A review of the recent research on vibration energy harvesting via bistable systems. Smart Mater. Struct., 22: 023001.

78. Beeby, S.P.; Cao, Z.; Almussallam, A. (2013) Kinetic, thermoelectric and solar energy harvesting technologies for smart textiles. Multidisciplinary Know-How for Smart-Textiles Developers; Woodhead Publishing: Cambridge, UK, pp. 306–328.

79. Muralt P. (2000) Ferroelectric thin films for micro-sensors and actuators: a review. J Micromech Microeng; 10(2): 136–146.

80. Zhou W, Liao WH, Li WJ. (2005) Analysis and design of a self-powered piezoelectric microaccelerometer. Proc SPIE ; 5763: 233–240.

81. Shahab, S. (2015) Vibration energy harvesting, biomimetic actuation, and contactless acoustic energy transfer in a quiescent fluid domain (Doctoral dissertation, Georgia Institute of Technology).

82. He C-H, Amer TS, Tian D, Abolila AF, Galal AA. (2022) Controlling the kinematics of a spring-pendulum system using an energy harvesting device. Journal of Low Frequency Noise, Vibration and Active Control. 41(3):1234-1257. Doi:10.1177/14613484221077474

Chapter 3

3. Design & Fabrication of a Bench-Scale Vibration-Enhanced Flooded Bed Dust Scrubber

3.1. Introduction

The proposed design of a vibration-enhanced flooded bed dust scrubber was evaluated through two different test setups: (1) a bench-scale scale system; and (2) a full-scale prototype system. The installation and construction stages of each test rig are described in separate chapters.

In this chapter, the design and construction stages of the bench-scale system are explained. This system was then tested from various aspects to determine the optimum range of operating conditions through detailed parametric tests. These tests included vibration frequency, amplitude, water flow rates, network design, surface modifications, and their coupling effects. Moreover, the smaller size of the system allowed for more detailed internal system analysis, especially in terms of particle deportment and fate through the system.

The bench-scale FBS was designed and manufactured to model the form and function of an industrial scrubber used on continuous miner applications. Figure 3.1 illustrates the bench-scale scrubber unit used in this study and identifies many of its components and sampling points. To provide a platform for evaluating a variety of operational system variables, the system was configured with several independent modules, including dust concentration, dust size, dust material type, mesh design, mesh vibrational frequency, mesh vibrational amplitude, water flow rate, water nozzle type, and tunnel dimensions.

Additionally, the system features several noteworthy components, including an innovative dust-feeding system, an air-handling puller fan, a dust collection unit, an assortment of air sampling ports down the length of the tunnel, and a shaker assembly mounted to the mesh screen.

3.2. Tunnel Structure

The tunnel structure itself is composed of four detachable ductwork sections, each of which has a matching cross-sectional dimension with a height of 0.152 m and a width of 0.152 m respectively. There are four separate detachable units in this system: (1) the upwind section from which coal dust is fed into the system and from which pre-mesh screen samples are collected, (2) the mesh screen unit, (3) the demister unit, and (4) the post-demister section where the final downwind samples are collected. A polyurethane sealer was used between each section of the chamber so as to prevent any unmeasured air and water from entering or leaving the chamber.

The mesh screen and demister housing sections are 0.36 m in length, and they have grated blackwater sumps underneath to collect wastewater for confirming the water flow rate measurements and supplying the required outlet for wastewater from the mesh screen and demister units' floor. The longer sections provide the place for the sampling ports and allow the dust-laden air to travel from one unit to another and share a common length of 1.22 m. Altogether, the full system spans nearly 3.8 m in total length.

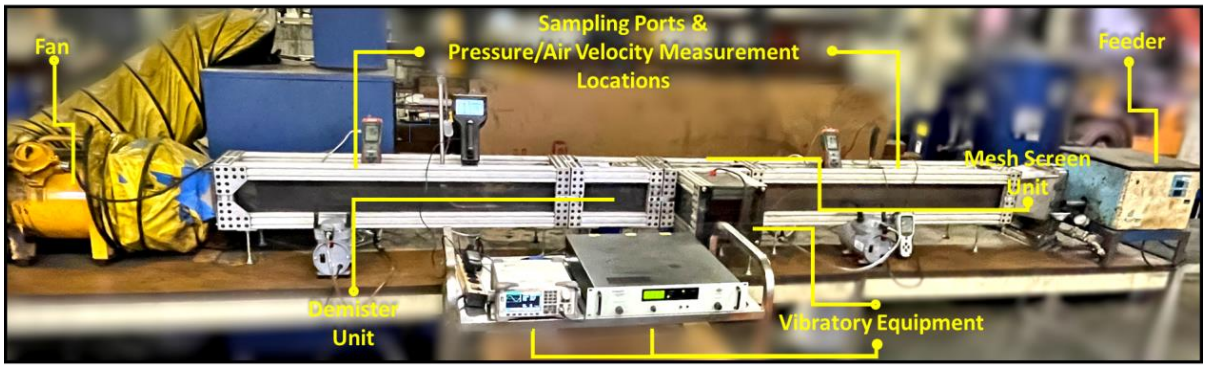

Figure 3.1: Bench-scale scrubber system.

The framework of the scrubber consists of 80/20 extruded aluminum framing with walls made from clear polycarbonate. The sections were made modular in nature and shared a new common

mode of fastening. This fastening, shown in Figure 3.2a, includes 6.35-mm inner alignment dowels and outer slide-locking alignment bars that are fastened with wing nuts for ease of assembly/disassembly during testing. In this modular configuration, sections can be separated and realigned quickly and in a matter that is both airtight and watertight. Flat neoprene rubber seals between each section (Figure 3.2b) were placed and barbed neoprene rubber seals (Figure 3.2c) running the length of each section around each joint containing the polycarbonate sheeting. This additional chamber sealing provided the airtight and watertight seal necessary for verifying that no unmetered air entered or left the chamber during testing. Figure 3.2d shows the entirety of these sealing shown on one of the four main assembly joints.

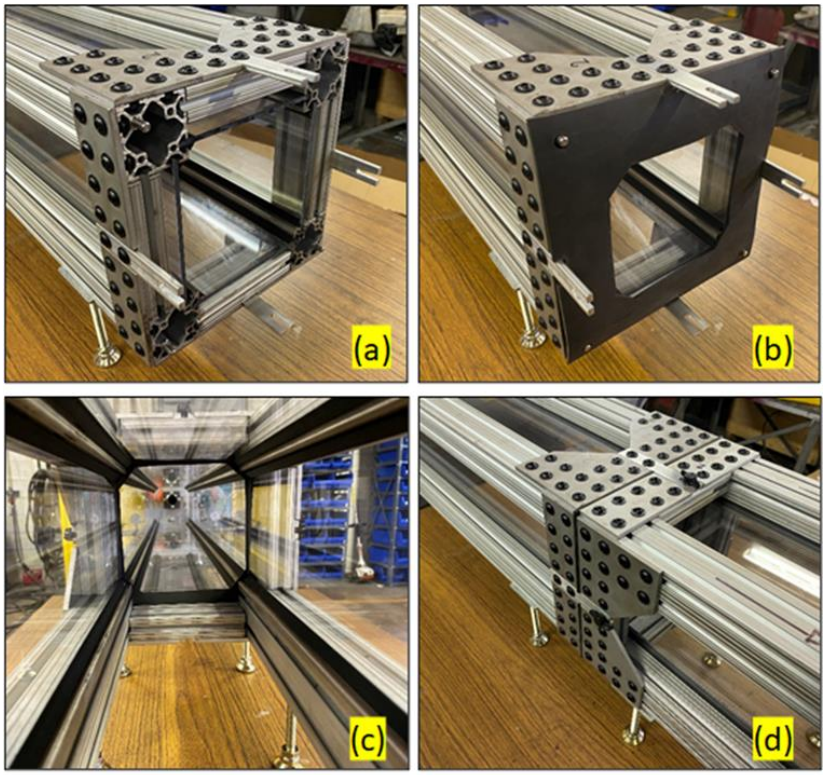

Figure 3.2: Tunnel structure: (a) alignment dowels and bars; (b) inter-chamber neoprene seals; (c) barbed rubber wall-joint seals; (d) chamber sections fully fastened.

3.3. Axial Fan

Tunnel airflow was regulated by a nominal 2,700 cfm portable ventilation fan. The fan was selected to more accurately represent the airflow rates and velocities, in scale, of an industrial flooded bed scrubber. The fan is positioned at the end of the tertiary downward section of the chamber with its output fed into an industrial dust collection system shown in Figure 3.3. The dust collection system ensures that no extraneous dust particles are entering the laboratory work area.

To properly size the exhaust fan for the laboratory-scale unit, the tunnel cross-sectional area was scaled down while maintaining a constant linear air velocity equal to that of a full-scale scrubber unit. The constant air velocity was selected as the scaling parameter, given that velocity dictates particle settling/suspension in the tunnel section. Data from NIOSH shows that typical measured volumetric flow rates in mine scrubbers are approximately 6,300 cfm [1]. Moreover, geometric data provided by Komatsu shows that typical scrubber filters have a cross-sectional area of 1.38 x 1.38 ft, though this value can vary significantly between models. Together, these values suggest that typical air velocities are on the order of 3,308 ft/min. Scaling this air velocity to the 6 x 6 in cross-section of the laboratory tunnel produced a target airflow rate of 827 cfm.

Figure 3.3: Exhaust fan and dust collector assembly.

After selecting and installing the fan, the actual airflow rate in the tunnel was measured using both a manual anemometer and a pitot tube. The results indicate that the airflow rate in the tunnel was slightly exceeding the target velocity of 827 cfm.

3.4. Feeding System

During testing, coal dust particles are injected into the scrubber by an innovative feeding system composed of a volumetric screw feeder and a Trost jet mill, as shown in Figure 3.4. Characterization of the volumetric screw feeder was found to be linear in nature and thus extremely predictable, which in turn enable to independently control dust concentration as an independent variable.

To reduce the size of coal particles and create fresh dust surfaces, a laboratory-scale Trost jet mill (Figure 3.5) was employed. The jet mill employs high-velocity jets of compressed gas to impart energy to particles for size reduction. This device contains no moving parts in the grinding chamber, and the energy for size reduction is solely brought by the carrier gas. The primary grinding action is by particle-particle attrition, and as such, no contamination is introduced during the grinding process. The compressed air, typically 50 to 55-psi, sweeps the original feed particles around the grinding chamber. The particle interactions reduce the size of particles until the particles are fine enough to leave through the centrifugal classifier located in the grinding chamber.

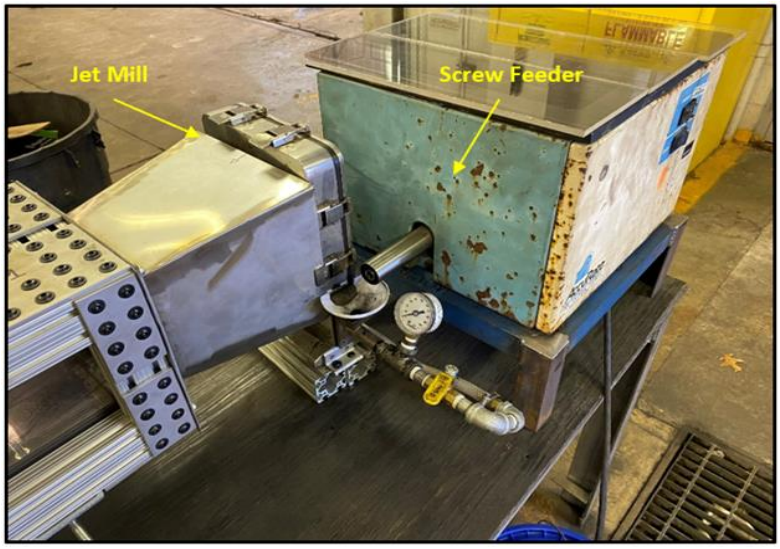

Figure 3.4: Scrubber particulate feed system.

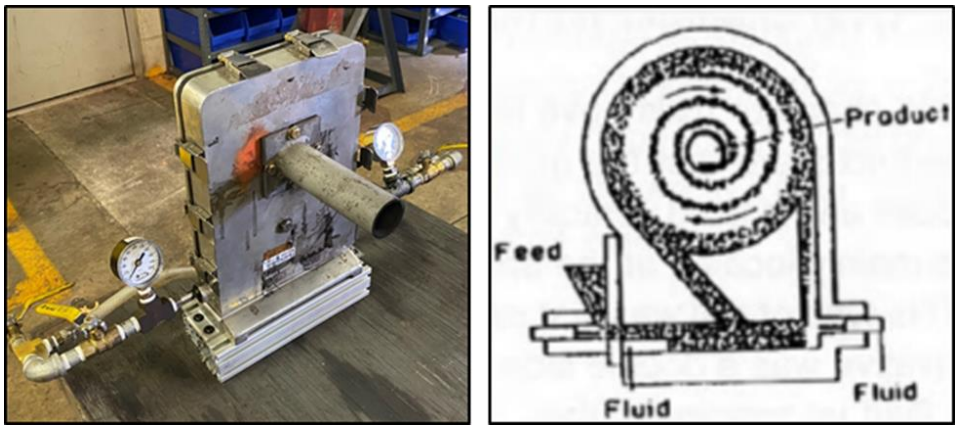

Figure 3.5: Trost jet mill used to feed the scrubber.

The original feed and jet mill product were analyzed for particle size distribution using a Microtrac S3500 laser particle size analyzer. Data from this evaluation are shown in Figure 3.6. Based on the particle size analysis data, the top size of the original feed is approximately 300 microns, with approximately 59% coarser than 20 microns. A further parametric study of the jet mill also indicates it produces particles typically finer than 5 microns when operated at 55 psi jet pressure, and nearly 54% of the product is within the respirable range of below 5 microns. The ash and moisture content of the coal dust feed were determined by content analyses. In the analyzed sample, there is a low moisture content of 1.2% and a dry ash content of 16.2%.

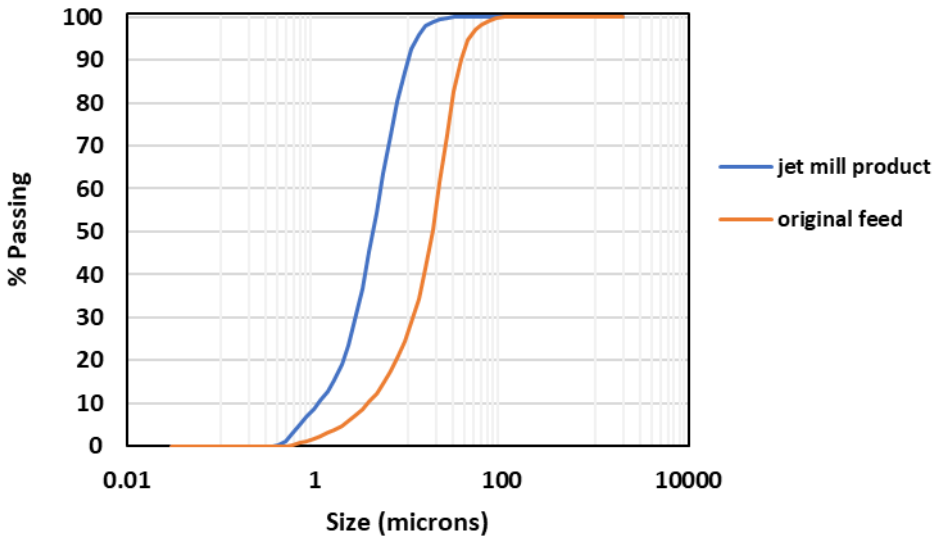

Figure 3.6: Particle size distribution analyses of the original dust sample and jet mill product.

3.5. Sampling System

During testing, dust samples are collected using 37-mm air sampling cassettes preloaded with Teflon filters. The first of the sampling locations, tasked with collecting pre-filtration data, is located within the preliminary upwind section, 0.2-m upstream from the secondary upwind section which contains the filter assembly. The second sampling port, tasked with collecting post-demister data, is located within the downwind section, 0.9-m upstream from the demister assembly. All sampling locations were placed in the long airflow sections to allow for more consistent air particulate mixing from the entrance and filter assembly sections of the scrubber. The mesh screen itself, mesh screen unit blackwater sump and the demister unit blackwater sump were also sampled to further analyze the particle size distribution along the scrubber system and determine overall particle deportment/partitioning. The sampling ports themselves consist of identical long radius 90° bends of 1/8” inner diameter copper tubing that are placed parallel to the incoming airstream at the centerline velocity of the chamber shown in Figure 3.7. Particulate matter capture testing was performed at all sampling locations with the chamber void of the filter and demister assembly

to confirm that the sampling locations were collecting similar amounts of particulate at their respective locations. Air velocity sampling was also performed with the chamber fully dressed to confirm that similar mass flow rates of coal rich air was entering all cassettes to aid in accurately gauging capture efficiency.

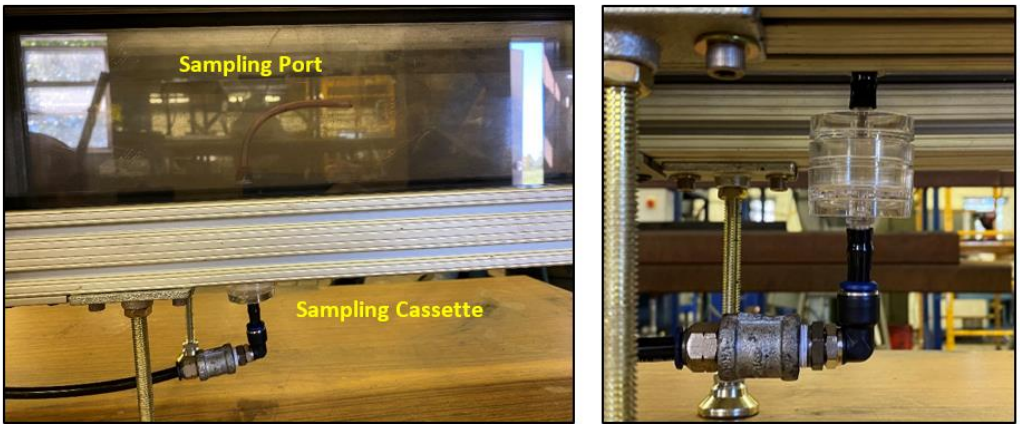

Figure 3.7: Gravimetric sampling system.

3.6. Water Management System

To control the egress of water into the scrubber unit, a system of gate valves along with flowmeter is teed off of the laboratory building's water supply. Mass flow rate and pressure of the incoming water is set up and checked before testing using a timing system and container of specified fluid volume. As with the introduction of air into the system, the amount and pressure of water was also scaled down with a cross-sectional-area scaling factor calculated from the information obtained from an operational scrubber unit.

The nozzle is housed within the preliminary upwards section utilizing a bulkhead fitting and directed towards the middle section of the filter assembly. Due to its higher wettability efficiency a brass 60° spray angle full cone nozzle which is capable of spraying at a rate of 0.25 gpm at 55 psi was employed in the test runs.

A demisting assembly added to the system to create a more accurate representation of a full-size scrubber assembly. An in-house and purpose-built demister assembly (curved vane demister) was designed, 3-D printed, and additively manufactured (Figure 3.8). This unit was then tested and

shown to increase airflow and water collection into the bottom sump that actively pulls excess water from clean charge air while maintaining sufficient flow rates through the chamber.

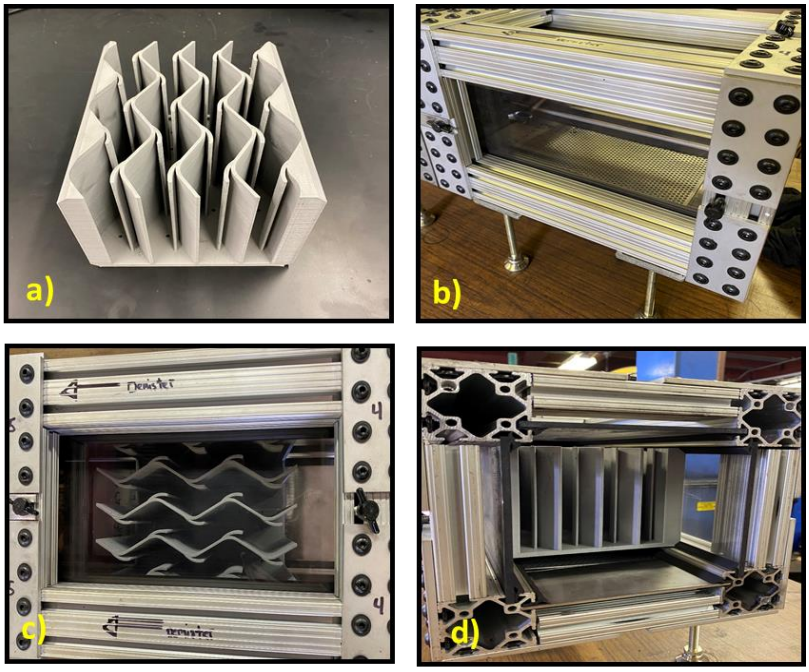

Figure 3.8: Demister assembly: (a) additively manufactured curved-vane demister; (b) bottom of the demister (water collection equipment); (c-d) Top and front view of the shaker assembly.

3.7. Mesh Screen

The filter mesh utilized in the scrubber unit was a small portion of an industrial-grade, steel-woven, scrubber mesh. The panel is approximately 6-mm in thickness and contains 20 layers of wire screen. The wire that the screen is composed of is 0.09-mm in diameter and is evenly spaced at 7 wires per centimeter of the screen. The panel is installed in the filter section of the scrubber, shown in Figure 3.9, at a downward sloping angle of 45° with a face area totaling 0.074 m2. The mesh screen housing includes two additively manufactured parts to hold the screen steady while it shakes including a quick-change stainless-steel mount for the upper part of the screen and a lower mesh mount. The additive parts were also optimized for water collection and mesh sealing (Figure 3.10).

As installed, the filter assembly can be easily interchanged to integrate design modifications (e.g. hydrophobic/hydrophilic treatment, modifications to mesh layering) as dictated by the experimental design.

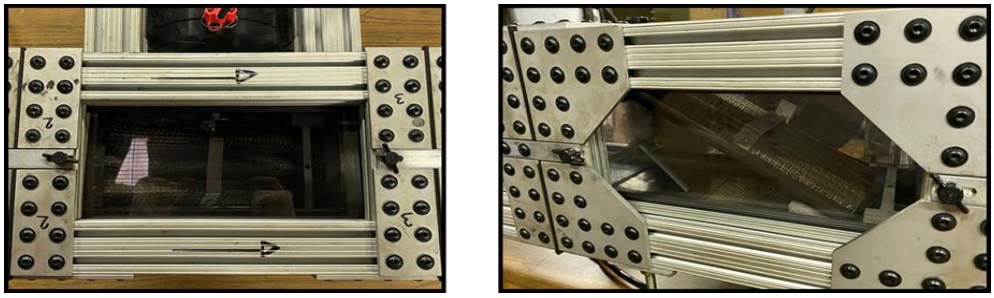

Figure 3.9: Top and longitudinal view of the filter assembly.

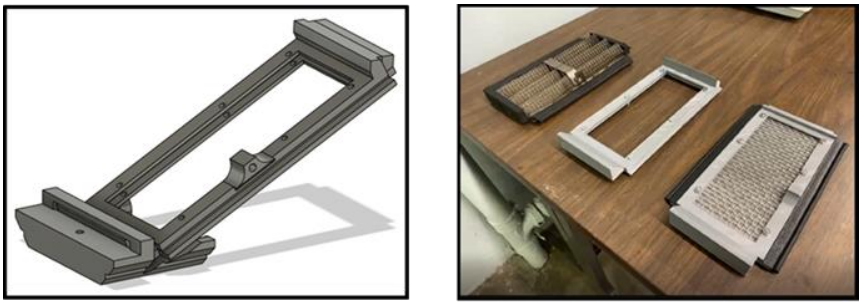

a) b)

Figure 3.10: The mesh frame-adapter assembly a) Illustrated in a CAD drawing, b) Additively manufactured frames

3.8. Vibratory Equipment

An extra unit containing the shaker was designed and mounted to the system in such a way that it can be attached to the mesh screen unit from the side (Figure 3.11). This unit completely protects the shaker from water and coal dust exposure and allows the mesh screen to be connected to the aluminum rod end of the shaker.

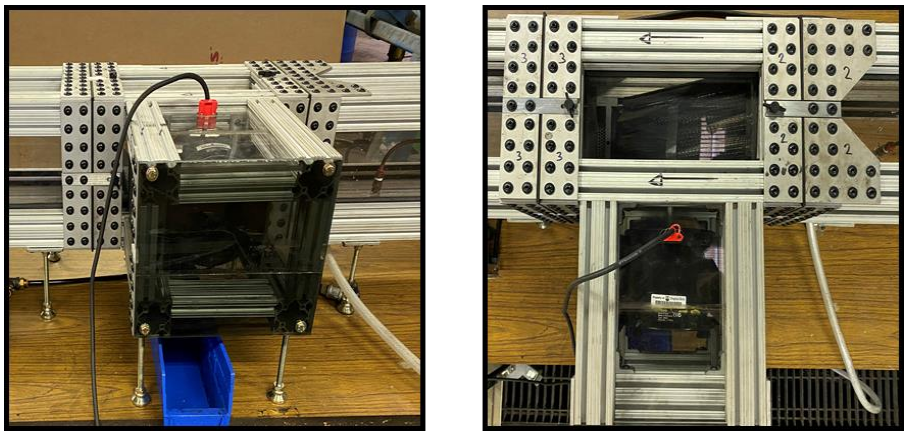

Figure 3.11: Top and longitudinal view of the shaker assembly.

The mesh screen itself was connected to an electromechanical shaker (Brüel and Kjær Type 4809) by an actuating rod and clamping mechanism (Figure 3.12). The square waves were generated by a SDG1000X function waveform generator and applied to the shaker through a Brüel and Kjær Type 2718 power amplifier for base excitation over a range of frequencies. The vibration equipment, as shown in Figure 3.13, are located around the mesh screen section.

Figure 3.12: Clamping mechanism between the shaker's actuator rod and mesh screen.

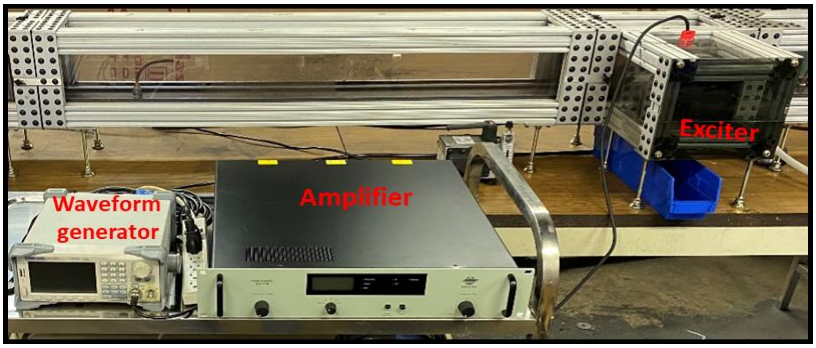

Figure 3.13: Vibration equipment utilized in the test set-up.

3.9. Conclusions

An evaluation of the vibration-enhanced design of a flooded bed dust scrubber was performed using two different test setups, which included a bench-scale system and a full-scale prototype system. The focus of this chapter is on explaining the design and construction stages of the bench-scale system. This system aimed to simulate an industrial scrubber used in continuous miner applications and was configured with various modules to assess operational variables.

This system consists of a tunnel structure made up of 4 detachable ductwork sections, each with a cross-sectional dimension that matches that of the previous one. Among these sections are the upwind section used for dust feeding, the mesh screen unit used for dust removal, the demister unit used for mist elimination, and the post-demister section used for collecting final downwind samples from the unit. The mesh screen housing and the demister housing sections also have grated blackwater sumps, which collect wastewater, which is then used to measure the water flow rates and to provide sampling outlets for the wastewater. Furthermore, the system is also equipped with several notable components, including an innovative dust-feeding system, an air-handling puller fan, a dust collection unit, an assortment of air sampling ports down the length of the tunnel, as well as a shaker assembly mounted on the side of the mesh screen unit.

Parameter tests using this setup and their results are presented in Chapter Four and Chapter Five. As a result of the experiences and lessons learned from this system, the configuration of this system was scaled up in the next part of this study. A wide range of efficiency tests were carried out in

the NIOSH dust gallery in a high-fidelity environment with an industry-scale prototype. Chapter 6 discusses the results of the full-scale prototype tests.

3.10. References

1. Colinet, J., Reed, W. R., & Potts, J. D. (2013). Impact on respirable dust levels when operating a flooded-bed scrubber in 20-foot cuts. Pittsburgh, PA Spokane, WA

Chapter 4

4. An Exploratory Investigation on the Effectiveness of a Novel Vibration-Enhanced Flooded Bed Dust Scrubber

This chapter was submitted for publication in the international peer-reviewed journal Mining& Metallurgy and Exploration. Citation details are provided below:

Uluer, M.E., Shigo, M., Amini, S. H., Noble, A., (under review). "An Exploratory Investigation on the Effectiveness of a Novel Vibration-Enhanced Flooded Bed Dust Scrubber", Mining& Metallurgy and Exploration.

(ABSTRACT)

Airborne coal mine dust is an unintended and unavoidable result of coal extraction operations that raises notable health and safety concerns. Modern mining techniques utilize several dust mitigation strategies, and the flooded-bed dust scrubber (FBS) is one such technology used extensively on continuous miners. The conventional static panel filter, instrumental in most scrubber designs, is fundamentally limited in collection efficiencies due to a high clogging rate and a tradeoff between mesh density and airflow rate. To overcome these deficiencies, a novel vibrating mesh panel is proposed. In this study, a laboratory-scale dust scrubber unit was used to investigate the efficacy of concept as compared to that of a static mesh. A statistical design of experiments study was first used to determine the effective vibrational parameters and scrubber operational parameters on dust collection and clogging mitigation. Optimized results from this study were then evaluated against those of a static mesh to determine performance improvement while investigate the mechanisms controlling dust collection and particle department through the scrubber system. Results show that the vibrating mesh conditions and higher water flow rates led to an improvement in the cleaning efficiency of the scrubber system. Compares to a static-mesh to FBS, the vibrating-mesh FBS

showed a significant reduction in pressure drop across the mesh screen indicating lower air loss through the test duration. Overall, the findings confirm that vibrating mesh conditions have the ability to improve filter clogging issues while maintaining high collection efficiencies. This research supports further technological advancement in mine dust mitigation technologies.

4.1. Introduction

4.1.1. Background

While modern mining techniques have drastically reduced the frequency and severity of health and safety concerns, dust production remains a significant challenge. Prolonged exposure to airborne respirable coal dust can cause permanent disability and deathly illnesses for coal workers such as pneumoconiosis, silicosis, emphysema, and chronic bronchitis, collectively known as black lung [1,2]. According to the National Institute for Occupational Safety and Health (NIOSH), coal workers' pneumoconiosis (CWP) has caused the deaths of more than 75,000 miners between 1970 and 2016 [3], and recent data has shown an increased prevalence of CWP since the late 1990s [4-7]. In addition, coal dust, if allowed to progress through the mining environment, can trigger catastrophic secondary explosions that can result in significant damage to life and property [8]. Given these issues, a new dust standard developed by the Mine Safety and Health Administration (MSHA), was fully implemented on August 1, 2016, and required the dust level at the working face to maintain levels below 1.5 mg/m3 with intake entries remaining below 0.5 mg/m3 [9]. While underground dust prevention and mitigation have been areas of inquiry for several decades, these new regulations have prompted new attention to the area, particularly with respect to new technology development.

Modern mining techniques utilize several complimentary approaches for dust control and mitigation, with the ventilation system itself being a major component [10]. Additional systems include cutter-mounted sprays and dust scrubbers, and over the past several decades researchers have investigated thee and other techniques for improved dust prevention and mitigation [11-16]. For continuous miners in underground coal mines, the flooded bed scrubber (FBS) is a widely

adopted technology that has been commercially deployed for several decades [17-19]. This technology, which is installed onto the continuous mining machine, provides a cleaning action by pulling in dirty air near the cutter head, moving the dust in scrubber, and discharging clean air at the rear of the machine. Dust removal is facilitated by a mesh screen that is continuously sprayed with water. As dusty air flows through the screen, water droplets adhere to the dust particles, and a downstream mist eliminator collects the dust-water agglomerates into a blackwater sump. Airflow is facilitated by an exhaust fan positioned at the discharge of the unit [20]. Figure 4.1 shows a cartoon depiction of an FBS and its constituent components.

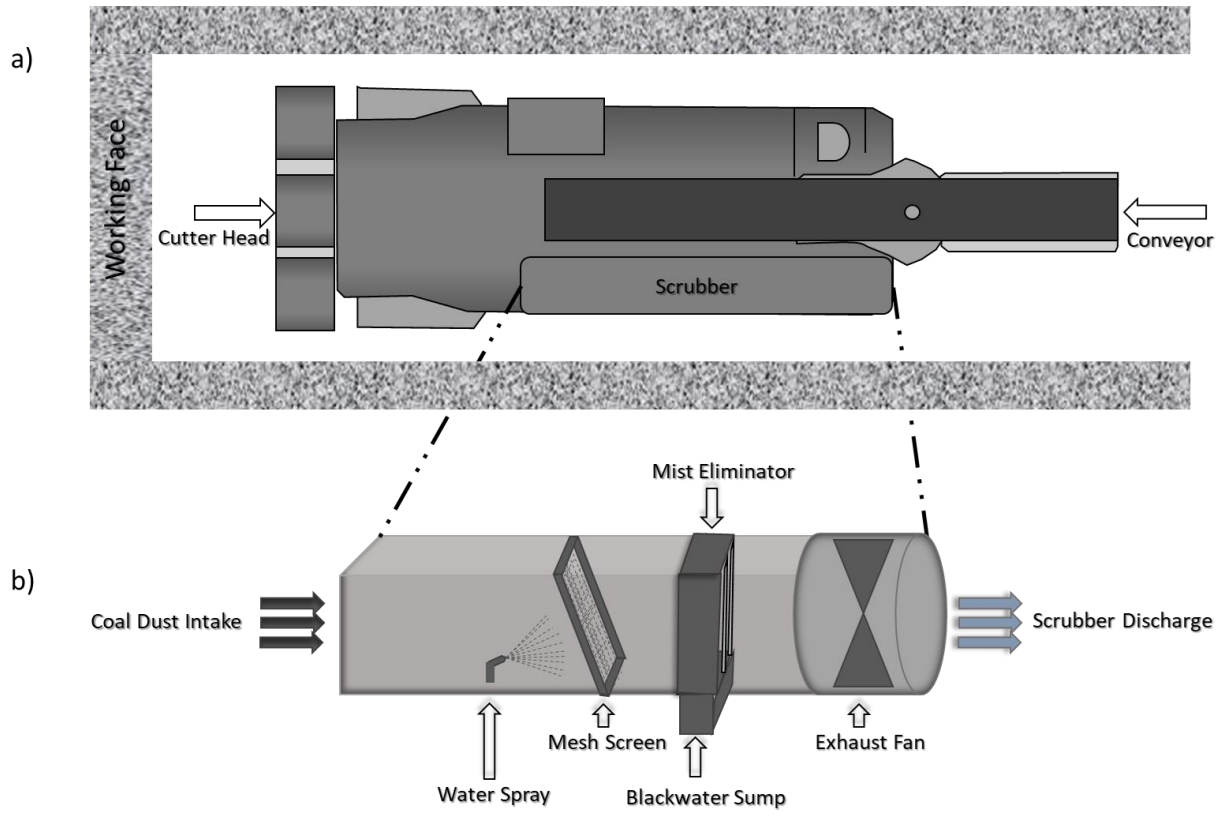

Figure 4.1: a) Continuous Miner Top View b) Flooded Bed Scrubber Side View

Despite the ubiquitous utilization of FBSs in continuous mining applications, numerous technical challenges limit their performance and efficiency. Fundamentally, FBS units exhibit a tradeoff between air flow and mesh density. Higher mesh densities can collect a higher portion of particles

that enter the scrubber; however, they also yield a higher pressure drop, which reduces the total volume of air that can be cleaned through the scrubber. Lower scrubber air flow rates cause more dirty air to bypass the scrubber, thus reducing overall system performance. For high mesh densities, this issue is exacerbated, as they have a higher tendency to clog during the cutting cycle, thus further increasing pressure drop and reducing air flow rate. At the other extreme, lower density meshes have the potential to maintain high air flow rates; however, the dust capture within the scrubber is reduced. These interactions have been well studied in real operational conditions [19].

To maintain suitable performance levels, the mesh screen is periodically removed from the scrubber and thoroughly cleaned by the operator. While cleaning practices and techniques vary, the frequency of cleaning has been studied and assessed. While previous recommendations required the filter to be cleaned after each 40-foot advance [21], a recent study showed that the reduction in the scrubber airflow can reach up to 35% after a 20 ft advance. Thus, NIOSH highly recommends cleaning the filter after each 20-foot [22]. In either case, the overall system performance deteriorates through the cutting process [23], and operational downtime caused by the cleaning process slows the production rate.

Recent efforts have sought to improve the FBS performance by directly addressing the challenges described above. In a recent study, a vortecone non-clogging wet filter, first developed by Salazar et al. and widely used in the automobile industry as an over-sprayed vehicle paint particle collector [24], was employed to replace the dust collection unit within the FBS. This system has a high collection efficiency of coal dust. While it was found to improve the system efficiency, it was also increasing the pressure drop to undesirable values. Later modifications were made to the structure of this system to minimize resistance to enable it to be used at much higher airflows [25]. It also requires significant modifications to the main structure of the FBS [26-28].

In a separate study, researchers proposed an impingement-type filter with large slits on three separate metallic surfaces mounted in series. While the first and third screens are identical, the second screen slits are displaced laterally by 6.0 mm in the screen plane to prevent the straight flow. With this configuration, dust particles impact the metallic surfaces and are subsequently captured [29]. Furthermore, the solid impermeable surface of the filter helps distribute water more evenly on the surface. Due to the filter surface being the dust-capturing element and water being

the surface-cleansing agent, the system requires a minimum amount of water inflow to keep the surface wet. Laboratory tests, however, showed that the filter can remain in unclogged state for extended periods.

4.1.2. Vibration-Enhanced Scrubbers

Enhanced particle filtering by vibrating filter media has been long recognized as an alternative approach and has been deployed in many industrial applications, including size classification, filtering, and dust collection/removal [30-32]. Vibration can be used to improve the efficiency of fibrous filters [33,34], and applying vibration directly to the filter element area can also reduce clogging problems with membrane filters [35,41]. In a separate application, researchers studied the effects of ultrasonic vibrations propagating through gaseous media in a natural gas filtration process [42,43]. As a result of ultrasonic agglomeration, particles coalescence was amplified, and the larger agglomerates were more easily trapped by the filter element. Lastly, the ultrasonic shaking can mitigate the clogging phenomenon during operation without removing the filter [44].

Through a computational study, Lu et al. examined and evaluated the use of vibrating filter meshes in FBS applications. Several two- and three phase computational fluid dynamic (CFD) simulations were used to evaluate the interaction of airflow, coal particulate matter, and water droplets in both vibrating and static mesh scenarios. In particular, the vibration conditions were studied in relation to dust particle-mesh interaction and mesh wetting. The results showed that a dynamic mesh screen can significantly improve dust capture on the screen surface, while also increasing the wetted area, thereby improving screening efficiency. As a result, the study showed that the vibrating mesh can provide an equivalent particle-mesh interaction level to the static mesh with a larger aperture [45].

To implement the vibrating mesh in an operational setting, one may exploit the natural vibrations on the continuous miner through an energy harvesting approach. Experimental and numerical studies conducted with continuous miners have shown that large vibrations occur immediately after the machine is operated, forming even before it comes into contact with coal and persisting throughout the operation [46-49]. Most vibration is caused by the motor gearbox, the dust collection unit exhaust fan, the conveyor system, the cutter head/cutting arm, and the machine's interaction with dynamic forces during the cutting cycle [50-53].

Even though very few studies have examined the vibrational energy of continuous miners, a technical report provided by Fuchs (1979) provides detailed raw vibrational characteristics of underground mining equipment including different types of continuous miners. Digitizing and analyzing the raw data produced demonstrable acceleration levels within the range of frequencies up to 5 kHz at the nearest locations to the filter. On the basis of Fuchs (1979) report, Figure 4.2 illustrates the overall average and variation of acceleration levels for the different types of continuous miners under all operating conditions. It is evident from the graph that peak acceleration levels occur around 100 Hz [46].

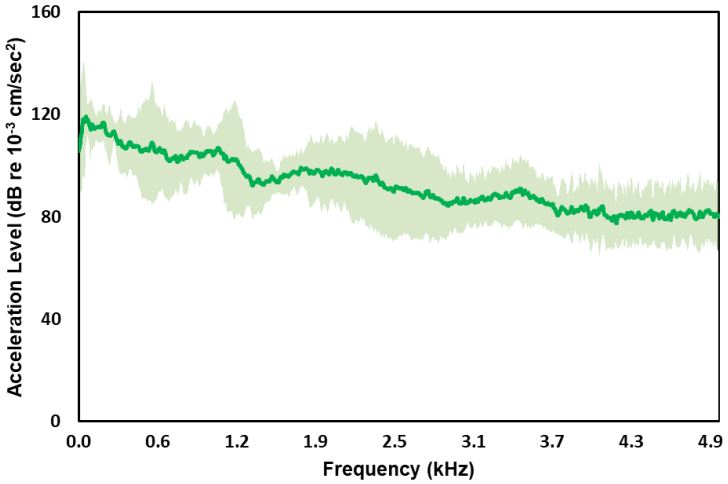

Figure 4.2: Vibration acceleration levels for four continuous miners at various working positions and operating conditions

Augmenting this direct observation of machine vibration, other researchers have investigated the sound power levels of the various surfaces of the continuous miner and determined that the most significant noise-radiating surfaces occur at the tail section. Experimental data shows that more than 80% of sound energy near the conveyor system that is located at the center of the continuous miner is emitted at frequencies between 500 and 2500 Hz [47-50]. In a separate study, a continuous miner cutting arm was also examined for its vibration characteristics and dynamic loads in separate studies. It was found that the vibration amplitude at the engine location was greater than at other locations on the cutting arm. According to the results, higher vibration amplitudes usually occur between 1-100 Hz [52, 54].

Altogether, these studies show that continuous mining equipment produces notable vibration energies in specific frequency ranges that may be exploited for improved dust capture. Through an energy harvesting approach, natural vibrations can be translated into an optimal frequency and amplitude range most appropriate for dust particle capture and minimal particle clogging [55]. By using specific spring configurations, these output vibrations can then be transmitted to the mesh screen. This concept is being more thoroughly explored in a separate communication [56].

4.1.3. Objectives

While several studies have shown that vibrating filter meshes have the potential to improve FBS performance though increased particle capture and reduced clogging, this technique has not been experimentally validated and compared against the performance of static mesh panels in laboratory or operational conditions. As such, the objective of this study is to provide a rigorous comparison based on extensive testing of a laboratory-scale FBS. In addition, the study will evaluate the influence of various vibrational and operational parameters through a statistical design of experiments test program. Optimal results will be directly compared to tests using static panels to determine the level of improvement with respect to both dust capture and clogging mitigation. This study is one of several explaining the technical development, scale-up, and testing of the vibration-enhanced FBS systems [45, 56].

4.2. Theory

Based on the challenges defined in the section 4.1.1, the overall goal of the study in this chapter is to design, develop, and test a working prototype of an improved flooded bed dust scrubber that can simultaneously increase dust capture and mitigate clogging potential. In a prior proof-of-concept study, Noble et al. investigated this concept and found that the addition of a vibrating mesh panel could improve dust collection efficiency over that of a static unit [57]. Given those findings, the current study sought to continue the technology maturation to next level through the detailed design and testing of an improved bench-scale prototype scrubber unit. Fundamentally, a

vibrating mesh screen has the capacity to capture more particles by creating a larger effective surface area, thus encouraging a greater number of water-particle interactions. Figure 4.3 shows this phenomenon as a simplified cartoon.

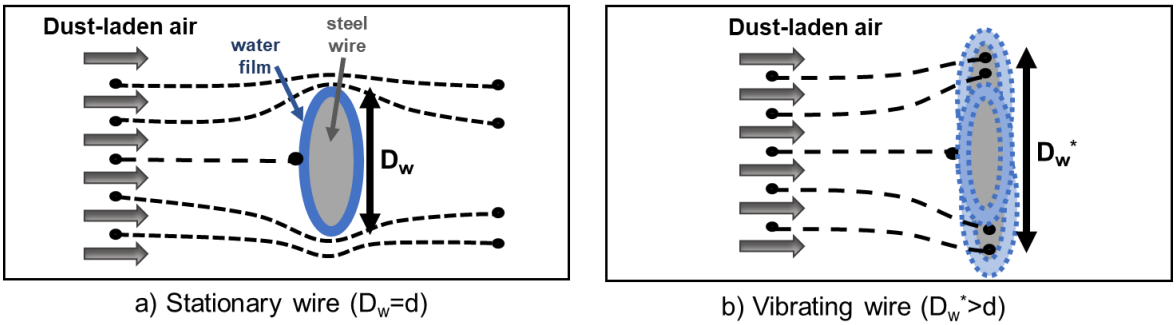

Figure 4.3: Particle-capture mechanisms of a mesh screen

The proposed design is mainly vibrating the screen to improve the filtering performance. The attractive Van der Waals force between the mesh and particles is an order of magnitude weaker than the force between the liquid interface and dust particles. Therefore, if some regions in the filter do not have moisture or liquid interfaces, the dust particles more likely slide through the mesh. When a sufficient amount of surface velocity is produced with the help of external excitation, the water spreads out the surface area better than a static mesh condition. Therefore, the investigated vibration-enhanced liquid interface modification is able to uniformly wet the filter panel. Despite many particles passing around the stationary mesh as seen in stationary wire, the vibrating mesh is able to capture a significant portion of dust laden air. This is because of the expanded surface created by vibrational movement. This will ensure that the surface is wetted to the greatest extent possible. Consequently, dust particles will have a better chance of being captured by water droplets as they pass through the filter. Eventually, this vibrational movement will increase adhesion between dust particles and liquid interfaces and improve dust particle amount trapped by water droplets.

4.2.1. The Impacts of Vibration on Surface Wettability

In practical applications, external fields, such as vibration, temperature, force, and electricity, inevitably affect the wetting characteristics of the filter surface. Researchers have shown that vibrations can overcome the energy barrier required to transition from Wenzel to Cassie states, which eventually expedites shedding coal dust water mixtures by periodically separating the particles from the interface and pulling them through the demister with the help of airflow [58]. Ku et al. found that when applied, vibration can change the surface's energy by changing its wettability [59]. Alternatively, Wang et al. studied the effects of vibration fields on the wetting behavior of droplets on the surface. By applying vibration fields to different surfaces, he developed a prediction model for the wetting process in vibration [60]. They derived a fundamental equation using Newton's second law:

$$(V_f - V_i)m/\tau = F_{C-D} \quad (1)$$

where m, τ is the mass of the droplet and the time interval from V_i (the initial velocity of the droplet) to V_f (the final velocity of the droplet), respectively. $F_{C\text{-}D}$ is the interaction force between surface and droplet. Wang et al. (2021) also rearranged Eq. (1) to find the acceleration of droplet (a_f) as:

$$a_f = -\frac{\tau \partial^2 z[E_{C-D}(r)]}{m \partial z(r) \partial z(t)} \quad (2)$$

where $E_{C\text{-}D}$ (r) the interaction energy between liquid and surface. Based on this mathematical model, the researchers concluded that the interaction between liquid droplets and the surface is positively correlated with their amplitude, vibration frequency, and contact area. As has been demonstrated, vibration can modify the surface-wetting characteristics of surfaces. Additionally, different vibration amplitudes could be used to adjust the surface wettability. The vibration field can improve the hydrophobicity of the surface of the filter and thereby facilitate the removal of coal dust, so this study adopted a similar approach to promote the wettability of the filter surface.

4.2.2. Effect of Vibration on Particle-Laden Drop Drainage

Dr. Jung's group, as reported in [61], investigated the effect of vibration on the drainage of a particle-laden drop from a mesh in a controlled laboratory environment. Tests were conducted

throughout the proof-of-concept testing campaign to examine the effect of vibration on particle-laden drop drainage rate at three different frequencies: 50 Hz, 100 Hz, and 150 Hz. It was found that in all cases, drop sliding speed increased as vibration frequency increased. In addition, they stated that when particle-laden drops are still sticky under low-frequency vibration, higher vibration frequencies increase the likelihood that they will slide due to higher inertia forces. For instance, Figure 4.4 illustrates how a particle-laden drop does not slide on a bare surface when vibrated at 100 Hz, but does slide at 150 Hz.

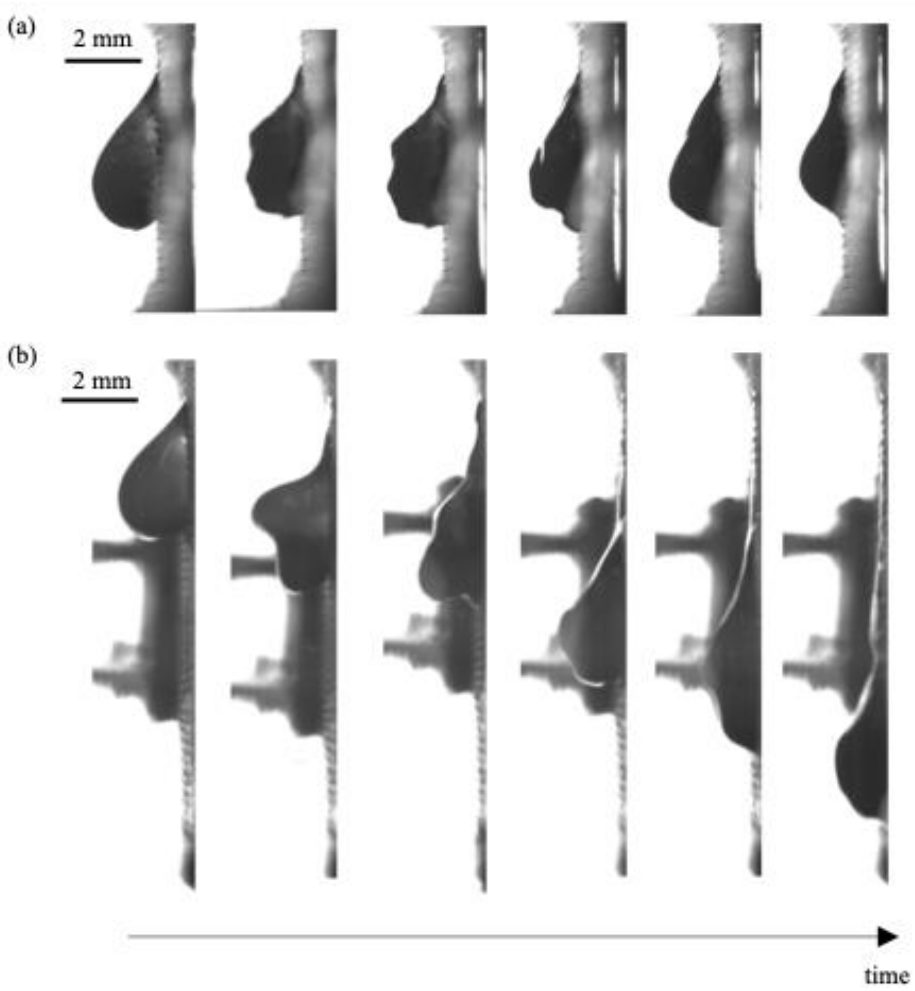

Figure 4.4: Snapshots of the time evolution of a 20 μL drop mix on surface at (a) 100 Hz, (b) 150 Hz vibration [61]

Based on their experimental findings, an optimal combination of parameters can be defined that leads to the highest particle collection rate. These parameters can ensure maximized particle collection while avoiding clogging. These findings were leveraged in the present work by establishing the optimal range of vibrational frequencies for testing. Specifically, their work showed that 150 Hz was superior to establish the best balance for wettability of the surface, and as such a similar frequency was selected for the initial FBS tests described in this chapter.

4.2.3. Vibration Efficiency Analysis

To investigate the geometric and vibrational system parameters and construct a theoretical baseline of the bench-scale testing campaigns in the context of this study, Janjua et al. (under review) performed computational fluid dynamics (CFD) simulations [56]. Figure 4.5 shows the efficiency of dust collection over the mesh screen at the end of the simulation. Based on the number of dust particles captured ($N_{captured}$) on the filter surface and the number of dust particles released into the domain per unit time ($N_{released}$), they calculated system efficiency as follows:

$$\mu = N_{captured}/N_{released}$$

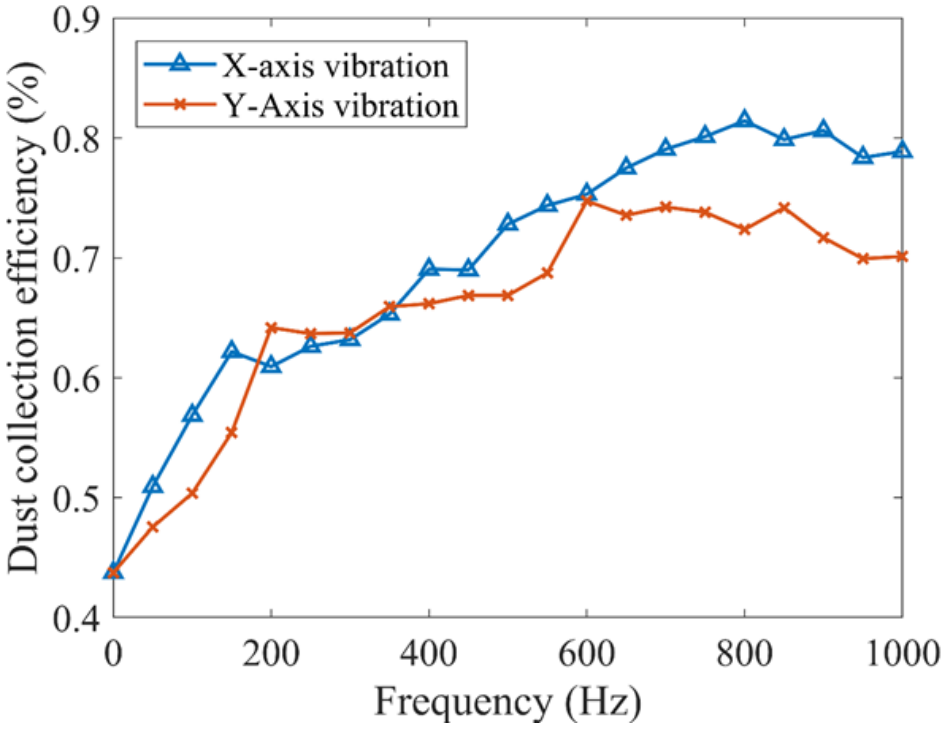

Figure 4.5: Vibration frequency-dependent dust collection [56]

The dust removal mechanism is determined by two key factors in the flooded-bed scrubber as described earlier. Firstly, the mesh screen needs to be wet so dust particles are caught by water droplets on its surface. The second factor is how strong the interaction is between dust particles and the filter surface, i.e., how likely it is that dust particles will come into contact with droplets.

One of the aims of their study was to examine numerically whether exciting the mesh panel with vibrations would improve both particle-droplet and particle-mesh interactions, thus improving dust collection efficiency. By introducing a vibrating mesh screen to the simulation, the researchers tested its efficiency at frequencies between 0 Hz and 1000 Hz in both the X and Y directions. Figure 4.6 shows how dust particles interact with meshes in a dust-laden flow simulation.

Simulation results are consistent with the original hypothesis. They found that even at 50 Hz, vibration in the X-direction increases the dust collection efficiency of the system. Their results also showed an increase in dust collection efficiency with increasing vibration frequency. Y-direction vibrations followed a similar trend but with a weaker response in collection efficiency. These observations led this study to keep the vibrational frequency range in small as dust collection

efficiency was predicted to be greater within low frequency range. They also found that the overall impact of vibrations was stronger when it was excited in X-direction. Their findings further supported the technique of the external shaker that provides one-way stimulation (X-direction) to the filter that was used in the present work by showing the dust collection was slightly more significant for vibration in the X-direction compared to the Y-direction for most frequencies.

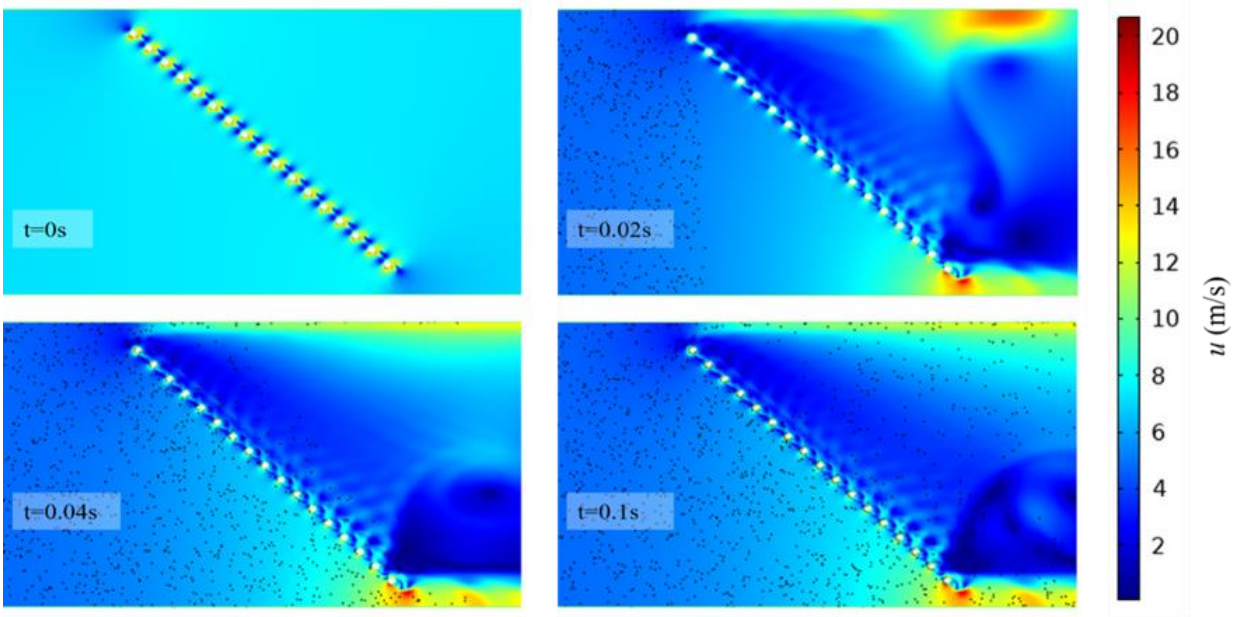

Figure 4.6: The velocity contour of the dust-laden flow [56]

4.2.4. The Effect of Spray Water on Filter Clogging

During the initial proof-of-concept tests in the wind tunnel, coal dust collected on the mesh. The experimental study results clearly demonstrate the driving mechanisms that influence scrubber performance and ultimately lead to better filter designs based on sound scientific principles. The collected dust volume strongly depends on its operation time. In the proof-of-concept testing, it was found out that the majority portion of the front side of the lab-scale mesh is significantly clogged after 10~15 minutes of operation. Obviously, the clogged mesh would block significant amount of air flow and further decrease the dust collection efficiency. This clogged matter is composed of dust particles and sprayed liquids, which becomes very viscous. It is known that the

particle-fluid mixture increases its viscosity nonlinearly depending on the particle density. A few such models relating the effective viscosity to the packing fraction, ϕ, are listed as follows:

$$\frac{\mu}{\mu f} = \left(\frac{9}{8}\right)\left(\frac{\phi}{\phi_m}\right)^{\frac{1}{3}} / \left(1 - \frac{\phi}{\phi_m}\right)^{\frac{1}{3}}$$ (Frankel & Acrivos,1967 [62]

$$\frac{\mu}{\mu f} = \left(1 - \frac{\phi}{\phi_m}\right) - \phi_m$$ (Krieger & Dougherty,1959) [63]

All these models predict that the viscosity of the clogged liquid increases nonlinearly (almost exponentially) with its particle packing fraction as it gets close to the random packing fraction (ϕ_m ~ 0.64). Therefore, different water flow rates were investigated in the present work to find the optimal spray amount that would provide sufficient liquid into the filter surface to avoid reaching to its critical particle concentration being extremely viscous.

4.3. Materials and Methods

The experimental data from the prior proof-of-concept shakedown tests confirmed the hypothesis and show that, when operated under optimal conditions, liquid-coated vibrating meshes can increase the dust capture performance of a flooded-bed dust scrubber. While the proof-of-concept technology showed promise, further laboratory testing was needed to validate and optimize the technical performance under different operational conditions. During this study, the proof-of-concept unit was refurbished, and further testing was conducted to fully demonstrate the distinct capabilities of liquid-coated vibrating mesh filters in reducing the mesh filter clogging and enhancing dust collection efficiency. To adequately simulate the mining environment, the level of dust concentration within the dust-laden air, the flow rate and pressure of water sprays, and the range of air flow rates in the prototype were adjusted according to the typical ranges for these

parameters in the operating (in-mine) conditions. The main objective of this chapter is to identify the optimal frequency and amplitude of the mesh panel, and to determine the optimal design of a water management system and scrubber mesh at which the minimum clogging and maximum collection efficiency can be achieved.

4.3.1. Testing Setup

A bench-scale FBS was designed and constructed to model the form and function of an industrial scrubber used on continuous miner applications. Figure 4.7 shows the bench-scale scrubber unit used in this study and identifies many of the constituent components and sampling points. The system was configured with several independent modules to provide a platform for evaluating several operational system variables, including dust concentration, dust size, dust material type, mesh design, mesh vibrational amplitude, mesh vibrational frequency, water flow rate, water nozzle type, and tunnel dimensions. Note that not all variables were assessed in this study; however, the system was designed with maximum flexibility in mind.

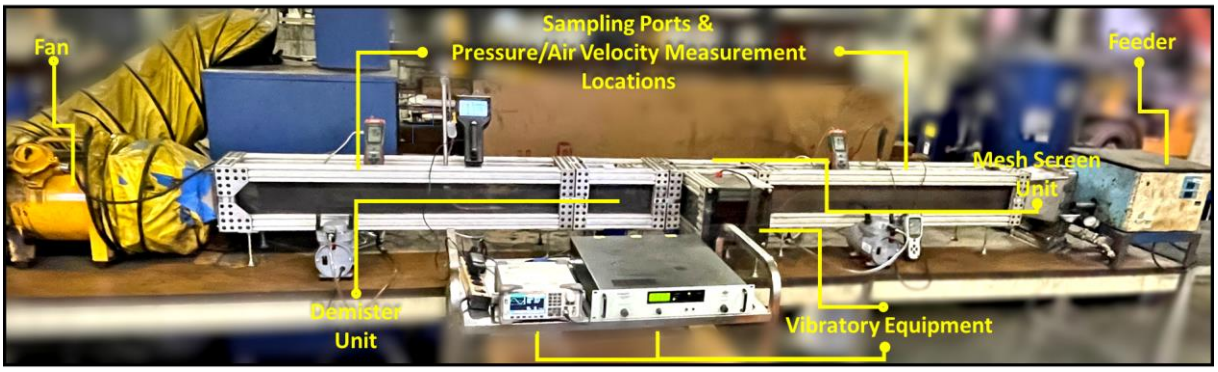

Figure 4.7: Bench-scale scrubber system

The overall tunnel structure consists of four detachable ductwork sections with each having a matching cross-sectional dimension of 0.152 m x 0.152 m. These detachable units include: (1) the upwind section where the coal dust is fed into the system and from where the pre-mesh screen samples are collected, (2) the mesh screen unit, (3) the demister unit, and (4) the post-demister

section where final downwind samples are collected. To ensure that no unmeasured air or water entered or left the chamber, polyurethane sealers were used between sections.

Tunnel airflow is regulated by a nominal 2,700 cfm portable ventilation fan. To properly size the exhaust fan for the laboratory-scale unit, the tunnel cross-sectional area was scaled down while maintaining a constant linear air velocity equal to that of a full-scale scrubber unit. The constant air velocity was selected as the scaling parameter, given that velocity dictates particle settling/suspension in the tunnel section. Data from NIOSH shows that typical measured volumetric flow rates in mine scrubbers are approximately 6,300 cfm [22]. Combining this data with typical mesh scrubber geometries suggests that the typical air velocities in industrial scrubbers are on the order of 3,300 ft/min. Scaling this air velocity to the cross-section of the laboratory tunnel produced a target airflow rate of 827 cfm.

The scrubber unit utilized a portion of a standard 20-layer steel-woven mesh filter used in industrial FBS units. The filter panel is installed at a downward angle of 45° in the scrubber's filter section. A custom-built demister assembly (curved vane demister) was designed and additively manufactured for the bench scale unit. With the help of an actuating rod and clamping mechanism, an offset unit containing the electromechanical shaker was mounted directly to the mesh screen (Figure 4.8). Electromechanical shaker vibrates the mesh screen perpendicularly to the airflow in the chamber.

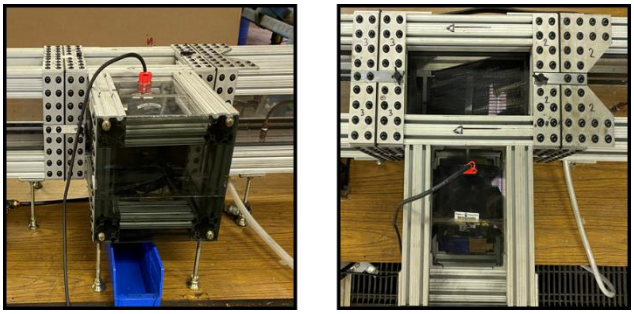

Figure 4.8: Side and top view of the shaker assembly

Dust is introduced to the system using the combination of a volumetric screw feeder and a Trost jet mill. These two units provide independent control of dust size and dust concentration and

ensure that the dust introduced to the scrubber has fresh surfaces, as would be the case in an operating FBS. Feed to the jet mill consisted of Keystone Black material obtained from Keystone Filler & Mfg. Co. with a low inherent moisture content of 1.4% ± 0.10% with a dry ash content of 14.6% ± 0.04%, and the jet mill was configured to produce feed dust that was 95% passing 10 microns and approximately 50% passing 5 mm microns. Figure 4.9 shows the particle size analysis of the jet mill feed and product as determined by a Microtrac S3500 laser particle size analyzer. As shown, the top size of the original feed is approximately 300 microns, with approximately 59% coarser than 20 microns, while the product matches the specifications mentioned above. The ash and moisture content of the coal dust feed were determined (by thermogravimetric analysis) to be 16.2% and 1.2%, respectively.

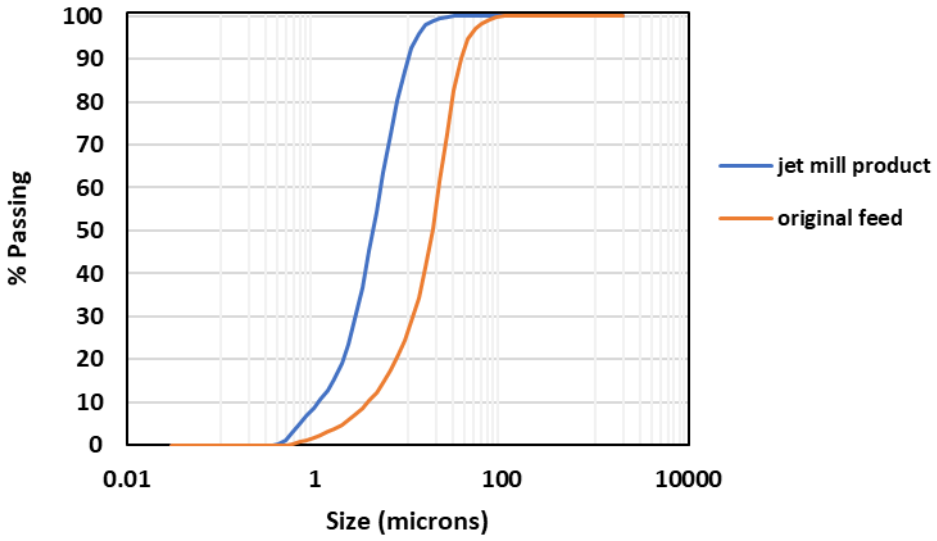

Figure 4.9: Particle size distribution analyses of the original dust sample and jet mill product

During testing, dust samples are collected from sampling ports located upwind of the scrubber's filter section and downwind of the demister section using linear IAQ sampling pumps and 37-mm air sampling cassettes preloaded with Teflon (PTFE) filters.

4.3.2. Experimental Design

Response surface methodology (RSM) was used in this study to empirically quantify the correlation between multiple independent variables and a response variable. Response surface designs are advanced design of experiments (DOE) methods used to study and optimize responses. For this study, a 3-factor Box-Behnken design (BBD) was employed. In this approach, each independent variable (factor) is distributed evenly across three values, symbolically represented as −1, 0, +1. For a BBD, the required number of experiments is, N=2*k*(k-1)+C where k is the number of variables and C is the number of central points.

For this study, vibrational amplitude (amplifier gain), vibrational frequency, and water flowrate were selected as the experimental parameters to be included in the experimental design. Based on the initial findings of the fundamental vibrational analysis (See Section 3.1), the vibrational energy of the system was found to be most prominent between 10 and 200 Hz. Additionally, the modal analysis indicated 133.84 Hz and 58.67 Hz as the natural frequencies of different modes of the mesh screen used in the test. As such, these values were chosen to define the range of low, medium, and high vibrational frequency values used in the test. Likewise, the amplifier gain values were determined to be 40 dB (high, +1), 30 dB (mid, 0), and 20 dB (low, -1). Lastly, based on the data obtained from a scrubber in operation, the water flow rate was scaled down by using the cross-sectional-area scaling factor. The scaled-down value is used as a medium value in the experimental design. To evaluate the effect of water flow rate on the system efficiency, the highest flow rate was set at 3 l/min, the midpoint was set at 2 l/min, and a 1 l/min flow rate was set as the lowest flow rate. Table 4.1 summarizes the factors and levels associated with the independent variables. Similarly, Table 4.2 shows the experimental parameters that were held constant through all tests.

Table 4.1: Experimental factors and range values for bench-scale scrubber tests

Factors	**Level**		
	Low (-1)	**Medium (0)**	**High (+1)**
Water flow rate (l/min)	1	2	3

Amplifier gain (dB)	20	30	40
Frequency (Hz)	58.67	96.26	133.84

Table 4.2: Fixed operating parameters for each trial

Property	**Value**
Dust feed rate	22.7 g/min
Respirable dust concentration in feed	2.7 g/m^3
Downwind airflow velocity	10 m/s
Sampling method	Gravimetric Sampling
Sampling duration	5 min
Sampling pump flow rate	5 l/min
Jet mill pressure	55 psi
Signal generator gain	20 Vpp

4.3.3. Laboratory Test Procedures

Before each trial, various portions of the system, including the mesh screen, demister, sampling ports, and black water sumps, were thoroughly cleaned with compressed air to ensure experimental integrity, and maintain a consistent airflow rate. In order to determine the dust mass differential collected in the specified time interval, sampling cassettes with the appropriate filters were weighed before and after each test. All experiments were conducted with the same cleaning procedure in order to compare the efficiency of all operational modes effectively. During testing, the fan, water spray, vibrational unit, dust feeder and jet mill were individually started in a

sequential manner. After a fixed operation time, samples were taken and subsequently analyzed. Given the system factors, gravimetric measurement is considered to be the most reliable and least likely to lead to bias. For reliable quantification of gravimetric filters, and for reducing the impact of weighing error, a minimum mass accumulation in the downwind cassette of 1 mg is required. As such, the following was used to calculate the time required for accumulating enough mass in the downwind sampling cassette for analysis:

$$t = m/[Qpump * Cfeed * (1 - \eta)]$$

where m is the mass accumulation in downwind sampling cassette, $Qpump$ is the sampling pump flow rate, $Cfeed$ is dust feeding concentration, η is the scrubber efficiency.

Gravimetric samples collected during these tests were used to determine the dust collection efficiency:

$$Collection\ Efficiency\ (\%) = \left(1 - \frac{weight\ of\ downwind\ sample}{weight\ of\ upwind\ \ sample}\right) * 100$$

After collecting samples, the coal dust particles were scraped from the Teflon filters. A Microtrac particle size analyzer were used to determine the particle size distribution of each sampling cassette.

It was also necessary to determine the particle size distribution of the mass accumulated on the cassettes, mesh screen and black water sumps underneath the system in different operational modes to identify overall system efficiency and self-cleaning potential of the mesh screen. A further set of tests was conducted to determine and analyze the size-by-size material balance. These experiments used the same fixed parameters as in Table 4.2. Following each run, the samples were taken from cassettes, from egressed water sumps and from the mesh screen surface, and they were analyzed with Microtrac laser particle size analyzer (S3500) to determine the particle size

distribution of accumulated mass for each sample region. The coded sampling locations along the chamber are shown in Figure 4.10.

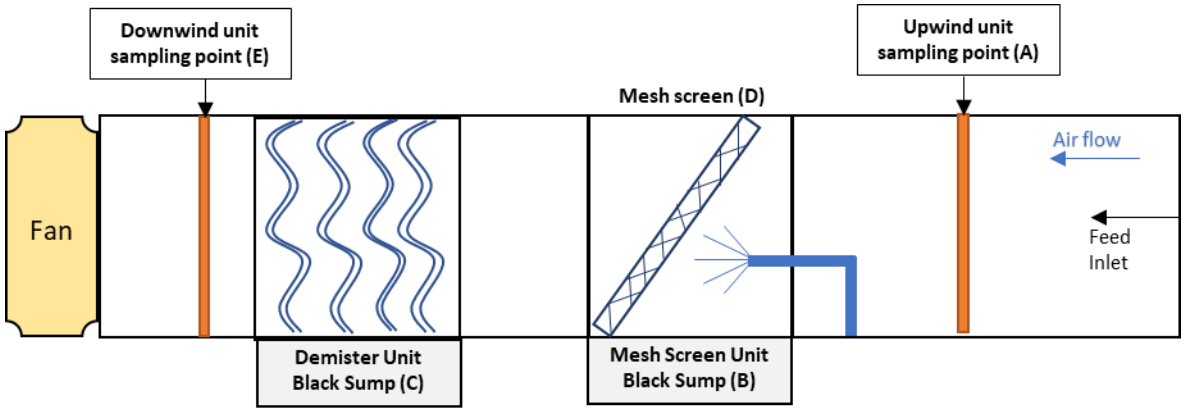

Figure 4.10: Visual illustration of sampling locations

Throughout testing, the system was monitored by measuring inner pressure continuously with pitot tubes and digital manometers to control the system's airflow loss and to further identify the filter's self-cleaning potential. The pressure drop data under different conditions was then determined by comparing the pristine condition with the post-experimental condition.

4.4. Results and Discussion

4.4.1. Mesh Vibrational Analysis

i. Geometry-based Modal Vibration Analysis:

Vibration characteristics, mode shapes and corresponding natural frequencies of a structure can be determined through modal analysis. The modes of a structure will change as the material properties (e.g. mass and stiffness) and boundary conditions (mountings) change. To investigate these attributes, a standard filter geometry was drawn and material properties were generated using CAD

software. In order to determine the natural frequencies of the filter geometry and the total deformation associated with those frequencies, a modal analysis was conducted with Ansys.

The mode shapes describe the spatial distribution of the vibrations at each natural frequency [64]. Each mode represents a unique vibration pattern of the geometry, and each of them introduces another variation of bending or twisting deformation. Modes are ordered according to their natural frequencies. Vibration patterns become more complex as the mode order increases. Through the higher modes, the natural frequency increases. Based on the color densities and the corresponding displacement simulation results of the modes, the 3rd and 5th modes showed the most vibrational energy in the entire surface of the mesh screen. Mode shapes of the framed mesh screen with the most obvious deformation are given in the Figure 4.11.

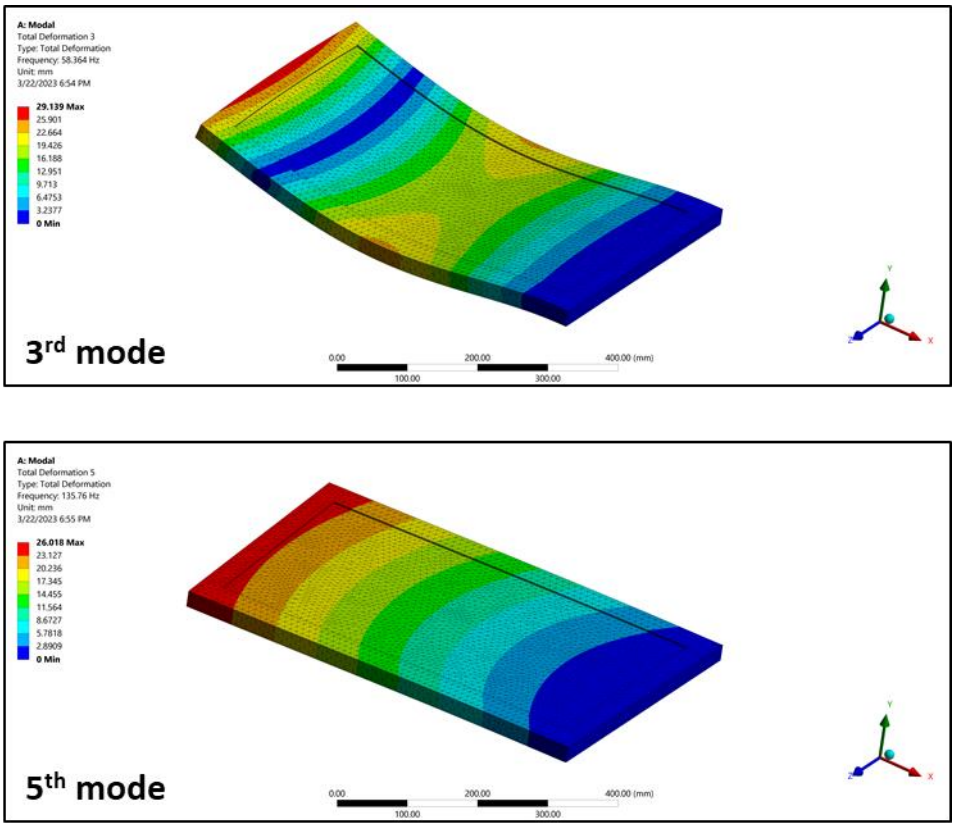

Figure 4.11: The most pronounced vibration modes associated with the filter geometry

ii. Accelerations at a Range of Frequencies:

In addition to the modal analysis, the peak acceleration of the mesh filter was determined by a series of experimental studies within a range of frequencies. The principal coordinates of the accelerometer and the filter were aligned appropriately. To generate the output vibration in the bench scale test setup, an electromechanical shaker (Brüel and Kjær Type 4809) was attached directly to the side of the mesh screen by an actuating rod and clamping mechanism. The filter media is then vibrated electromechanically by the shaker. The signal waves were generated by an SDG1000X function waveform generator and transferred to the shaker through a Brüel and Kjær Type 2718 power amplifier for base excitation over a range of frequencies (Figure 4.12).

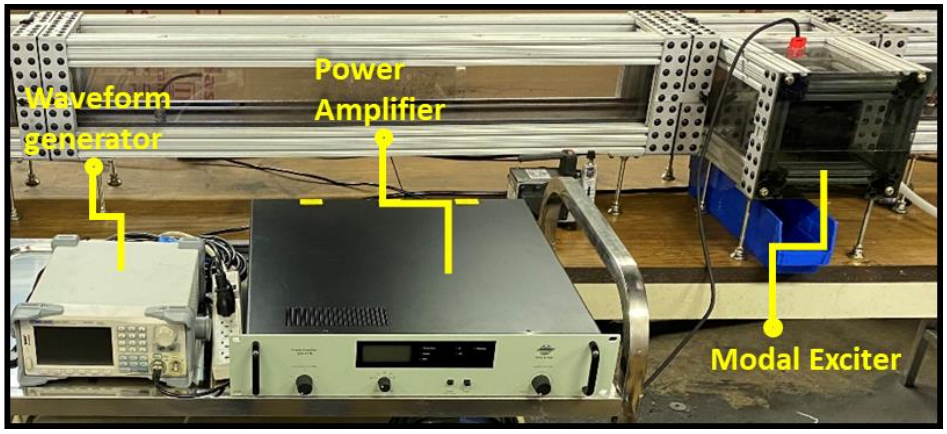

Figure 4.12: Vibrational equipment

Acceleration data was collected using a Lutron-BCB-8217SD three-axis vibration meter datalogger. The sensor was positioned on the middle of filter surface and X direction vibration data along was obtained. Figure 4.13 shows the mesh screen's responses to a predetermined frequency range when it is subjected to a sweep test. As shown in Figure 4.13, peak acceleration levels occur in a frequency range of 10 and 200 Hz. These values were subsequently used to guide the experimental design, setting thresholds for the parameter ranges.

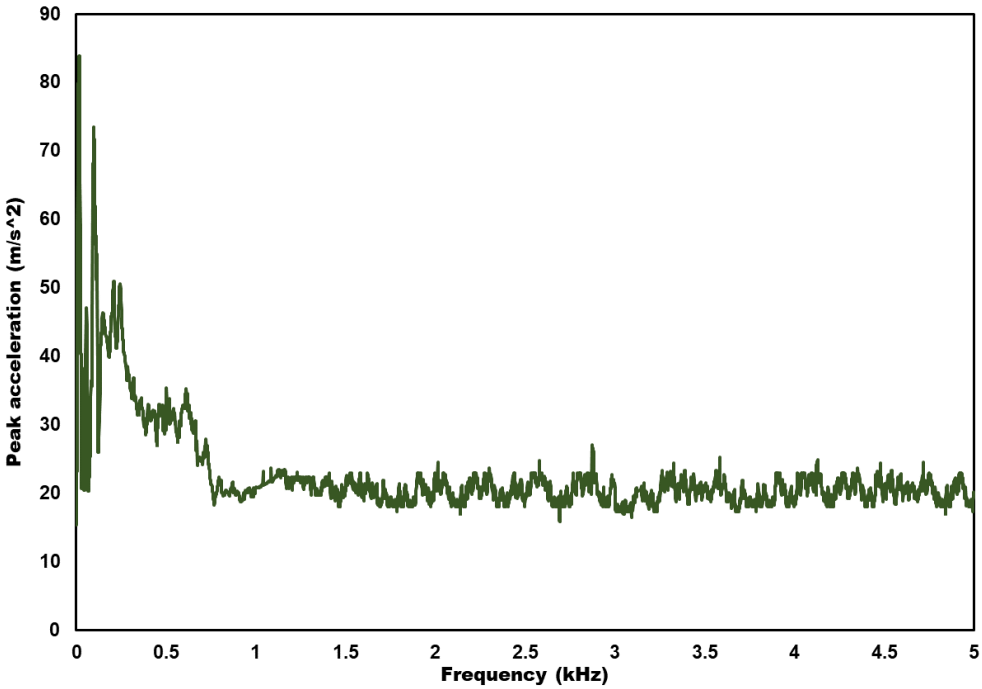

Figure 4.13: Frequency-Peak Acceleration test results

4.4.2. Vibrational Parameter Optimization

An experimental program was developed in Minitab using a three-factor BBD as described above. This modeling approach provides a rigorous means of assessing the individual and combinatory influence of water flow rate, amplifier gain, and vibrational frequency on FBS performance. The raw experimental results from the test program are shown in Table 4.3, while Table 4.4 shows the model summary and ANOVA table. Analysis of Table 4.3 shows the significance of the mentioned operational factors in determining mesh screen dust collection efficiency. Alternatively, no major differences were observed in the pressure drop values, suggesting that no significant clogging was experienced during the vibrationally-enhanced tests.

Table 4.3: Experimental program results

Run Order	Variables			Collection Efficiency (%)	Increase in Pressure Drop (mbar)
	Water Flow Rate (lt/min)	Amplifier Gain (dB)	Frequency (Hz)		
1	2	20	58.67	85.1%	0.11
2	2	20	133.84	86.5%	0.15
3	2	40	58.67	85.8%	0.10
4	2	40	133.84	87.1%	0.11
5	1	30	58.67	80.7%	0.13
6	1	30	133.84	84.6%	0.11
7	3	30	58.67	89.2%	0.12
8	3	30	133.84	92.9%	0.11
9	1	20	96.26	82.9%	0.09
10	1	40	96.26	83.1%	0.18
11	3	20	96.26	90.1%	0.15
13	3	40	96.26	91.8%	0.13
C1	2	30	96.26	87.8%	0.14
C2	2	30	96.26	89.1%	0.09
C3	2	30	96.26	88.7%	0.10

As shown in the ANOVA and model summary table (Table 4.4), several statistical tools were used to measure statistical reliability, including variance analysis, coefficients of determination,

adjusted coefficients of determination, and the lack of fit test. Each term in the model was estimated at a 95% confidence level, and as such p-values less than 0.05 indicate that the factor exhibits a statistically significant association. Based on the model terms, frequency and water flow rate were found to be significant at the 0.05 level. Alternatively, amplifier gain and the non-linear levels (2-way interactions between terms) were not found to be significant. This result indicates that the 2-way interaction results do not show substantial interdependencies between the parameters. Rather than affecting collection efficiency in a combinatory way, each factor has a direct effect on the system response.

Table 4.4: ANOVA table and model summary

Source	DF	Coef	Adj SS	Adj MS	F-Value	P-Value
Linear	3		148.203	49.401	61.23	0.000
Freq. (Hz)	1	1.287	13.261	13.261	16.44	0.010
Amp. Gain (dB)	1	0.4	1.28	1.28	1.59	0.263
W. Flow (lt/min)	1	4.087	133.661	133.661	165.66	0.000
2-Way Interaction	3		0.575	0.192	0.24	0.867
Freq. (Hz)*Amp. Gain (dB)	1	-0.025	0.003	0.003	0	0.958
Freq. (Hz)*W. Flow (lt/min)	1	-0.05	0.01	0.01	0.01	0.916
Amp. Gain (dB)*W. Flow (lt/min)	1	0.375	0.563	0.563	0.7	0.442
Lack-of-Fit	3		3.147	1.049	2.37	0.311
Pure Error	2		0.887	0.443		
Model Summary			**R^2**			**R^2_{adj}**
			97.53%			93.07%

The BBD results were also used to generate contour plots showing the 2-way interaction between the independent variables and the system's collection efficiency (Figure 4.14). Typically, the collection efficiency reaches its highest value in the dark green range, while lighter colors indicate that lesser effects of the parameters are visible.

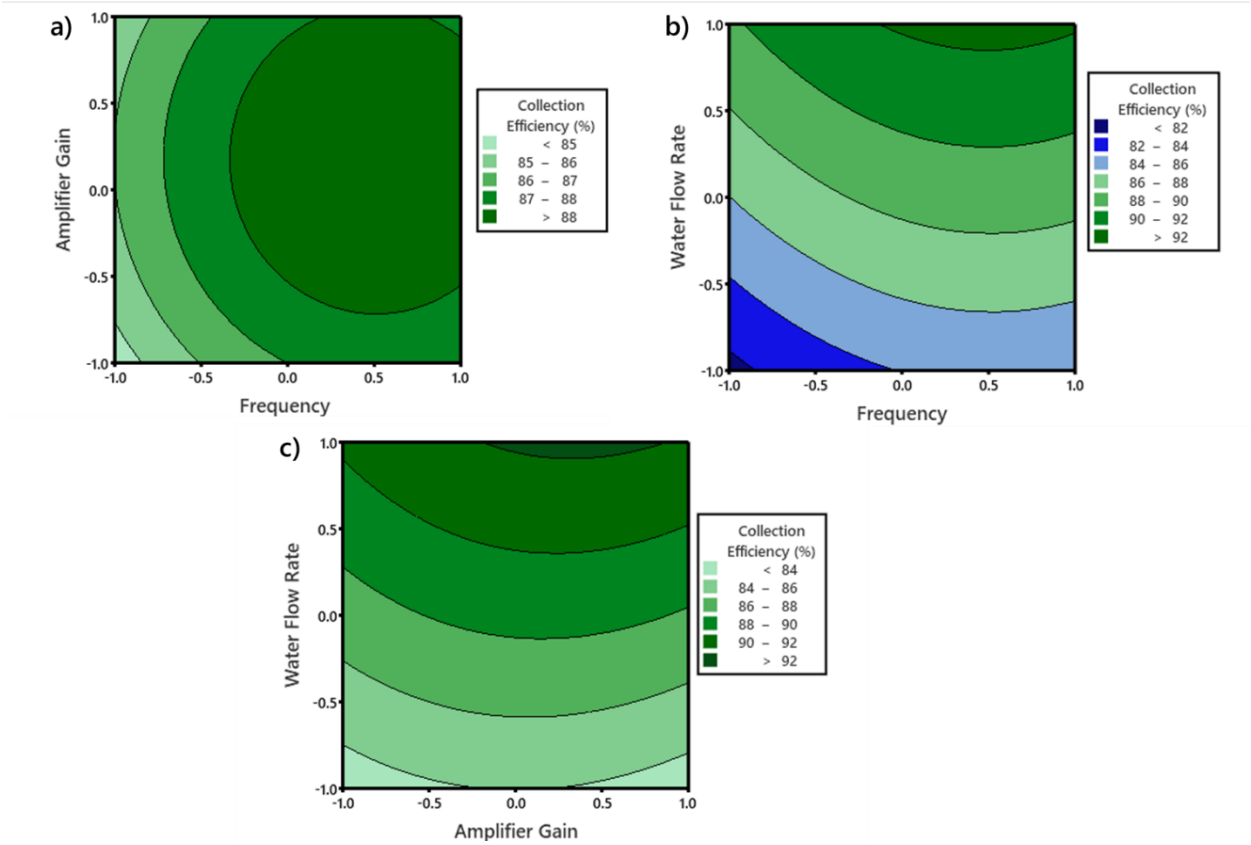

Figure 4.14: Contour Plots of Collection Efficiency vs Coded Units of a) Amplifier Gain-Frequency b) Water Flow Rate-Frequency c) Water Flow Rate-Amplifier Gain

Overall, the results show that the dust collection efficiency increased as the water flow rate and frequency were increased; however, the amplifier gain, had a minimal effect on the response. Amplifier gain is fundamentally one of the important parameters which determines the energy level of a signal. However, the sensitivity within the tested range does not significantly affect the system's performance. Considering that the experimental design includes relatively high amplifier gain values, almost no significant effect of amplifier gain was noticed between experiments. A vibration-free environment, however, can produce results comparable to signals with very low amplitudes.

Altogether, these results provide empirical support for the optimal conditions that maximize dust collection efficiency while maintaining acceptable pressure drop values. Specifically, the test results show that the optimum collection efficiency can be achieved when the water flow rate is at

its maximum (+1 or 3 lt/min), the amplifier gain is at its midpoint (+0.5 or 30 dB), and the vibration frequency is at its highest level (+1 or 133.84 Hz).

The results of this study are in agreement with Nawaz et al., 2023 simulation study results in general. Based on the simulation study, it appears that the vibrating mesh allows for stronger dust particle-mesh interactions than the static mesh, and the strength of the interaction increases as the vibrational energy increases, which results in a higher level of dust collection efficiency. They observed that the lowest amplification values tested in the simulation caused more particle collection than the others. According to researchers, this phenomenon occurs when the flow regions in front of the wire are perturbed because of the large amplitudes, resulting in the deflection of dust particles and their escape through the gap between the wires [56].

4.4.3. Size-by-Size Performance Results

Using the optimized parameter values identified in the previous section, a series of follow-on trials were conducted to investigate the size-by-size deportment of particles through the system. In this study, representative samples were taken at predetermined locations across the system. The coded sampling locations along the chamber are illustrated in Figure 4.10.

After collecting samples from these locations, the coal dust particles from the Teflon filters as well as coal dust & water mixture from the mesh screen itself, mesh screen section blackwater sump and demister section blackwater sump were analyzed with Microtrac laser particle size analyzer to determine the particle size distribution of each sample.

Table 4.5 to Table 4.8 and Figure 4.15 and Figure 4.16 show the size-by-size results of this study for both vibration free and vibration enhanced operation in both dry and wet modes. The particle amounts sampled at the predetermined locations are listed in the results as both a percentage of stream (i.e. the size distribution of the sample stream) and a percentage of feed (i.e. mass recovery to the stream).

In the dry operational conditions (Table 4.5 and Table 4.6), over half of the feed mass accumulated on the floor of the duct between the mesh screen and demister and was thus not found in the various sampling endpoints. While this result does hinder the interpretation of the material balance, the

data does provide evidence that intermediate sized particles (10 x 2.5 microns) are being preferentially recovered in the mesh screen, as indicated by the higher % of feed recovery for this size class as compared to the other classes. In addition, the dry data indicates that the vibration leads to lower accumulation in the mesh screen, as the total % of feed recovered to this stream was reduced from 7.59% to 4.51% with the addition of vibration.

Table 4.5: Summarized size-by-size material balance data for dry and vibration-free operational mode

Size (μm)	Feed (A)		Sump (Screen Unit) (B)		Sump (Demister Unit) (C)		Mesh Screen (D)		Ejected Air (E)		U/S – D/S Collection Efficiency (%)
	% of stream	Mass (g)	% of stream	% of feed	% of stream	% of feed	% of stream	% of feed	% of stream	% of feed	
+10	35.04	39.77	NA	NA	NA	NA	28.28	6.12	28.27	29.7	70.29
-10*2.5	37.23	42.26	NA	NA	NA	NA	54.78	11.1	35.59	35.2	64.80
-2.5	27.73	31.47	NA	NA	NA	NA	16.94	4.64	36.14	47.9	52.01
Total	**100.00**	**113.5**	**NA**	**NA**	**NA**	**NA**	**100.00**	**7.59**	**100.00**	**36.8**	**63.18**

Table 4.6: Summarized size-by-size material balance data for dry and vibration operational mode

Size (μm)	Feed (A)		Sump (Screen Unit) (B)		Sump (Demister Unit) (C)		Mesh Screen (D)		Ejected Air (E)		U/S – D/S Collection Efficiency (%)
	% of stream	Mass (g)	% of stream	% of feed	% of stream	% of feed	% of stream	% of feed	% of stream	% of feed	
+10	46.08	52.30	NA	NA	NA	NA	33.98	1.53	45.89	14.8	67.83
-10*2.5	43.51	49.38	NA	NA	NA	NA	47.92	2.16	38.33	12.3	71.54
-2.5	10.41	11.82	NA	NA	NA	NA	18.10	0.82	15.78	5.10	51.03
Total	**100.00**	**113.5**	**NA**	**NA**	**NA**	**NA**	**100.00**	**4.51**	**100.00**	**32.3**	**67.70**

Data from the wet testing (Table 4.7 and Table 4.8) provide better accounting of the mass and as such provide better insight on particle deportment. As expected, the majority of the feed mass ultimately reports to the demister sump (53% for vibration free; 59% for vibration enhanced)

however, a notable portion is also retained in the screen sump (23% for vibration free; 25% for vibration enhanced). Moreover, the data shows that the vibration enhanced unit has a higher collection efficiency (92.6% versus 87.2%) and lower accumulation in the mesh screen (2.9% versus 3.2%) when compared to the static mesh. As in the dry tests, the intermediate particles (10 x 2.5 microns) were preferentially recovered to the mesh screen; however, this trend was not as prominent as that found during the dry testing.

Table 4.7: Summarized size-by-size material balance data for wet and vibration-free operational mode

Size (µm)	**Feed (A)**		**Sump (Screen Unit) (B)**		**Sump (Demister Unit) (C)**		**Mesh Screen (D)**		**Ejected Air (E)**		**U/S – D/S Collection Efficiency (%)**
	% of stream	**Mass (g)**	**% of stream**	**% of feed**	**% of stream**	**% of feed**	**% of stream**	**% of feed**	**% of stream**	**% of feed**	
+10	17.59	19.96	16.77	3.78	15.51	8.27	40.75	1.29	6.45	0.83	95.30
-10*2.5	54.79	62.19	56.81	12.8	56.75	30.2	57.14	1.81	54.55	7.00	87.23
-2.5	27.62	31.35	26.42	5.95	27.74	14.7	2.11	0.07	39.00	5.00	81.88
Total	**100.00**	**113.5**	**100.00**	**22.5**	**100.00**	**53.3**	**100.00**	**3.17**	**100.00**	**12.8**	**87.17**

Table 4.8: Summarized size-by-size material balance data for wet and vibration operational mode

Size (µm)	**Feed (A)**		**Sump (Screen Unit) (B)**		**Sump (Demister Unit) (C)**		**Mesh Screen (D)**		**Ejected Air (E)**		**U/S – D/S Collection Efficiency (%)**
	% of stream	**Mass (g)**	**% of stream**	**% of feed**	**% of stream**	**% of feed**	**% of stream**	**% of feed**	**% of stream**	**% of feed**	
+10	30.33	34.42	36.60	9.12	29.81	17.5	14.12	0.40	21.67	1.61	94.73
-10*2.5	48.94	55.55	45.09	11.2	52.71	31.0	60.05	1.72	39.02	2.87	94.11
-2.5	20.73	23.53	18.31	4.56	17.48	10.3	25.83	0.74	39.31	2.90	86.00
Total	**100.00**	**113.5**	**100.00**	**24.9**	**100.00**	**58.9**	**100.00**	**2.86**	**100.00**	**7.38**	**92.62**

As shown in Figure 4.15, vibration improves overall collection efficiency in both wet (93% versus 87%) and dry (68% versus 63%) conditions. Similarly, the data shows that the presence of vibration generally has a positive effect on the collection efficiency of the system in finer size classes. While almost the same results are obtained in dry conditions for particles below 2.5 micron (52% versus 51%), a significant improvement in collection efficiency is observed in this size class under wet conditions (86% versus 82%). In the coarse size class, very slight decreases in collection efficiency were observed. While these decreases were more pronounced in dry conditions (70% under vibration versus 68% with no vibration), the difference was less significant in wet conditions (95% in both conditions).

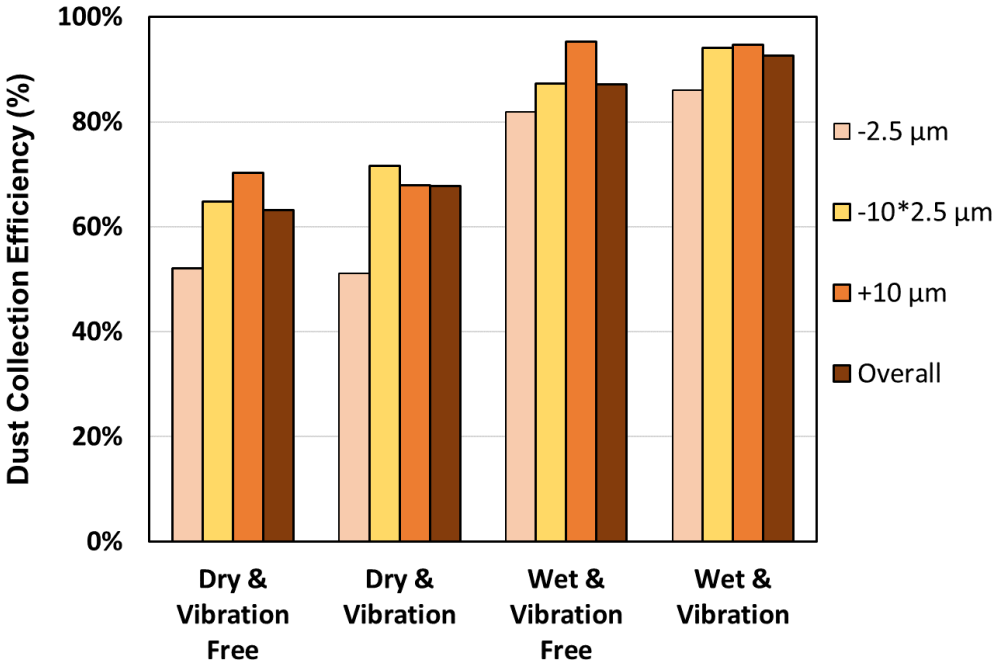

Figure 4.15: Collection efficiency by particle size class for various operational modes

To further assess the data, Figure 4.16 shows the Rosin-Rammler size distribution curves of the various product streams for the evaluated operational conditions. By comparing curves for the different conditions, the variations in particle size characteristics can be assessed and the distribution profiles can be understood better. When the operational conditions change from dry

and vibration-free condition to wet and vibration condition, the sharpness of the curves are usually increasing. This is most prominent in the mesh screen section. It has a slope of 1.03 for the dry & vibration-free condition while it has a slope of 1.46 for the wet and vibration condition. This means in the wet vibration condition the mesh screen has a narrower particle size distribution.

The d80 values obtained from the curves also show the significant change in mean particle size between the dry and vibration free conditions (d80 = 24.5 microns) versus that of the wet with vibration condition (d80 = 9.7 microns) (Figure 4.16). The decrease in this value shows that adding water to the system and vibrating the mesh screen at the same time will increase the possibility of finer dust particles getting captured by water droplets due to the increased surface wettability and improve the efficiency of the screening activity. It is also important to note that more amount of dust particles that were introduced to the stream were eliminated in the upwind section of the mesh screen. The blackwater sump located in the upwind section of the mesh screen is largely collecting the particles that are shed from the mesh screen surface. While the percentage of feed in the mesh screen section black water sump under the wet & vibration-free condition is 23%, the same parameter for the wet & vibration condition increased to 25%.

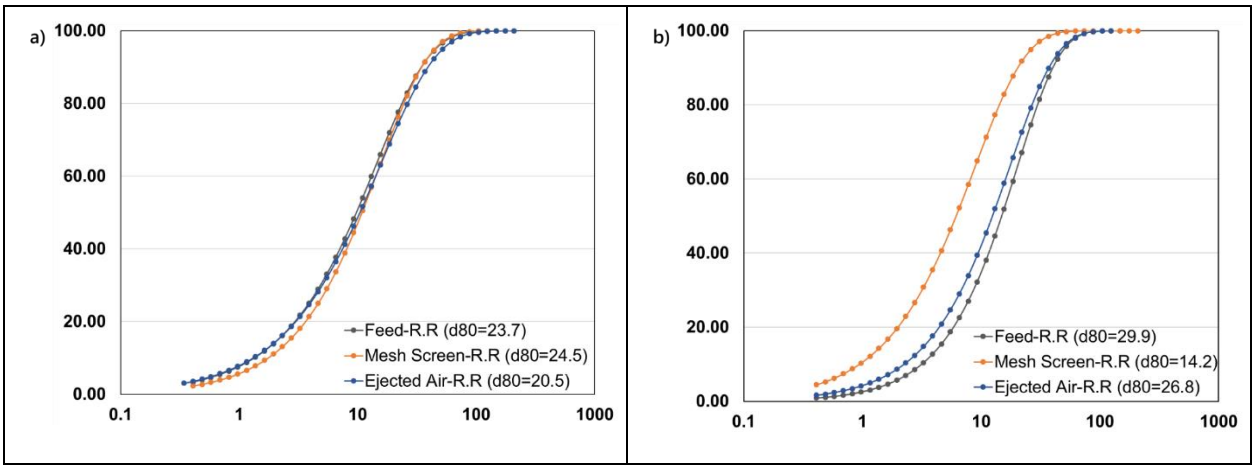

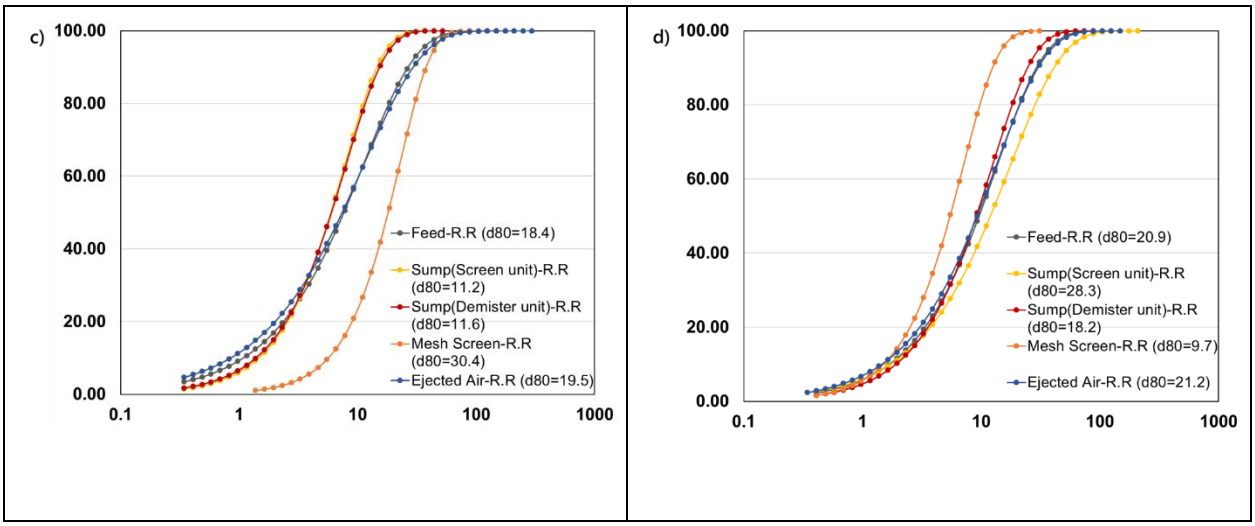

Figure 4.16: Size distributions of a) Dry and vibration-free mode b) Dry and vibration mode c) Wet and vibration-free mode d) Wet and vibration mode

Mass accumulation on the mesh screen and pressure drop across the mesh screen are two important indicators of the mesh screen's self-cleaning ability when vibration is applied. These data are given and illustrated in the Table 4.9 and Figure 4.17. When vibration was induced, pressure drop across the mesh screen decreased by 23% and filter accumulation decreased by 9.7% in the wet environment compared to vibration-free test. In the dry condition, when the vibration was applied, a 43% decrease in pressure drop and a 41% decrease in mass accumulation were observed. The reductions supporting the proposed vibration enhanced mesh screen design can provide the mesh screen with a self-cleaning mechanism and enable the mesh screen to operate longer.

Table 4.9: Summarized clogging data for various scrubber operational modes

Operational Mode	Increase in Pressure Drop (mbar)	Total Mass Retain on Filter (g)
Dry & Vibration-Free	0.78	8.61
Dry & Vibration	0.45	5.11
Wet & Vibration-Free	0.13	3.6
Wet & Vibration	0.1	3.25

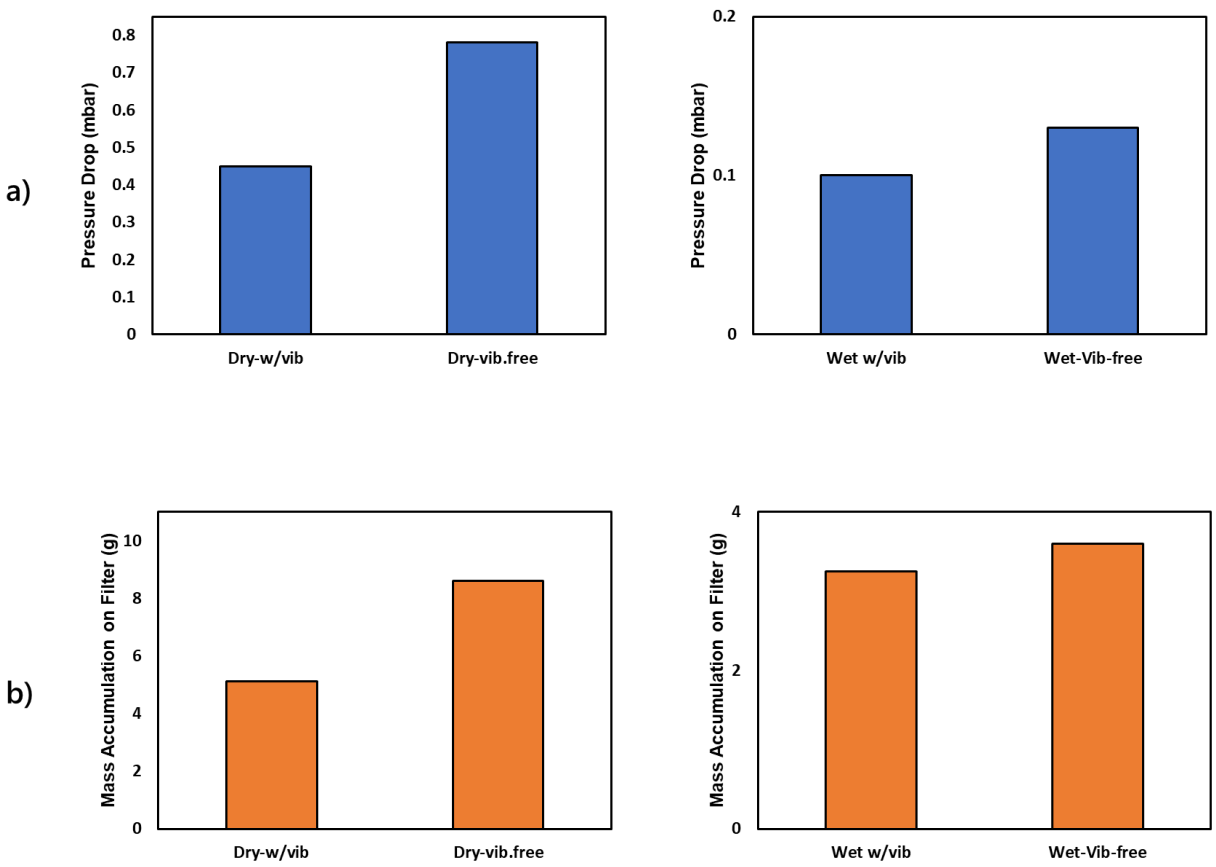

Figure 4.17: a) Pressure drop data across mesh screen in dry and wet operational conditions, b) Total accumulation between wire meshes in dry and wet operational conditions

4.5. Conclusions

Traditional flooded bed scrubber units use a static panel filter, which is has fundamental limitations that are amplified by their high clogging rate. As an alternative approach, we have proposed a vibration-enhanced filter mesh, which improves wetting uniformity and provides a mechanism for self-cleaning. In this study, a bench-scale prototype was constructed and tested. Through a statistically designed experimental program, the vibrational frequency, water flow rate, and

vibrational amplitude were empirically evaluated with respect to their influence on dust collection efficiency and mesh pressure drop. Statistical modeling showed that vibrational frequency and water flow rate were significant factors influencing performance, and both had a direct, rather than a combinatory, influence on the results. Follow on tests, using the optimal test conditions, compared the performance of the vibrating mesh to that of a static mesh tested under similar operating conditions. Test results showed that the vibrating mesh significantly outperformed that of the static mesh, improving collection efficiencies by over 6% in wet condition and over 7% in dry condition while reducing mass accumulation in the filter by almost 10% in wet condition and over 40% in dry condition. Overall, results of this bench-scale prototype study have validated that the vibration-enhanced mesh system can improve operational outcomes over that of a static mesh system. Future studies will evaluate other components of the system, including parameters significant for further scale up and implementation.

Authorship contribution statement

Mahmud Esad Uluer: Conceptualization, Methodology, Testing, Formal analysis, Data Curation, Writing - Original Draft, Writing - Review & Editing, Visualization

Matt Shigo: Test setup manufacturing

Hassan Amini: Conceptualization

Aaron Noble: Resources, Writing - Review & Editing, Supervision, Project administration, Funding acquisition

Role of Funding Source

This study was sponsored by the Alpha Foundation for the Improvement of Mine Safety and Health, Inc. (Alpha Foundation). The views, opinions, and recommendations expressed herein are solely those of the authors and do not imply any endorsement by the Alpha Foundation, its directors, and staff.

Declaration of Competing Interest

The authors declare that they have no known competing financial interests or personal relationships that could have appeared to influence the work reported in this manuscript.

4.6. References

1. U.S. Department of Labor (2014) Lowering miners' exposure to respirable coal mine dust, including continuous personal dust monitors. Fed Regist Vol 79, Number 84. http://arlweb.msha.gov/regs/fedreg/final/2014finl/2014-09084.asp. Accessed June 5, 2022.

2. Sinclair J (1958) Environmental conditions in coal mines: including fires, explosions, rescue and recovery work. Pitman, 1958.

3. CDC (2019) Centers for Disease Control and Prevention, National Institute for Occupational Safety and Health, Occupational Respiratory Disease Surveillance, National Occupational Respiratory Mortality System (NORMS) National Database.

4. E. Suarthana, A.S. Laney, E. Storey, M.D. Attfield (2011). Coal workers' pneumoconiosis in the United States: regional differences 40 years after implementation of the 1969 Federal Coal Mine Health and Safety Act, Occup. Environ. Med., 68 (12), 908-913. https://doi.org/10.1136/oem.2010.063594

5. J.F. Gamble, R.B. Reger, R.E. Glenn (2011). Rapidly progressing coal workers pneumoconiosis as a confounding risk factor in assessing coal mine dust safe exposure levels, J. Clin.Toxicol., S1:003. https://doi.org/10.4172/2161-0495.S1-003

6. V.C. dos S. Antao, E.L. Petsonk, L.Z. Sokolow, A.L. Wolfe, G.A. Pinheiro, J.M. Hale, M.D. Attfield (2005). Rapidly progressive coal workers' pneumoconiosis in the United States: geographic clustering and other factors, Occup. Environ. Med., 62 (10), pp. 670-674. https://doi.org/10.1136/oem.2004.019679

7. M. Attfield, N. Seixas (1995). Prevalence of pneumoconiosis and its relationship to dust exposure in a cohort of U.S. Bituminous coal miners and ex-miners, Am. J. Ind. Med., 27 (1), pp. 137-151.

8. Cashdollar KL, Sapko MJ (2006) Explosion hazards of coal dust in the presence of methane. Handbook for methane control in mining, pp 147–150

9. U.S. Department of Labor (2014) Final rule.

http://arlweb.msha.gov/regs/fedreg/final/2014finl/2014-09084.asp. Accessed June 5, 2022.

10. Reed W, Taylor C (2007) Factors affecting the developing of mine face ventilation systems in the 20th century, SME Annual Conference and Expo, Denver, CO

11. Wang W, Peng FF (1991) Analyses of respirable dust distributions with multiple dust sources on longwall faces. Proc. of Soc. for Mining, Metallurgy & Exploration. pp 367–375

12. Colinet JF, Spencer ER, Jankowski RA (1997) Status of dust control technology on U.S. longwalls. Proceedings of 6th International Mine Ventilation Congress. pp 345–351

13. Arya S, Sottile J, Novak T (2018) Development of a flooded-bed scrubber for removing coal dust at a longwall mining section. Saf Sci 110:204–213. https://doi.org/10.1016/j.ssci.2018.08.003

14. Arya S, Sottile J, Rider JP, Colinet JF, Novak T,Wedding C (2018) Design and experimental evaluation of a flooded-bed dust scrubber integrated into a longwall shearer. Powder Technol 339:487–496. https://doi.org/10.1016/j.powtec.2018.07.072

15. Arya S, Novak T, Saito K et al (2019) Empirical formulae for determining pressure drop across a 20-layer flooded-bed scrubber screen. Mining, Metallurgy & Exploration, 36(6), 1169-1177. https://doi.org/10.1007/s42461-019-0091-5

16. Arya S (2018) Investigation of the effectiveness of an integrated flooded-bed dust scrubber on a longwall shearer through laboratory testing and CFD simulation. Doctoral Dissertation, Mining Engineering, University of Kentucky. https://doi.org/10.13023/ETD.2018.074

17. S. R. Cowley, B.S. McCoy (1993) “Wet scrubber apparatus,” U. S. Patent 5,178,654.

18. Campbell, J. A., Moynihan, D. J., Roper, W. D., & Willis, E. C. (1983). U.S. Patent No. 4,380,353. Washington, DC: U.S. Patent and Trademark Office.

19. Colinet, J. F., & Jankowski, R. A. (2000). Silica collection concerns when using flooded-bed scrubbers. Mining Engineering (Littleton, Colorado), 52.

20. Colinet, J., Halldin, C. N., & Schall, J. (2021). Best Practices for Dust Control in Coal Mining, Second Edition. National Institute of Occupational Safety and Health, Pittsburgh. PA; Spokane, WA. https://doi.org/10.26616/NIOSHPUB2021119

21. Colinet, J., Potts, J. D., & Reed, W. R. (2011). Evaluation of face dust concentrations at mines using deep-cutting practices.

22. Colinet, J., Reed, W. R., & Potts, J. D. (2013). Impact on respirable dust levels when operating a flooded-bed scrubber in 20-foot cuts. Pittsburgh, PA Spokane, WA

23. National Institute for Occupational Safety and Health (2002) Exposure to Silica Dust on Continuous Mining Operations Using Flooded-Bed Scrubbers, Applied Occupational and Environmental Hygiene, 17:5, 322-323, https://doi.org/10.1080/10473220252864888

24. Salazar, A. J., Saito, K., Alloo, R. P., & Tanaka, N. (2000). U.S. Patent No. 6,093,250. Washington, DC: U.S. Patent and Trademark Office.

25. Taylor A., Schafrik S., Kumar A.R. (2019). The Vortecone: A new maintenance-free wet scrubber device. Future Mining, Sydney, NSW.

26. Kumar, A. R., Levy, A., Kumar, A., Schafrik, S., & Novak, T. (2020). Computational fluid dynamics modeling and laboratory analysis of aerosol particles' capture on thin swirling water film in a Vortecone. Powder Technology, 361, 499-506. https://doi.org/10.1016/j.powtec.2019.11.093

27. Kumar, A. R., & Schafrik, S. (2020). Multiphase CFD modeling and laboratory testing of a Vortecone for mining and industrial dust scrubbing applications. Process Safety and Environmental Protection, 144, 330-336. https://doi.org/10.1016/j.psep.2020.07.046

28. Kumar, A. R., Schafrik, S., & Novak, T. (2020). Multi-phase computer modeling and laboratory study of dust capture by an inertial Vortecone scrubber. International Journal of Mining Science and Technology, 30(3), 287-291. https://doi.org/10.1016/j.ijmst.2020.03.014

29. Kumar, A. R., Schafrik, S., & Velasquez, O. (2020). Designing, modeling, and laboratory testing of a non-clogging impingement type filter for mining dust scrubbers. Mining, Metallurgy & Exploration, 37(6), 1911-1918. https://doi.org/10.1007/s42461-020-00311-9

30. King, R. P. (2001). Classification based on sieving–vibrating screens. Modeling and simulation of mineral processing systems. Elsevier. 81-86.

31. Chen, Z., Zhou, Z., & Peng, J. (2022). Dust Removal Mechanism of the Vibrating String Filter with Charged Water Mist. International Journal of Rotating Machinery, 2022. https://doi.org/10.1155/2022/5713983

32. Mishin, I. F., El'bert, E. I., Belikov, V. I., Tumanov, A. N., & Kachaev, V. K. (1975). Cleaning coal tar by vibrating-screen filtration, surfactant treatment, and short-term clarification. Coke Chem., USSR (Engl. Transl.);(United Kingdom), 4.

33. Yang, X., Wang, H., & Chase, G. G. (2015). Performance of hydrophilic glass fiber media to separate dispersed water drops from ultra low sulfur diesel supplemented by vibrations. Separation and Purification Technology, 156, 665-672. https://doi.org/10.1016/j.seppur.2015.10.062

34. Kim, S. C., Wang, H., Imagawa, M., Chen, D. R., & Pui, D. Y. (2006). Experimental and modeling studies of the stream-wise filter vibration effect on the filtration efficiency. Aerosol science and technology, 40(6), 389-395. https://doi.org/10.1080/02786820600640541

35. Genkin, G., Waite, T. D., Fane, A. G., & Chang, S. (2006). The effect of vibration and coagulant addition on the filtration performance of submerged hollow fibre membranes. Journal of membrane science, 281(1-2), 726-734. https://doi.org/10.1016/j.memsci.2006.04.048

36. Coster, H. G. L., Farahani, T. D., & Chilcott, T. C. (2011). Production and characterization of piezo-electric membranes. Desalination, 283, 52-57. https://doi.org/10.1016/j.desal.2011.04.071

37. Bilad, M. R., Discart, V., Vandamme, D., Foubert, I., Muylaert, K., & Vankelecom, I. F. (2013). Harvesting microalgal biomass using a magnetically induced membrane vibration (MMV) system: filtration performance and energy consumption. Bioresource technology, 138, 329-338. https://doi.org/10.1016/j.biortech.2013.03.175

38. Kuscer, D., Rojac, T., Belavič, D., Santo Zarnik, M., Bradeško, A., Kos, T. & Faccini, M. (2017). Integrated piezoelectric vibration system for fouling mitigation in ceramic filtration membranes. Journal of membrane science, 540, 277-284. https://doi.org/10.1016/j.memsci.2017.06.054

39. Khairuddin, N. F. M., Idris, A., & Irfan, M. (2019). Towards efficient membrane filtration for microalgae harvesting: a review. J Kejuruteraan, 2, 103-112. https://doi.org/10.17576/jkukm-2019-si2(1)-13

40. Nurra, C., Clavero, E., Salvadó, J., & Torras, C. (2014). Vibrating membrane filtration as improved technology for microalgae dewatering. Bioresource technology, 157, 247-253. https://doi.org/10.1016/j.biortech.2014.01.115

41. Niţoi, D., Amza, G., Amza, Z., Radu, C., & Teodorescu, M. (2018). PRACTICAL REALISATION AND FINITE ELEMENT MODELING OF ULTRASONIC FILTERS DESIGN FOR AIR FILTRATION. International Multidisciplinary Scientific GeoConference: SGEM, 18(4.2), 555-562. https://doi.org/10.1088/1757-899X/400/2/022003

42. Amza, C. G., Nitoi, D. F., Chivu, O., Radu, C., & Teodorescu, M. C. (2015). Contributions of the possibility of use of ultrasound in the air filter and purification. In 15th International Multidisciplinary Scientific GeoConference SGEM 2015 (pp. 897-904). https://doi.org/10.1088/1757-899X/95/1/012010

43. Nakamura, K. (2012). Ultrasonic transducers. Material and design for sensors, actuators and medical applications, (Woodhead Publishing USA). https://doi.org/10.1016/B978-1-84569-989-5.50022-X

44. Niţoi, D., & Amza, G. (2019). Industrial Air Purification System Using Ultrasonic Vibration. Current Trends in Natural Sciences Vol, 8(15), 17-22.

45. Lu, Z., Rath, A., Amini, S. H., Noble, A., & Shahab, S. (2022). A computational fluid dynamics investigation of a novel flooded-bed dust scrubber with vibrating mesh. International Journal of Mining Science and Technology, 32/3, 525-537, https://doi.org/10.1016/j.ijmst.2022.03.002

46. Fuchs, E.P (1979) Coal Mining Equipment Vibration Data Report, Donaldson Company, Inc.

47. Smith, A. K., Peterson, J. S., & Kovalchik, P. G. (2008). Continuous mining machine conveyor system sound power levels.

48. Mężyk, A., Klein, W., Pawlak, M., & Kania, J. (2015). Numerical simulation of the vibration control system designed for Continuous Miner machines. Mathematical and Numerical Approaches, 363.

49. Mężyk, A., Klein, W., Pawlak, M., & Kania, J. (2017). The identification of the vibration control system parameters designed for continuous miner machines. International Journal of Non-Linear Mechanics, 91, 181-188. https://doi.org/10.1016/j.ijnonlinmec.2017.02.005

50. Yantek, D. S. (2003). Estimated sound power radiated by surfaces on a continuous miner tail section using vibration measurements. National Institute for Occupational Safety and Health, Pittsburgh, PA.

51. Stander, C. J., & Heyns, P. S. (2005). Instantaneous angular speed monitoring of gearboxes under non-cyclic stationary load conditions. Mechanical systems and signal processing, 19(4), 817-835. https://doi.org/10.1016/j.ymssp.2004.10.006

52. Wang, J., Zhang, Y., & Dong, L. (2016). Analysis of vibration characteristics and dynamic load identification in continuous miner cutting arm. Int J Simul Syst Sci Technol, 17(13), 20-1. https://doi.org/10.5013/IJSSST.a.17.13.20

53. Mężyk, A., Pawlak, M., Klein, W., & Kania, J. (2013). Methodology for optimization modal parameters in the engineering design process on the example on the example of continuous miner cutter boom. https://doi.org/10.1007/s00419-014-0955-6

54. Zhang, X. K. (2011). Optimal Placement ot Vibration Sensor about Heavy Mining Equipment. Meikuang Jixie (Coal Mine Machinery), 32(3), 173-175. https://doi.org/10.3390/s19020340

55. Shahab, S. (2015). Vibration energy harvesting, biomimetic actuation, and contactless acoustic energy transfer in a quiescent fluid domain (Doctoral dissertation, Georgia Institute of Technology).

56. Janjua, A.N., Shaefer M., Amini, S.H., Noble, C.A., Shahab, S. (2023). Vibration Energy Harvesting in Underground Continuous Mining: Dynamic Characteristics and Experimental Research of Field Data. Applied Energy. (Manuscript submitted for publication.)

57. Jung S., Noble A., Pan L., Shahab S. (2017) Collecting Mine Dust Particles with Liquid-Coated Vibrating Meshes, Alpha Foundation for the Improvement of Mine Safety and Health, Inc. (Technical Report). https://www.alpha-foundation.org/wp-content/uploads/2019/03/AFC518-25_VirgTech_FinalRpt.pdf Accessed January 5, 2023.

58. J.B. Boreyko, C.H. Chen, (2009) Restoring superhydrophobicity of lotus leaves with

vibration-induced dewetting, Phys. Rev. Lett., 103/17, DOI:https://doi.org/10.1103/PhysRevLett.103.174502

59. J.L. Kou, H.J. Lu, F.M. Wu, J.T. Fan, (2011) Toward the hydrophobic state transition by the appropriate vibration of substrate, EPL 96, DOI 10.1209/0295-5075/96/56008

60. Pengyu W., Xiaokun S., Hongqing L., Shang M., Zhenqing W., (2021) Investigation of surface wettability and their influencing mechanisms under vibration field: A molecular dynamics simulation study. Computational Materials Science, Vol 197, https://doi.org/10.1016/j.commatsci.2021.110615.

61. Noble A., Jung S., Pan L., Shahab S., Amini H., (2023) Collecting Mine Dust Particles with Liquid-Coated Vibrating Meshes, Alpha Foundation for the Improvement of Mine Safety and

Health, Inc. (Final Report). https://www.alpha-foundation.org/wp-content/uploads/2023/07/AFC518SP-89_VirgTech_FinalRpt.pdf Accessed September 5, 2023.

62. Frankel, N. and A. Acrivos, (1967) On the viscosity of a concentrated suspension of solid spheres. Chemical Engineering Science, 22 (6): p. 847-853.

63. Krieger, I.M. and T.J. Dougherty, (1959) A mechanism for non - Newtonian flow in suspensions of rigid spheres. Transactions of the Society of Rheology, 3 (1): p. 137-152.

64. Schwarz, B. J., Richardson, M. H. (1999). Experimental Modal Analysis. Vibrant Technology Inc., CSI Reliability Week, Orlando, FL.

Chapter 5

5. Influence of Mesh Design and Surface Treatments on Particle Transport and Fate in a Vibration-Enhanced Flooded Bed Dust Scrubber

This chapter is in preparation to be submitted for publication in the international peer-reviewed journal Mining& Metallurgy and Exploration. Citation details are provided below:

Uluer, M.E., Noble, A., (in preparation). "Influence of Mesh Design and Surface Treatments on Particle Transport and Fate in a Vibration-Enhanced Flooded Bed Dust Scrubber"

(ABSTRACT)

Respirable coal mine dust (RCMD) is one of the biggest occupational health hazards for underground coal miners. Dusty mining environments can cause long-term health problems, including pneumoconiosis and progressive massive fibrosis. The Mine Safety and Health Administration (MSHA) has recently revised regulations promoting enhanced dust mitigation technologies, which have sparked renewed interest in the development of dust mitigation technologies. The flooded bed dust scrubber (FBS) is one of the most widely used technologies; however, it is limited by technical challenges, the most notably being the potential to clog. Recent studies (Lu et al., 2022; Uluer et al, under review; Janjua et al., under review) have shown that applying vibration to filter mesh can improve the overall efficiency of the scrubber and that the system can be readily integrated to existing continuous mining equipment using an energy harvesting approach. In this follow-up study, the impact of mesh design and surface modification on system efficiency was examined using different vibrating liquid-coated stainless-steel mesh panels in a laboratory-scale FBS. Based on the two-way interaction data from a multi-factor experimental design, the results show that the performance of the system can be optimized by using hydrophilic 20- or 30-layer filters and by excitation frequencies between 67 and 134 Hz.

This laboratory study suggests that a 20-layer mesh screen with hydrophilic surface applications and optimized vibration parameters can perform similar to that of a 30-layer static mesh, which is typically used in industrial units.

5.1. Introduction

Respirable coal mine dust (RCMD) is one of the most significant occupational health hazards in the coal industry [1-5]. RCMD is defined as a particulate matter that has an aerodynamic diameter of below 10 μm and a median cut point of 4 μm [6]. It has been reported that this substance can be deposited anywhere along the lung's gas-exchange region [4]. According to recent research, smaller particles may pose more risk to health within their respirable range than larger particles [7]. In addition, technological advances in mining equipment have led to more powerful cutting, which, in turn, may cause smaller particles to be released into the mine area during the mining and drilling processes [8, 9]. Coal miners who work in dusty mining environments have been shown to suffer from long-term health effects, including but not limited to coal workers pneumococis (CWP) and progressive massive fibrosis (PMF) [10]. The Federal Coal Mine Health and Safety Act (Public Law 91-173) was enacted in 1969 to prevent the development of CWP in coal miners. It sets a limit at 2 mg/m3 [11] for RCMD level with a minimum of 5% quartz. Regulations limiting respirable dust exposures, along with better ventilation and dust mitigation techniques, have contributed heavily to the decline in disease incidence in the US over the following several decades [4, 12-14]. However, since the late 1990s, the disease incidences have been on the rise [12, 14, 15] with some studies suggesting even 0.1-0.2 mg/m3 exposure [6] can be harmful to the lungs. As a result of these issues, the Mine Safety and Health Administration (MSHA) implemented a new dust standard on August 1, 2016, requiring dust levels at the working face to remain below 1.5 mg/m3 and intake entries below 0.5 mg/m3. Even though underground dust control has been the subject of research and inquiry for several decades, these revised regulations have prompted renewed interest in the area, particularly in the development of new technologies [16].

Dust control and mitigation strategies in modern mining include cutter-mounted sprays and dust scrubbers [17-22], while the ventilation system itself is also essential [23]. Augmenting these primary approaches, the flooded bed scrubber (FBS) mounted on the continuous mining machine

is a widely adopted technology found in nearly all modern coal mines [24,25]. The FBS works by drawing dirty air near the cutting head into a scrubbing duct. Here the dirty air passes through a mesh screen where water is continuously sprayed. The interaction of the water spray and mesh panel wets or captures the dust particles, which are subsequently captured in a mist eliminator. The dry clean air is then discharged at the rear of the machine where an exhaust fan induces the airflow needed for the scrubber [26]. Figure 5.1 shows a depiction of the FBS, with the slight adaptation of a vibration inducer that prompts controlled vibration to the mesh screen.

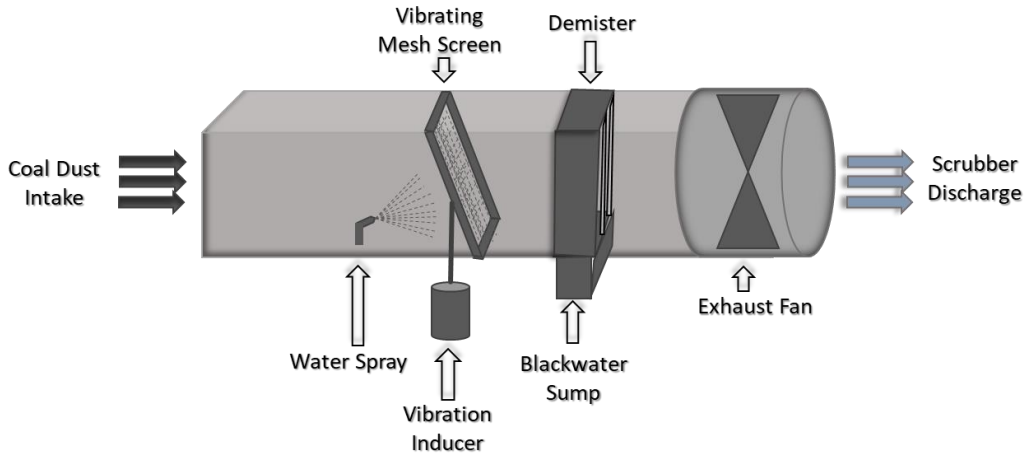

Figure 5.1: Visual illustration of bench-scale flooded bed dust scrubber

While FBSs are ubiquitously in continuous mining applications, they face numerous technical challenges. Most significantly, the units exhibit a fundamental tradeoff between airflow and mesh density. Higher mesh densities typically have higher particle capture rates; however, they also produce higher pressure drops, which reduce the amount of air that can be cleaned through the scrubber. Alternatively, low-density meshes can achieve higher air flow rates, however, the dust capture capacity is poor [26]. These issues are further compounded when the filter mesh is clogged, which reduces overall efficiency and necessitates frequent cleaning. At least one study shows that even a 20-foot advancement can reduce scrubber airflow by 35% [28]. Operational downtime caused by the cleaning process slows the production rate because of overall system degradation [29].

In recent years, research and development efforts have sought to directly address these challenges. In one example, a vortecone non-clogging wet filter used in the automobile industry to collect oversprayed vehicle paint particles [30] was used to replace the dust collector within the FBS [31]. Later, this structure was modified to minimize resistance for use at much higher airflows [32]. In a separate study, researchers proposed an impingement-type filter facilitating dust removal by preventing the straight flow [33]. Recent attempts have been made to improve system performance by utilizing vibration-enhanced filter panels [27,34,35]. Many industrial applications have benefited from enhanced particle filtering using vibrating filter media, including size classification, filtering, and dust collection/removal [36-40]. It has also been shown that directly stimulating the filter media can reduce clogging problems in membrane filters [41,42]. In-mine vibrational analysis on continuous miners data exhibit peak acceleration levels occur around 100 Hz [43]. Additionally the authors observed that the mesh screen responded with maximum vibrational energy when it excites in the range of 10-200 Hz [27].

Recent studies by the authors and colleagues have demonstrated the utility of vibration-enhanced FBS units. In an initial study, vibration-enhanced mesh panels were simulated through three-phase computational fluid dynamic (CFD) models [34, 35], and the results indicated that the vibrating mesh provides stronger dust particle-mesh interactions than the static mesh and that the strength of the interaction increases as vibrational energy increases, resulting in a greater level of dust collection. It was found that the lowest amplification values produced more particle collection than the higher values simulated. More recently, and experimental study validated that adding a vibration-enhanced mesh panel to a laboratory scale FBS can improve dust collection efficiency over that of a static unit by 6% [27]. As a result of the induces vibration, more dust particles can be captured by water droplets, surface wetting can be improved, and airflow rates can be sustained for a longer period of time [27,34,35]. To implement the concept, energy harvesting approaches and specific spring configurations enable natural vibrations generated by continuous mining machines to be transmitted to mesh screen panels in FBSs [35,44].

Previous Chapter (Chapter 4) is experimentally studying the pressure drop across the mesh filter. Pressure drop across the filter has been investigated under different operating conditions, i.e. water spray flow rate and vibration. The results showed that the pressure drop with a water spray is significantly higher compared with that without a water spray, and the pressure drop is insensitive to the flowrate of the water spray.

As a follow-up study of Uluer et al., (under review), this study proposes further modifications to the standard FBS through surface modifications of the mesh filter. Many prior studies have evaluated the use of wetting agents and other modifications to the spray water; however, the results are largely inconsistent between studies and even within the same study [45 – 49]. In the current study, an alternative approach was applied, whereby, the modification is applied to the filter media rather than the spray water. Vibration-enhanced and surface-modified stainless-steel mesh panels with a variety of thicknesses were tested in this study to evaluate the combined effect of mesh design and surface modification on dust collection. For this purpose, several tests were conducted using a laboratory-scale FBS equipped with a vibration-enhanced mesh screen.

5.2. Theory

5.2.1. Effect of Surface Chemistry on System Performance

It is significantly important to evaluate the effect of mesh vibration with different surface coatings for improving the particle-laden liquid drainage collected on a mesh to avoid clogging. During the bench-scale prototype testing, a parallel study conducted by Dr. Jung et al. investigated how modification on filter surface affects system performance [50]. They coated the filter surfaces with three different coatings (NeverWet, Naisol, and Cytonix) and vibration was induced on the mesh. They also compared the results with the untreated filter surface. They used a high-speed camera to record the behavior of drops under vibration. The time evolution snapshots shown in Figure 5.2 illustrate the behavior of a particle-laden drop when vibration is applied to a bare surface and a Naisol-coated surface. As indicated in the figure, in the same conditions the coating causes the drop to slide, compared with a drop adhering to the untreated surface.

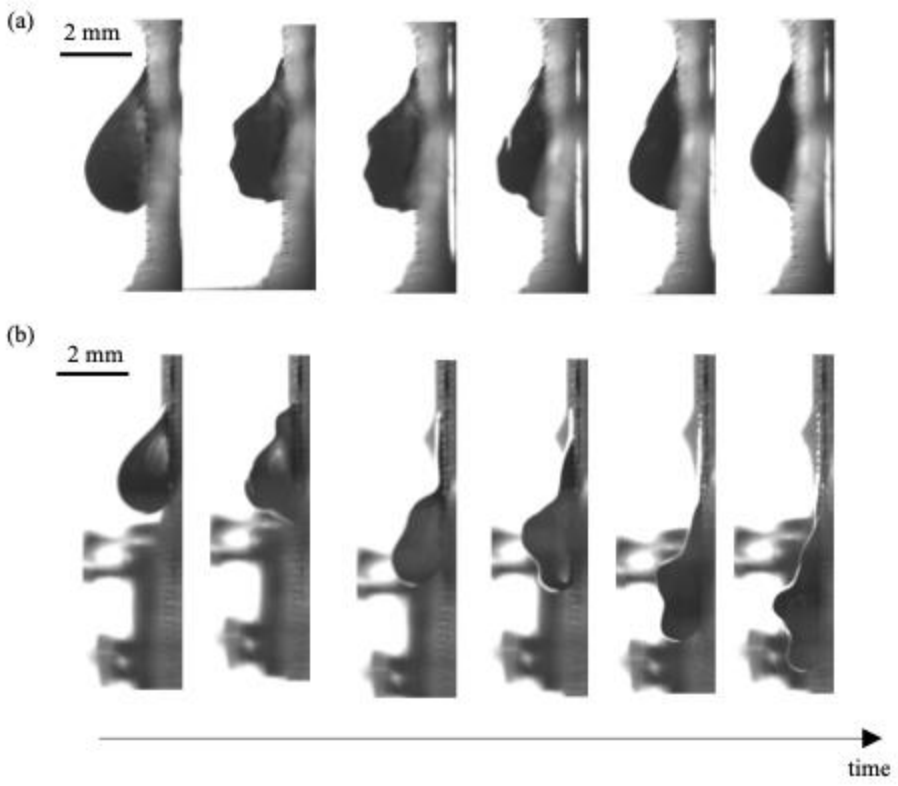

Figure 5.2: Time evolution snapshots of a 20 μL drop under 100 Hz vibrations on (a) untreated surface, and (b) Naisol-coated surface [50]

After collecting the data, they measured the wettability of these filter surfaces and compared them. The difference between maximum advancing and minimum receding contact angles ($\Delta\Theta$) is proportional to the wettability of the surface. Accordingly, higher $\Delta\Theta$ relates to more hydrophilic surfaces, whereas lower $\Delta\Theta$ refers to more hydrophobic surfaces. Their findings showed that Naisol-coated surfaces achieved the optimal balance (optimum $\Delta\Theta$) between particle collection via a hydrophilic surface and droplet mixture drainage via a hydrophobic surface.

The current study was able to make use of these results by identifying the most appropriate surface treatment types for greater system performance. These surface modifications can increase adhesion between dust particles and liquid interfaces by increasing evenly wetting the mesh screen surface with liquid. A hydrophilic surface (higher $\Delta\Theta$) will enable water droplets to remain on the mesh for a longer period of time and thus allowing the drops to capture more dust particles. Hydrophobic surfaces, as presented in Dr. Jung's group study, enhances the rate of drop drainage, allowing

droplets to continue their path to the mist eliminator. Considering these two competing effects, different coatings have been tested which provide a variety of surface wettability properties.

5.2.2. Effect of Mesh Type on System Performance

Sczap et al. (2023) studied the mechanisms involved in clogging filter media using a test setup which is modeled the filtering mechanism in the scrubber. Using differential pressure data across the filter, they fitted a modified model to the data and compared the model results with the experimental results.

In fibrous filters, Davies' equation (1973) governs the pressure drop. A filter's dimensions are related to its dimensional characteristics and its air velocity in this equation. This includes air velocity (V), porosity (α), air viscosity (μ), and mean filter size (df) as follows:

$$\frac{\Delta P}{Z} = 64\mu V \frac{a^{\frac{3}{2}}(1 + 56a^3)}{d_f^2} \quad (1)$$

Based on the research they conducted, Sczap et al. concluded that the total pressure drop across a filter is an accumulation of the pressure drops across individual layers of a filter pack or assembly. Pressure drop is increased by a decrease in both porosity and pore size.

In addition, they stated that coarse dust particles tend to accumulate at the front layer of the filter, causing caking, while fine dust particles tend to accumulate inside the filter. They utilized Bergman et al.'s (1978) mathematical pressure drop model as it considered various clogging mechanisms:

$$\frac{\Delta P}{Z} = 64\mu V \left(\frac{a_f}{d_f^2} + \frac{a_c}{d_c^2}\right)^{1/2} \left(\frac{a_f}{d_f} + \frac{a_c}{d_c}\right) \quad (2)$$

Where αf and αc stand for the porosity of the filter medium and cake medium and df and dc are the average particle size of the filter medium and cake medium. In Eq. (2), two different clogging mechanisms are taken into account, namely front caking and internal caking.

Sczap et al. (2023) modeled the impact of clogging on the pressure drop across the filter by modifying Bergman's equation [51]. They suggested that the front section could play a role in contributing to the overall pressure drop across the filter when caking is formed. Therefore, they rearranged Eq. (2) to include the thickness of the front (z_f) and back (z_b) sections:

$$\Delta P = 64\mu V\left(z_f \frac{a_f^{3/2}}{d_f^2} + z_b \frac{a_b^{3/2}}{d_b^2}\right) \quad (3)$$

There are three parameters here: thickness (z), porosity (α), and pore size (d). Based on their model, the cake thickness increases linearly when coarse dust particles are clogged at the front layers of the filter medium. Additionally, they found that the porosity (α_f) and mean pore size (d_f) of the clogged cake at the front layer remained constant during operation.

The mathematical model developed by Sczap et al. (2023) reveals the mechanism of filter clogging in flooded-bed dust scrubbers. This model successfully explains the increase in pressure drop across a filter panel. That study demonstrates the relationship between the pressure drop across the filter and the total accumulation of clogged dust particles within the filter. The theoretical approach was incorporated into the study presented in this chapter. Specifically, pressure drops across the mesh screen and the mass accumulation on the filter surface and within the filter package were continuously monitored. This was to establish a more accurate way for a better understanding of filter clogging and also to achieve more precise results about system performance.

5.3. Materials and Methods

5.3.1. Testing setup

The test setup used in this study is identical to that of Uluer et al. (under review). Salient details from that study are provided here for reader convenience.

A bench-scale scrubber was manufactured by scaling down the parameters of a typical underground coal mine FBS. With an internal cross-section of 0.152 m x 0.152 m, the chamber features a feeder, a jet mill grinder, an upwind section, a mesh screen unit, a shaker unit mounted

on the side of the mesh screen unit, a demister unit, a downwind section, a fan and a dust collector (Figure 5.3). Both the upwind and downwind sections are 1.22 meters long and have sampling stations for measuring air velocity and pressure. Each mesh screen and demister housing section is 0.36 m long, and both sections are equipped with grated blackwater sumps underneath. Through an actuating rod and clamping mechanism, the mesh screen was mounted to a Brüel and Kjær Type 4809 electromechanical shaker. SDG1000X function waveform generator generated the signals, which were applied to the shaker through a Brüel and Kjær Type 2718 power amplifier for base excitation (Figure 5.4).

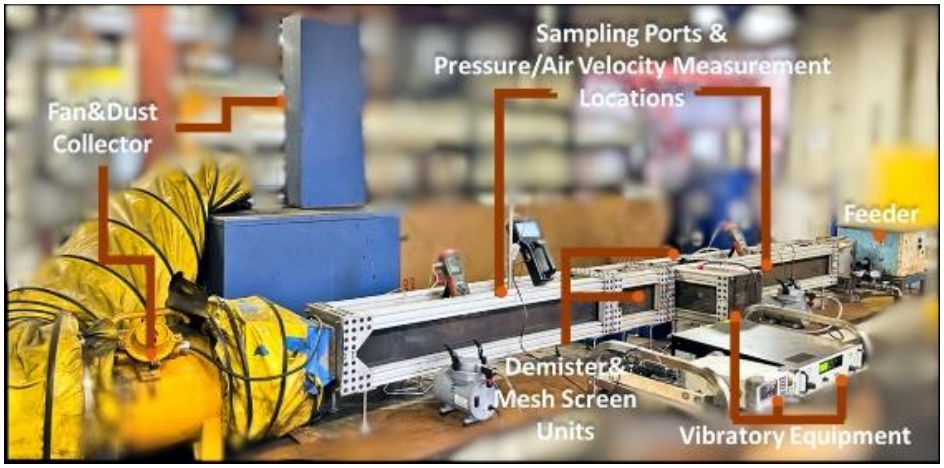

Figure 5.3: Testing setup

Figure 5.4: Vibratory instrument; Waveform generator (left), Power Amplifier (middle), Electro-mechanic shaker (right)

A volumetric screw feeder and a Trost jet mill are used to introduce dust material into the system. The two units are independent of one another and control dust size and concentration. This ensures that the dust introduced to the scrubber has fresh surfaces, as in a fully operational FBS. Keystone Black material obtained from Keystone Filler & Mfg Co. was fed to the jet mill. This coal dust contains a low inherent moisture content of 1.4 ± 0.10% with a dry ash content of 14.6% 0.04%. 95% of the feed dust produced by the jet mill passed approximately 10 microns and roughly 50% of it passed 5 mm microns. The dust material was selected because of its highly hydrophobic properties and high carbon content which mimics most RCMD materials. Air sampling cassettes preloaded with Teflon filters were used to collect dust samples from upwind and downwind sections during testing. Figure 5.5 shows the sampling ports positioned parallel to the incoming airstream at the chamber's centerline velocity.

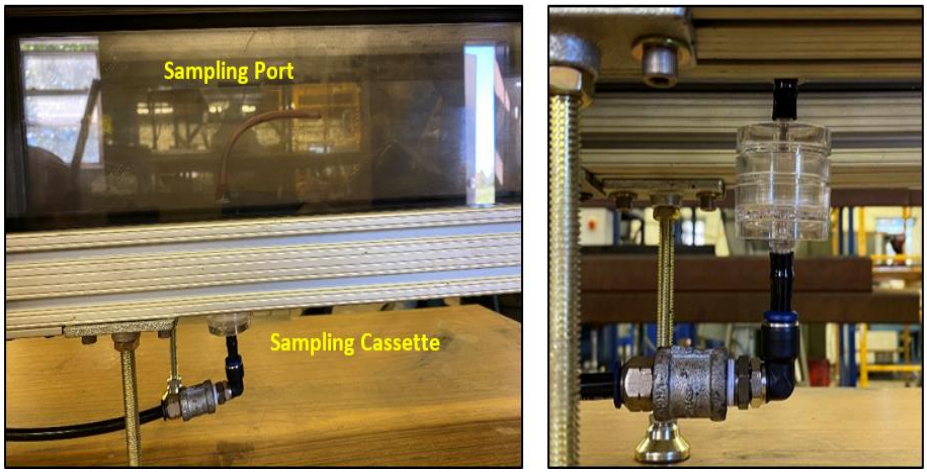

Figure 5.5: Gravimetric sampling system.

5.3.2. Methodology

An efficiency study was conducted to determine the effects of vibrating filter panels with various mesh designs. Each test was conducted for 5 minutes, during which pressure drop and air velocity were continuously measured using pitot tubes, hot wire anemometers, and digital manometers to

determine the level of mesh screen clogging. Each trial was conducted at an initial airspeed of approximately 9.5 m/s, and post-run air velocity measurements were taken to measure airflow loss. Dust particles were introduced into the system at a rate of 22.7 g/min. The sampling pump flow rate was kept at 5 lt/min. Previously optimized parameters for water flow rate and vibrational parameters were used in the tests [27]. These values were respectively 3 lt/min for water flow rate, 30 dB for amplifier gain, and 134 Hz for frequency. These values were maintained throughout the test runs to ensure consistency in the experiments.

Dust collection efficiency was determined by gravimetrically collecting dust-laden air samples upwind and downwind of the filter assembly. Following is an equation for calculating the collection efficiency (η) associated with each individual test trial:

$$\eta\ (\%) = \left(1 - \frac{m_{ds}}{m_{us}}\right) * 100$$

(m_{ds} = downstream sample weight, m_{us} = upstream sample weight)

Throughout the test, the dust particles on the mesh screen surface are also measured to determine how much dust accumulation is present on the mesh screen. After each run, the mesh screen was immersed in an ultrasonic bath for three minutes to remove dust particles and weighed after drying.

Customized filter frames were designed using a computer-aided design program and additively manufactured using a 3-D printer using the original mesh screen dimensions (Figure 5.6). In order to investigate how altered mesh design affects system performance, various layers of woven mesh and surface modifications were used. 10 layers, 20 layers, and 30 layers of 316 stainless steel woven mesh were used to fill the frames.

Figure 5.6: The mesh frame-adapter assembly is illustrated in a) CAD drawing, b) Additively manufactured frames

The performance of the system was also examined by testing modified screen chemistry with different surface treatments. The woven filter packages were made from 316 stainless steel with varying surface hydrophobicities. There are three types of screens: an untreated screen, a hydrophilic enhanced screen, and a hydrophobicized screen (Figure 5.7). The bare steel had a contact angle of 92.6±1.45 indicating that it was slightly hydrophobic [52]. Hydrophilic stainless steel meshes were made by heating them at 750° Cs for 20 minutes in a low-oxygen environment furnace. During this process, a blue magnetite layer formed on the surface. In response to this application, hydrophilic filters were produced by reducing the contact angle of bare steel to 37.1±1.00 [52]. The superhydrophobic filters were produced by coating the bare steel meshes with a commercial polymer agent. This application increased the contact angle of the steel to 156.6±0.88 [52].

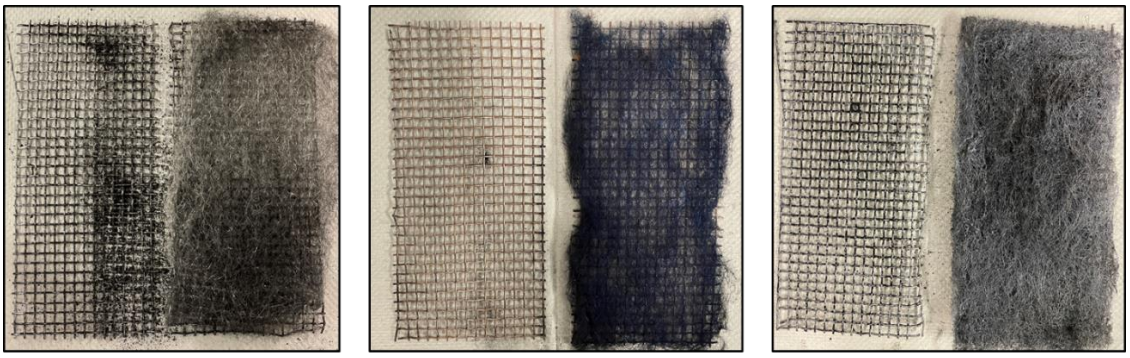

Figure 5.7: Appearance of the screen after a trial; a) Untreated (bare) screen, b) Hydrophilic screen, c) Hydrophobic screen

5.4. Results and Discussion

To evaluate the combined influence of mesh density and induced vibration on system efficiency, several tests were conducted using the bench-scale dust scrubber system. An in-house and purpose-built filter assembly was utilized to modify the filter package thickness (Figure 5.6). In this trial, three separate mesh densities, namely 30 layers, 20 layers, and 10 layers of woven stainless steel, were evaluated in both vibration-enhanced and vibration free settings.

Dust collection efficiency data from these tests is shown in Figure 5.8. The data obtained from the dust collection efficiency calculations showed that regardless of what filter package were used when the mesh screen is enhanced with the vibration, better results are obtained in both wet and dry conditions compared to the tests conducted in static condition. These differences are sometimes negligibly small for some operational conditions. However, an improvement of about 3.5% was obtained in the collection efficiency with the 30-layer screen in the wet vibration-enhanced operational condition compared to the same screen type under the wet vibration-free condition. The 30-layer wet vibration-enhanced operational condition was the most efficient run (92%). This is followed by the 30layer-wet vibration-free state with 89% efficiency. When each operational condition is evaluated in its own class, it will be seen that the lowest efficiency of that operational condition is always taking place with a 10-layer screen. The maximum achieved

efficiency with the 10-layer screen was under the wet vibration-enhanced operational condition (80%) and the lowest was about 77% under the dry vibration-free condition.

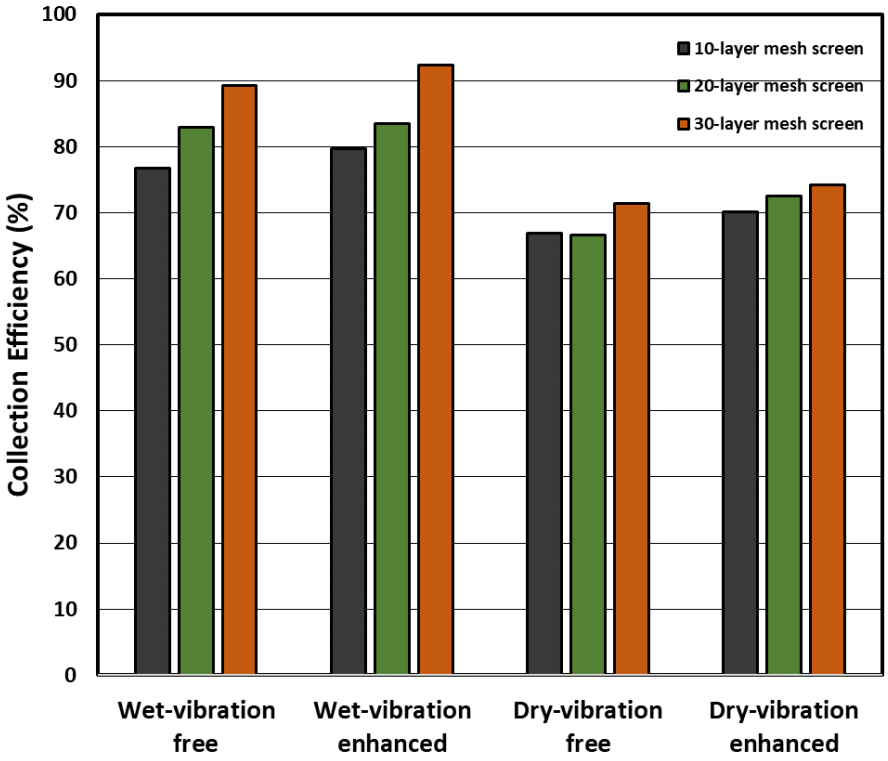

Figure 5.8: Collection efficiency by different mesh screen packages with various filter layering under various operational modes

While collection efficiency is one evaluation metric, it must be considered alongside other metrics of performance. As such, throughout the same tests, the pre-test and post-test conditions of the downstream airflow were monitored. The difference of these two values shows how much airflow loss occurs through the test duration. The greater the detected loss in airflow implies greater mesh clogging and thus lower the overall system efficiency. Data from this analysis is shown in Figure 5.9. The highest airflow loss occurred in the test with a dry and vibration-free operational condition with 30-layer screen (3.5 m/s). The conditions with the least air loss were the tests with a 10-layer screen in each operational condition. The lowest airflow loss occurred when a 10-layer mesh screen was used under the wet vibration-enhanced operational condition (0.81 m/s).

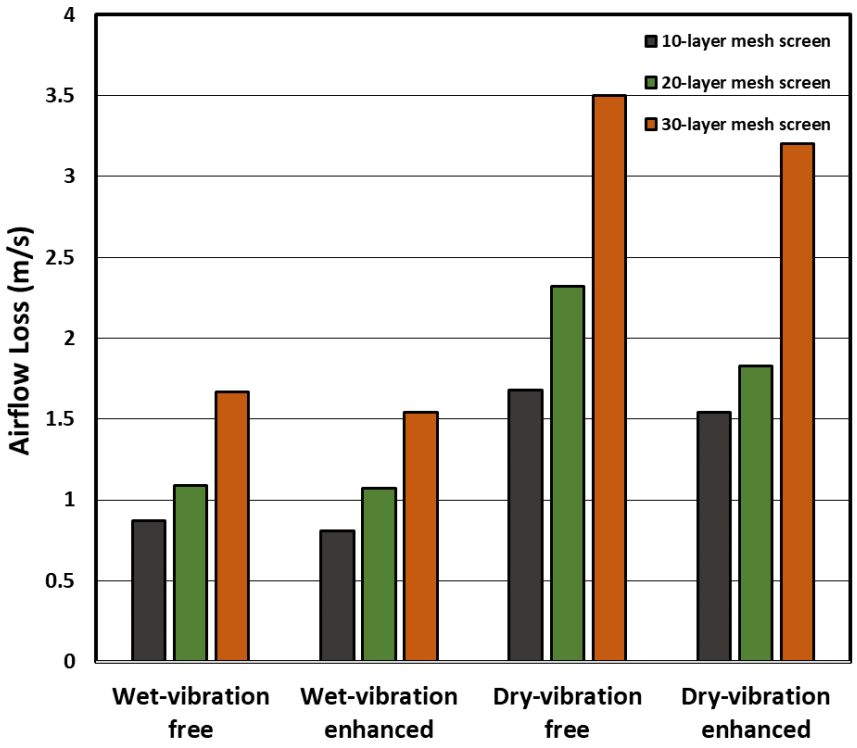

Figure 5.9: Downwind section airflow loss on mesh screen with different filter layering under various operational modes

As a supportive indicator to the airflow loss parameter, the pressure difference data read digitally from the downstream and upstream directions of the system continuously throughout each run (Figure 5.10). This data shows that the pressure in the wet condition tests always starts higher than the dry condition test, likely due to the water layer that coats the mesh and reduces mesh porosity. However, when the pressure change is monitored throughout the test, the data shows that the pressure changes in the tests performed under wet conditions is much less than the increase in pressure changes under dry conditions. Because the initial pressure created by the water sprayed on the screen causes the initial pressure in the tests performed in wet conditions to start from high. The data show that the pressure difference in dry condition reaches much higher values (avg. 20% increase) than in wet condition (avg. 3.13% increase). The pressure drop increase throughout the test explains the partial clogging of the mesh screen. In the wet condition, no significant differences

were observed in the vibrating and non-vibrating conditions. In addition, in each operational condition, the minimum increase in pressure difference was obtained in the tests performed with the 10-layer filter assembly under wet vibration-enhanced operational condition (2.2% increase), and the maximum pressure difference is obtained in the tests performed with the 30-layer filter assembly (22.4% increase).

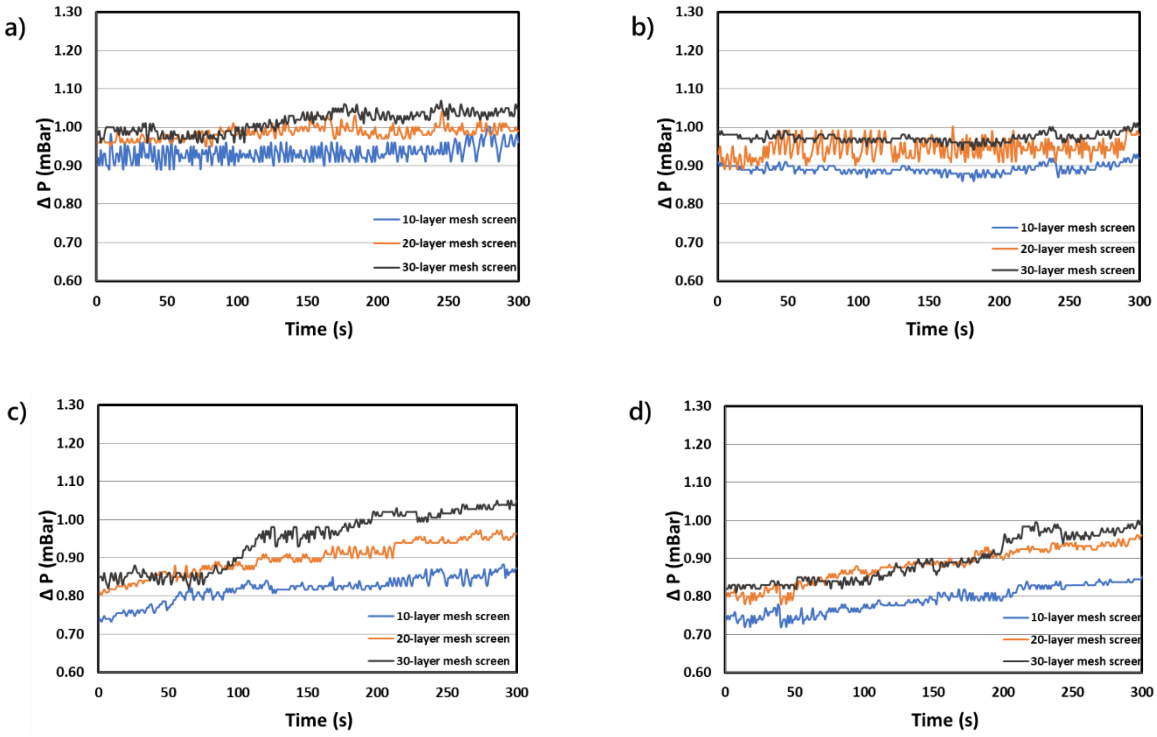

Figure 5.10: Δp across mesh screen with different screen packages of a) Wet and vibration-free mode b) Wet and vibration mode c) Dry and vibration-free mode d) Dry and vibration mode

In addition to these data, in order to further support the assessment of system efficiency, after each test, the filter assembly of that test was passed through an ultrasonic bath. The mass of material obtained from this procedure is indicative of the amount of dust accumulated on the filter during the test. This parameter is one of the most important parameters showing the clogging of the filter. As shown in Figure 5.11, the operational condition in which the largest mass of particles accumulated on the filter during the test was the test with a 30-layer filter assembly under dry vibration-free condition (7.2 g). The operational condition where the least dust accumulation

occurred on the mesh screen surface was the test with a vibrating 10-layer filter assembly under wet condition (2.9 g).

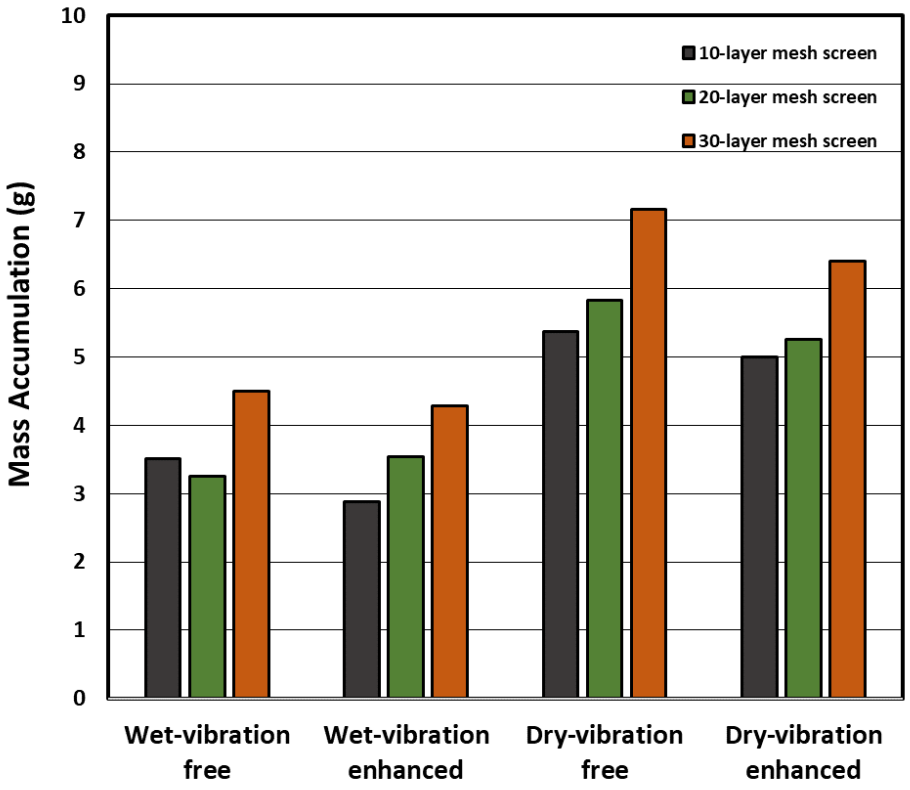

Figure 5.11: Mass Accumulation on mesh screen with different layering under various operational modes

Although vibrating the mesh screen has been promising in many cases, it can be inferred from the combined data that there are a few situations where the static state is more advantageous. For example, while the air loss in the wet vibrating condition decreased by 7.78 % compared to the vibration-free condition in the tests performed with the 30-layer mesh screen, the airflow loss in the wet test using the 20-layer vibrating filter increased by 1.87 % compared to the vibration-free condition. Similarly, a decrease of 4.77% is observed in the vibrating 30-layer screen under the wet condition compared to the vibration-free condition, while an increase of 9.14% is observed in the amount of dust accumulated on the filter surface with the vibrating 20-layer mesh screen

compared to the vibration-free condition. When all these data are combined, the performance of the 10-layer screen is remarkable in terms of air loss and dust accumulation on the filter. However, when the system efficiency is also considered, significant decreases are observed in the 10-layer screen compared to the higher-layer filter packages in each operational situation. The reason for its less overall efficiency is that the dust-laden air passes the 10-layer filter screen without getting captured by water droplets more easily than others. Since less dense screens cause an increase in the amount of material that can move downstream of the system, they are negatively affecting the system efficiency.

When all the test results are considered together, the data show that the lowest air velocity and pressure loss and the lowest amount of mass accumulated on the screen is the test performed under the wet vibrating operational condition performed with a 20-layer filter.

These results correlate well with a study conducted by Sczap et al. (under review) which investigated the clogging of a flood-bed scrubber filter panel both experimentally and theoretically. The results indicated that the pressure drop evolved differently with the pore structure of the filter medium. In addition, the pressure drop increased with dust accumulation within the filter [51]. Increasing the density of the filter media results in increased dust accumulation within the mesh screen panel, which increases the pressure drop across the mesh screen.

The surface of the filter panels can be coated in different ways to increase wettability and enhance particle-liquid adhesion. Following the protocols explained in methodology section, super hydrophobic filter coatings were obtained using a commercial polymer agent using the application instructions provided by the vender. Alternatively, the hydrophilic filters were obtained by heating them in a high-temperature low-oxygen environment furnace at 750° C for 20 minutes, allowing the formation of a blue magnetite layer on the surface of the stainless-steel filter.

Data from these tests are shown in Figure 5.12 to Figure 5.15 and include measured of both dust collection efficiency and clogging mitigation. First, Figure 5.12 shows the dust collection efficiency for the specified operational conditions. Across all conditions, the hydrophilic surfaces imparted the highest collection efficiency, with the differences being more pronounced for the vibration free conditions as opposed to the vibration enhanced conditions.

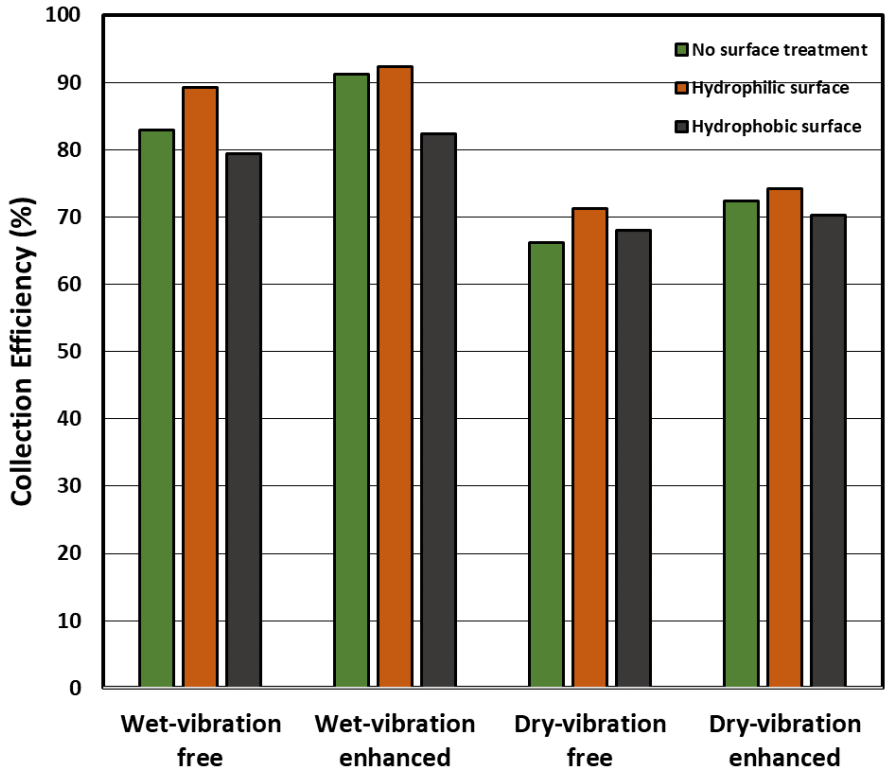

Figure 5.12: Collection efficiency by different mesh screens with various surface treatments under various operational modes

Airflow loss data for the tested operational conditions are shown in Figure 5.13. As anticipated, the dry conditions showed the highest airflow loss, and in all cases, the hydrophilic mesh outperformed the other two. Overall, this data follows the same trend as that of collection efficiency with the difference between the various treatments being more pronounced in the vibration free cases.

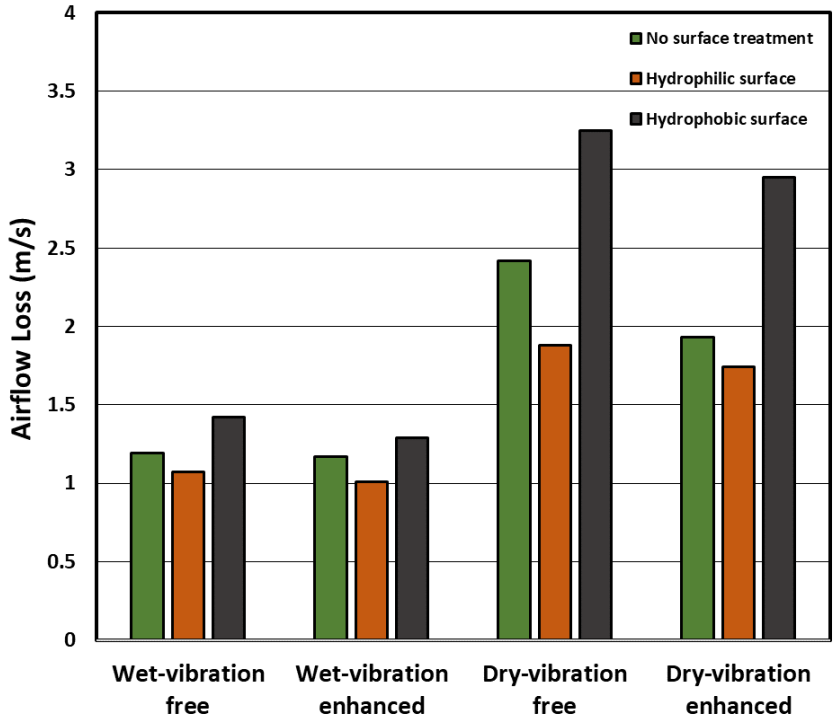

Figure 5.13: Downwind section airflow loss on mesh screen with different surface treatment applications under various operational modes

Similarly, Figure 5.14 shows the real time pressure drop data through the test duration. For the wet-condition tests, the pressure drop was similar for all three surface treatments; however, significant deviations were observed in the dry tests. Generally, the hydrophilic and bear meshes performed similarly, with the hydrophobic mesh exhibiting a significantly higher pressure drop.

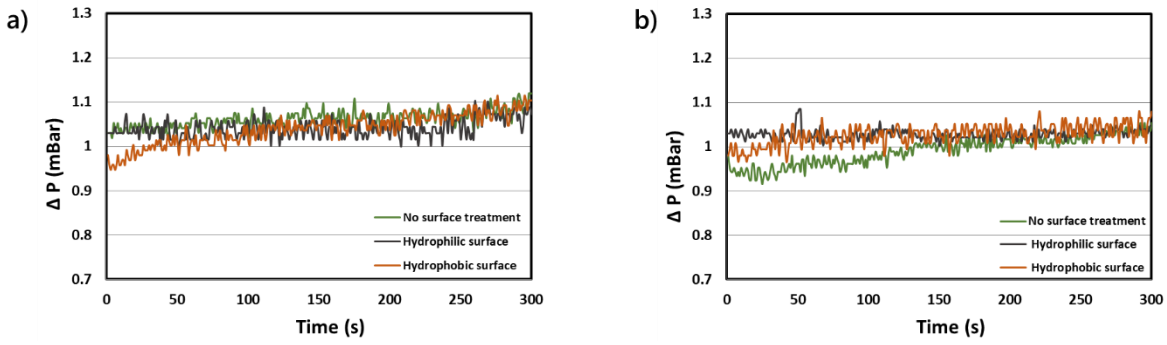

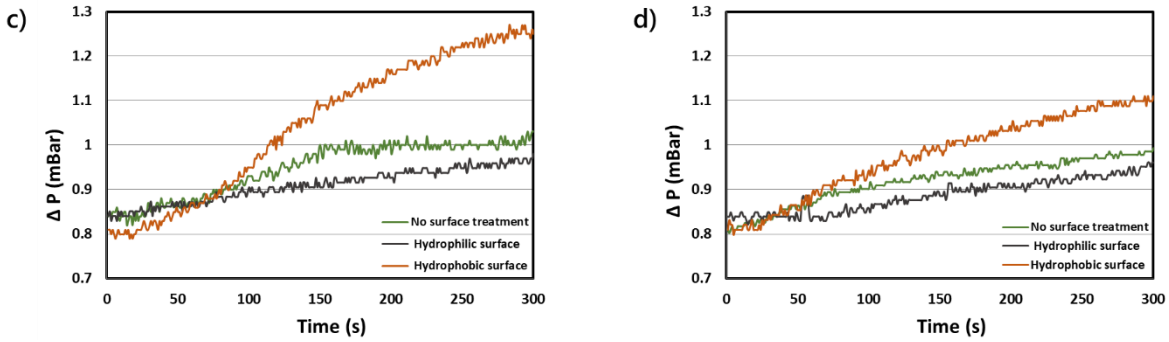

Figure 5.14: Δp across mesh screen with different surface treatments of a) Wet and vibration-free mode b) Wet and vibration mode c) Dry and vibration-free mode d) Dry and vibration mode

Lastly, the mass of particle accumulation on the filter, which is another parameter that indicates the clogging process of the mesh screen and shows the self-cleaning capacity of the filter, was examined. Data from this analysis is shown in Figure 5.15, and closely follows the trends of airflow loss shown in Figure 5.13.

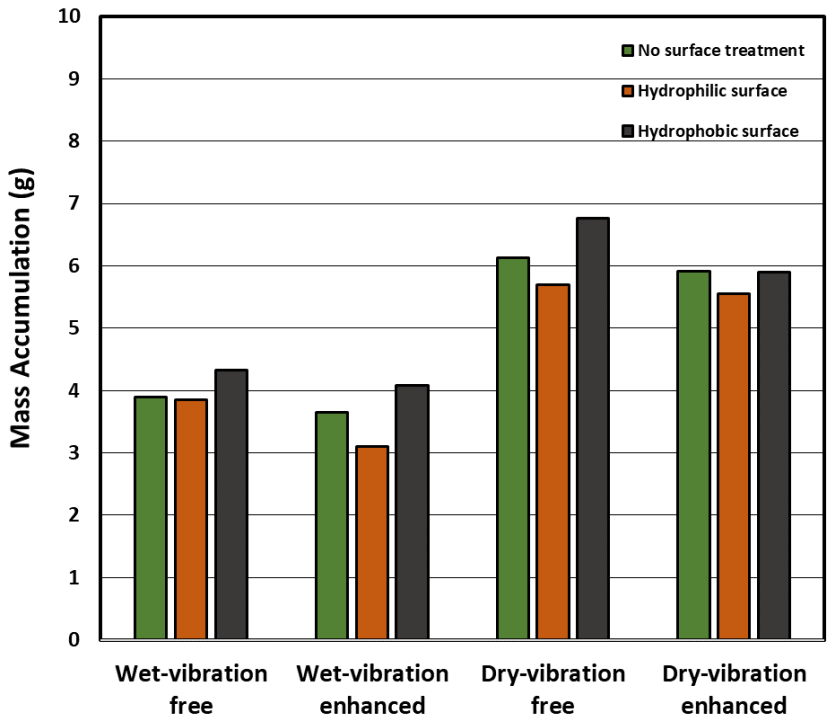

Figure 5.15: Mass Accumulation on mesh screen with different surface treatments under various operational modes

When the tests carried out under various operational conditions with different surface modifications are examined together, hydrophobic surface modifications tended to reduce system efficiency relative to the baseline, while hydrophilic treatment tended to improve conditions. This results closely aligns with that of the laboratory testing and validates the approach employed in that section. In explaining the findings, when water contacts hydrophilic surfaces, it forms a film, whereas when it contacts hydrophobic surfaces, it beads up. Since water droplets are highly mobile, if the surface becomes hydrophobic, the area covered by water droplets is significantly reduced of the total mesh wire surface area. Besides, hydrophilic coating is increasing the amount of liquid surface area on mesh, which increases chances of dust particles getting captured by the water droplets.

The final portion of the study utilized a three-factor Box-Behnken design (BBD) to examine the combinatory effects of mesh design, surface modifications, and vibrational frequency on system performance. The factors and levels associated with the independent variables are listed in Table

5.1. In total, 15 tests were carried out with different combinations of the variables. To determine the size distributions of the dust removed by the filter, upwind and downwind dust samples were analyzed using a Microtrac S3500 laser particle size analyzer.

Table 5.1 Independent variables and their respective values

Factors	**Level**		
	Low (-1)	**Medium (0)**	**High (+1)**
Filter Density (layering)	10-layer	20-layer	30-layer
Surface Treatment	Hydrophobic Treatment	No Surface Treatment	Hydrophilic Treatment
Frequency (Hz)	0	67	134

Response surface plots were created with the results and are shown in Figure 5.16 through Figure 5.20. Each figure shows the effect of two different variables on response by keeping one of the three variables used during the experiment constant. The collection efficiency surface (Figure 5.16) was plotted from the data obtained with the gravimetric sampling. In Figure 5.16a, the effect of the interaction of the filter density with the surface treatment on the efficiency is examined. The effect of the interaction of the filter density with the frequency on the efficiency shown examined in Figure 5.16b. The highest efficiencies (over 90%) were obtained when the filter frame filled with 30-layer, and at the same time the mesh surface was hydrophilic. Figure 5.16c shows the combinatory effects of vibrational frequency and surface modification. Compared to the filter density and surface modifications, the frequency had little impact on the collection efficiency. However, it is worth noting that the collection efficiencies approached maximum levels under the conditions where the densest hydrophilic filter excited with 134 Hz.

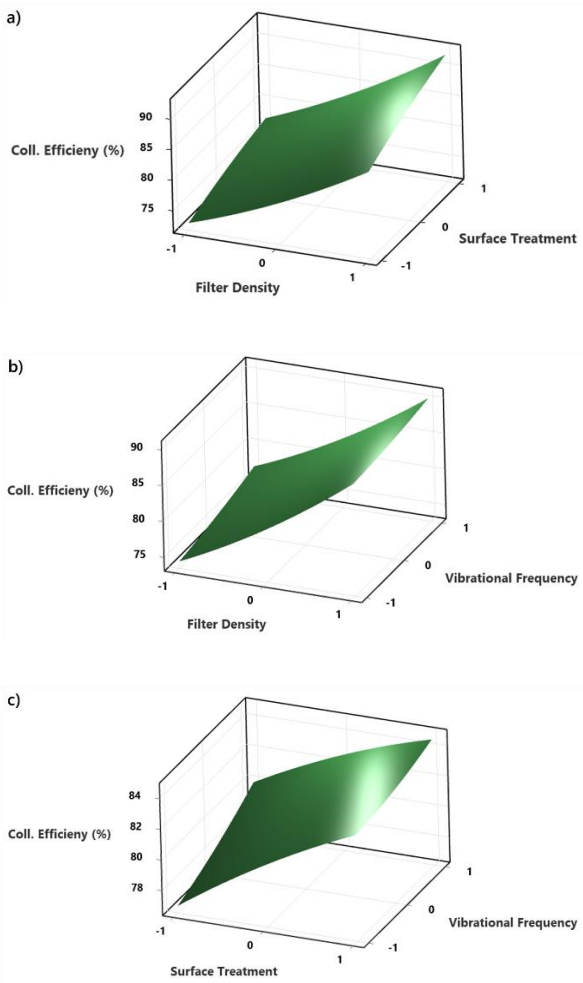

Figure 5.16: Surface Plots of Collection Efficiency (%) vs a) Filter density (-1: 10-layer, 0: 20-layer, +1: 30-layer) and surface treatment (-1: Hydrophobic, 0: Bare surface, +1: Hydrophilic), b) Filter density (-1: 10-layer, 0: 20-layer, +1: 30-layer) and frequency (-1: 0 Hz, 0: 67 Hz, +1: 134 Hz), c) Surface treatment (-1: Hydrophobic, 0: Bare surface, +1: Hydrophilic) and frequency (-1: 0 Hz, 0: 67 Hz, +1: 134 Hz).

In Figure 5.17, the effects of the binary interactions of the variables used in the test on the air velocity lost during the test were examined. In Figure 5.17a where the effect of the filter density with the surface treatment pair on air velocity loss is examined, the data shows that the air velocity loss is most pronounced (over 1.4 m/s) when the filter density is at its densest level (30-layer), and when the hydrophobic coating was applied to the mesh screen. Figure 5.17b shows that the air velocity loss reaches the highest levels with the 30-layer mesh screen in a vibration-free

environment. Similarly, the hydrophobic surface modification increases the airflow losses by over 1.2 m/s in a vibration-free environment. Altogether, the data show that air velocity loss can be minimized by using hydrophilic mesh screen package with lower mesh density and when vibrating the mesh screen around 134 Hz. Additionally, Figure 5.18 shows the effect of the binary interactions of the variables used in the experimental design on the pressure drops across the mesh screen. As Bernoulli's equation defines, the changes in the pressure drop between upstream and downstream in a chamber and the air velocity in the system are directly related. Thus, the increases in pressure drop tended to be similar to the losses in air velocity. A 30-layer hydrophobic filter tested in a vibration-free environment produced the greatest increase in pressure drop. The least increase in pressure difference was found with the highest frequency value (134Hz) and the least dense (10 layers) hydrophilic filter package.

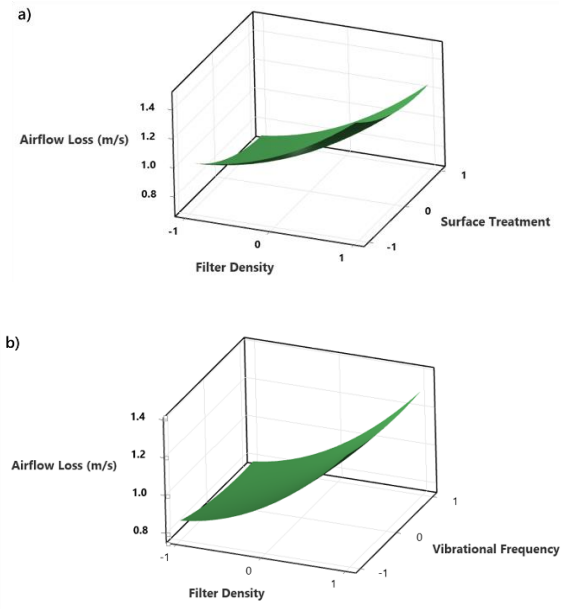

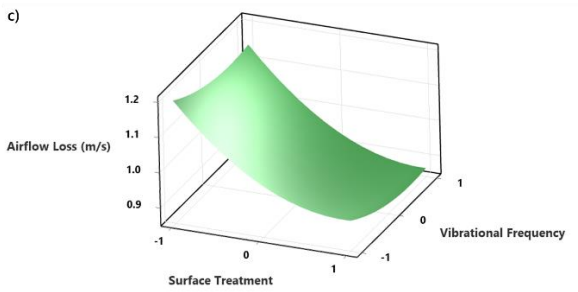

Figure 5.17: Surface Plots of Upstream Airflow Loss (m/s) vs a) Filter density (-1: 10-layer, 0: 20-layer, +1: 30-layer) and surface treatment (-1: Hydrophobic, 0: Bare surface, +1: Hydrophilic), b) Filter density (-1: 10-layer, 0: 20-layer, +1: 30-layer) and frequency (-1: 0 Hz, 0: 67 Hz, +1: 134 Hz), c) Surface treatment (-1: Hydrophobic, 0: Bare surface, +1: Hydrophilic) and frequency (-1: 0 Hz, 0: 67 Hz, +1: 134 Hz).

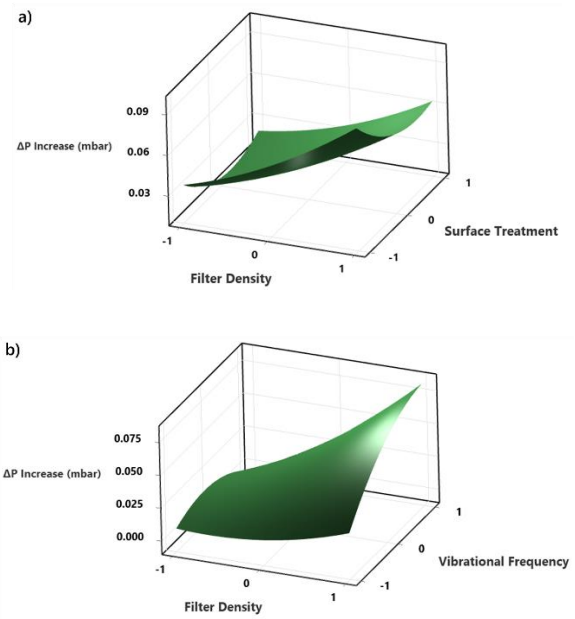

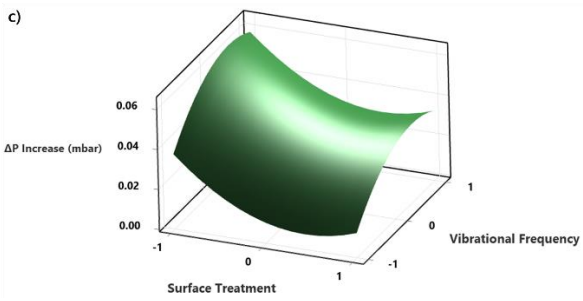

Figure 5.18: Surface plots of pressure drop across the mesh screen (mbar) vs a) Filter density (-1: 10-layer, 0: 20-layer, +1: 30-layer) and surface treatment (-1: Hydrophobic, 0: Bare surface, +1: Hydrophilic), b) Filter density (-1: 10-layer, 0: 20-layer, +1: 30-layer) and frequency (-1: 0 Hz, 0: 67 Hz, +1: 134 Hz), c) Surface treatment (-1: Hydrophobic, 0: Bare surface, +1: Hydrophilic) and frequency (-1: 0 Hz, 0: 67 Hz, +1: 134 Hz).

To determine the self-cleaning capacity of the mesh screen, the amount of mass accumulations within the figure was measured after each test. Figure 5.19 shows the data from this analysis. As anticipated from the pressure drop data, the static test with a 30-layer mesh screen and increased hydrophobicity yielded the highest mass accumulation (over 4.8 g collected over a five-minute test). Under the conditions tested, frequency did not have a significant effect on the dust accumulation (Figure 5.19b); however, a hydrophilic mesh combined with vibration was shown to be most effective, accumulating less than 3 g over the test period.

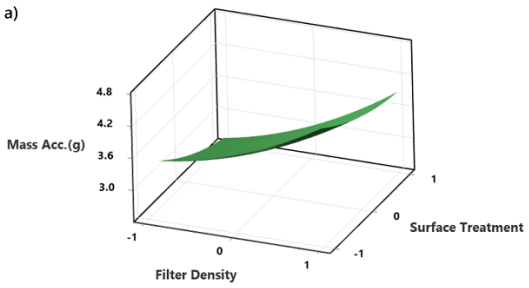

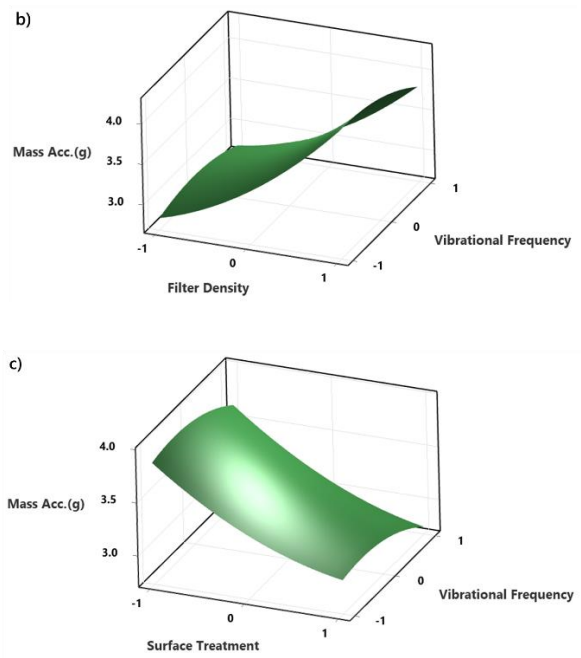

Figure 5.19: Surface plots of mass retain within the mesh screen (g) vs a) Filter density (-1: 10-layer, 0: 20-layer, +1: 30-layer) and surface treatment (-1: Hydrophobic, 0: Bare surface, +1: Hydrophilic), b) Filter density (-1: 10-layer, 0: 20-layer, +1: 30-layer) and frequency (-1: 0 Hz, 0: 67 Hz, +1: 134 Hz), c) Surface treatment (-1: Hydrophobic, 0: Bare surface, +1: Hydrophilic) and frequency (-1: 0 Hz, 0: 67 Hz, +1: 134 Hz).

Lastly, Figure 5.20 shows the interaction between vibration, filter density, and surface treatment in the reduction of fine respirable dust material (-2.5 μm). In Figure 5.20a, the test with a hydrophobic mesh screen shows the lowest values for respirable material reduction (below 60%), regardless of the number of layers in the filter pack. In contrast, when all figures are combined, when the surface is hydrophilic and the filter thickness is 30 layers, the amount of respirable substances eliminated increases by over 80%.

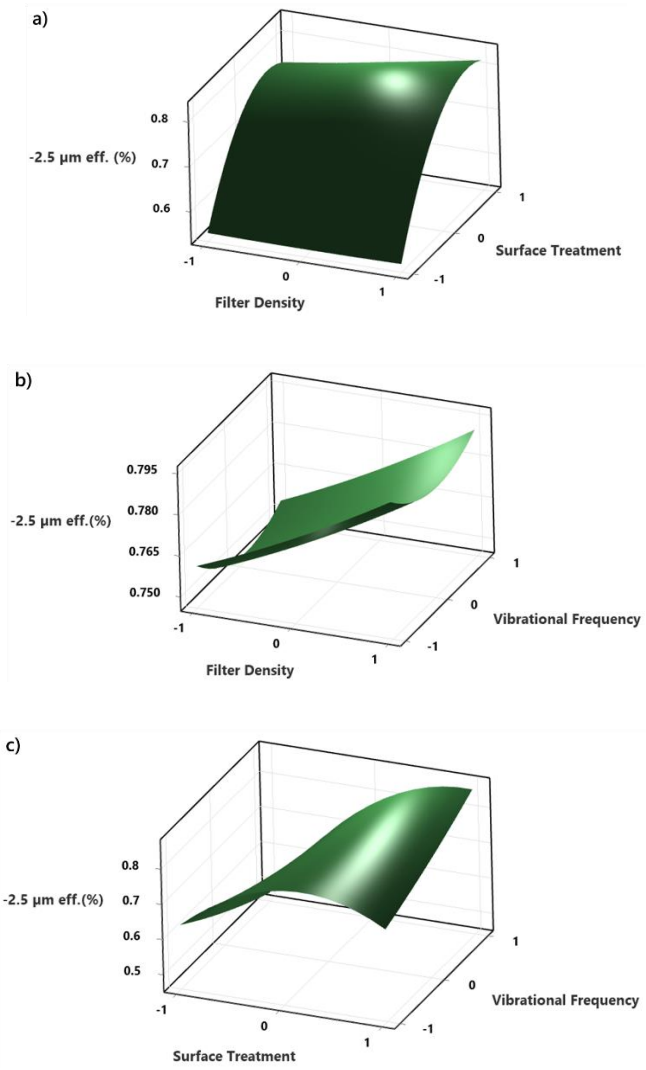

Figure 5.20: Surface plots reduction in respirable size (%) vs a) Filter density (-1: 10-layer, 0: 20-layer, +1: 30-layer) and surface treatment (-1: Hydrophobic, 0: Bare surface, +1: Hydrophilic), b) Filter density (-1: 10-layer, 0: 20-layer, +1: 30-layer) and frequency (-1: 0 Hz, 0: 67 Hz, +1: 134 Hz), c) Surface treatment (-1: Hydrophobic, 0: Bare surface, +1: Hydrophilic) and frequency (-1: 0 Hz, 0: 67 Hz, +1: 134 Hz).

These results compare well with a study by Sczap et al., 2023 which reports that mesh design and surface hydrophobicity significantly impact the clogging rate of the filter in an FBS. Decreasing the contact angle of the mesh screen surface improves the system performance and extends the life of the filter panel by preventing rapid mass accumulation within the filter. Additionally, as mesh

screen package thickness increases, dust particles accumulate more rapidly within the filter panel, increasing pressure drop and lowering system performance [51]. Inversely, as the filter media density decreases, more void areas appear within the filter media. As a result, some dust material passes through the mesh panel without being captured by water droplets. The less dense filter media does not offer better dust collection efficiency for this reason. The hydrophilic and vibrationally enhanced mesh screen, however, sustains more airflow through the system, slows the increase in pressure drop, and improves mass retention within the filter. Therefore, less dense hydrophilic and vibrating mesh screen panels can outperform higher-density panels for longer periods of time.

5.5. Conclusion and Summary

Flooded bed dust scrubbers utilized in underground mining operations are particularly susceptible to clogging. As dirty areas in the mesh become loaded with particles, the pressure drop across the screen increases, resulting in reduced airflow volumes and lower overall air cleaning efficiency. Thus, one way to improve overall system efficiency is to continuously remove particles from congested regions, which allows the system to maintain higher interior airflow rates. In this study, modifications to the filter surface and mesh thicknesses were examined to determine their combined effect on vibration-enhanced flooded bed dust scrubber performance. Tests were performed in laboratory-scale scrubber unit using mesh screens with different surface treatments and filter media densities. The effects of various factors were measured in both a wet and dry environment, as well as with and without vibrations. As part of the tests, air velocity, pressure drop, and the weight of dust particles accumulated inside the mesh screen were measured.

Overall, the results confirm the benefit of a vibrating mesh FBS, as has been demonstrated in prior studies [27,34,35]. Moreover, the results show that the system can be further optimized through control of the mesh density and particularly the mesh hydrophobicity. Results with different mesh thicknesses generally confirm prior studies showing that higher mesh density increased dust collection; however, also shows higher clogging potential as demonstrated through both mass accumulation and pressure drop. Interestingly, testing with different mesh surface modifications showed that optimal results were obtained with hydrophilic mesh surface, which exhibited reduced

clogging but similar dust collection as compared to the hydrophobic and untreated counterparts. In summary, the results showed that the system performance can be optimized when using hydrophilic 20- or 30-layer filters that are excited by frequencies between 67-134 Hz. These benefits were most notable in the -2.5 micron size class, where proper optimization of the mesh frequency, mesh wettability, and mesh density can lead to nearly 30% increases fine dust removal. Ultimately, this study provides a substantial contribution to the understanding of mesh design, surface modifications, and vibrational effects in shaping dust scrubber system efficiency.

Authorship contribution statement

Mahmud Esad Uluer: Conceptualization, Methodology, Testing, Formal analysis, Data Curation, Writing - Original Draft, Writing - Review & Editing, Visualization

Aaron Noble: Resources, Writing - Review & Editing, Supervision, Project administration, Funding acquisition

Role of Funding Source

This study was sponsored by the Alpha Foundation for the Improvement of Mine Safety and Health, Inc. (Alpha Foundation). The views, opinions, and recommendations expressed herein are solely those of the authors and do not imply any endorsement by the Alpha Foundation, its directors, and staff.

Declaration of Competing Interest

The authors declare that they have no known competing financial interests or personal relationships that could have appeared to influence the work reported in this manuscript.

5.6. References

1. IARC, 1997 International Agency for Research on Cancer (IARC), Working Group on the Evaluation of Carcinogenic Risks to Humans, International Agency for Research on Cancer and World Health Organization, Silica, Some Silicates, Coal Dust and Para-Aramid Fibrils (No. 68) World Health Organization (1997)

2. ISO, 1995 International Organization for Standardization (ISO) Air Quality-Particle Size Fraction Definitions for Health Related Sampling ISO Standard 7708 (1995)

3. OSHA, 2010 Occupational Safety and Health Administration (OSHA) Occupational Exposure to Respirable Crystalline Silica – Review of Health Effects Literature and Preliminary Quantitative Risk Assessment, OSHA-2010-0034 (2010)

4. WHO, 1999 World Health Organization (WHO) Hazard Prevention and Control in the Work Environment: Airborne Dust Who/Sde/Oeh/99.14 (1999), pp. 1-96

5. V. Castranova, V. Vallyathan (2000), Silicosis and coal workers' pneumoconiosis, Environ. Health Perspect., 108 (Suppl. 4), pp. 675-684

6. ACGIH (1999), Particle size-selective sampling for health-related aerosols J.H. Vincent (Ed.), American Conference of Governmental Industrial Hygienists Air Sampling Procedures Committee, Cincinnati, OH, USA (ISBN 1-1882417-30-5)

7.S.E. Mischler, E.G. Cauda, M.Di Giuseppe, L.J. McWilliams, C.S. Croix, M. Sun, J. Franks, L.A. Ortiz, (2016), Differential activation of RAW 264.7 macrophages by size-segregated crystalline silica, J. Occup. Med. Toxicol., 11 (1), p. 57, 10.1186/s12995-016-0145-2

8. J. Colinet, J.M. Listak, J.A. Organiscak, J.P. Rider, A.L. Wolfe, (2010), Best Practices for Dust Control in Coal Mining, Department of Health and Human Services, Centers for Disease Control and Prevention, National Institute for Occupational Safety and Health, Office of Mine Safety and Health Research.

9. M.J. Sapko, K.L. Cashdollar, G.M. Green, (2007), Coal dust particle size survey of US mines J. Loss Prev. Process Ind., 20, pp. 616-620, 10.1016/j.jlp.2007.04.014)

10. Thomas Sporn, V.R., 2013. Consideration of Occupational Lung Disease and Pneumoconiosis in Forensic Pathology. Sage, 3(4).

11. MSHA, Code of Federal Regulations Title 30, Part 70.100 (Respirable Dust Standards). 2016.

12. Centers for Disease Control (CDC), (2006), Advanced cases of coal workers' pneumoconiosis-two counties, Virginia MMWR, 55, p. 33

13. National Institute for Occupational Safety and Health (NIOSH), 1974. Criteria for a Recommended Standard – Occupational Exposure to Respirable Coal Mine Dust, DHEW Publication No. 95-106.

14. E. Suarthana, A.S. Laney, E. Storey, J.M. Hale, M.D. Attfield, (2011), Coal workers' pneumoconiosis in the United States: regional differences 40 years after implementation of the 1969 Federal Coal Mine Health and Safety Act Occup. Environ. Med., 68, pp. 908-913, 10.1136/oem.2010.063594

15. D.J. Blackley, C.N. Halldin, A.S. Laney, (2014), Resurgence of a debilitating and entirely preventable respiratory disease among working coal miners, Am. J. Respir. Crit. Care Med., 10.1164/rccm.201407-1286LE

16. U.S. Department of Labor (2014) Final rule.

http://arlweb.msha.gov/regs/fedreg/final/2014finl/2014-09084.asp. Accessed June 5, 2022.

17. Wang W, Peng FF (1991) Analyses of respirable dust distributions with multiple dust sources on longwall faces. Proc. of Soc. for Mining, Metallurgy & Exploration. pp 367–375

18. Colinet JF, Spencer ER, Jankowski RA (1997) Status of dust control technology on U.S. longwalls. Proceedings of 6th International Mine Ventilation Congress. pp 345–351

19. Arya S, Sottile J, Novak T (2018) Development of a flooded-bed scrubber for removing coal dust at a longwall mining section. Saf Sci 110:204–213. https://doi.org/10.1016/j.ssci.2018.08.003

20. Arya S, Sottile J, Rider JP, Colinet JF, Novak T,Wedding C (2018) Design and experimental evaluation of a flooded-bed dust scrubber integrated into a longwall shearer. Powder Technol 339:487–496. https://doi.org/10.1016/j.powtec.2018.07.072

21. Arya S, Novak T, Saito K et al (2019) Empirical formulae for determining pressure drop across a 20-layer flooded-bed scrubber screen. Mining, Metallurgy & Exploration, 36(6), 1169-1177. https://doi.org/10.1007/s42461-019-0091-5

22. Arya S (2018) Investigation of the effectiveness of an integrated flooded-bed dust scrubber on a longwall shearer through laboratory testing and CFD simulation. Doctoral Dissertation, Mining Engineering, University of Kentucky. https://doi.org/10.13023/ETD.2018.074

23. Reed W, Taylor C (2007) Factors affecting the developing of mine face ventilation systems in the 20th century, SME Annual Conference and Expo, Denver, CO

24. S. R. Cowley, B.S. McCoy (1993) "Wet scrubber apparatus," U. S. Patent 5,178,654.

25. Campbell, J. A., Moynihan, D. J., Roper, W. D., & Willis, E. C. (1983). U.S. Patent No. 4,380,353. Washington, DC: U.S. Patent and Trademark Office.

26. Colinet, J. F., & Jankowski, R. A. (2000). Silica collection concerns when using flooded-bed scrubbers. Mining Engineering (Littleton, Colorado), 52.

27. Uluer, M.E., Shigo, M., Amini, S. H., Noble, A., (under review). "An Exploratory Investigation on the Effectiveness of a Novel Vibration-Enhanced Flooded Bed Dust Scrubber", Mining& Metallurgy and Exploration. (Manuscript submitted for publication.)

28. Colinet, J., Reed, W. R., & Potts, J. D. (2013). Impact on respirable dust levels when operating a flooded-bed scrubber in 20-foot cuts. Pittsburgh, PA Spokane, WA

29. National Institute for Occupational Safety and Health (2002) Exposure to Silica Dust on Continuous Mining Operations Using Flooded-Bed Scrubbers, Applied Occupational and Environmental Hygiene, 17:5, 322-323, https://doi.org/10.1080/10473220252864888

30. Salazar, A. J., Saito, K., Alloo, R. P., & Tanaka, N. (2000). U.S. Patent No. 6,093,250. Washington, DC: U.S. Patent and Trademark Office.

31. Kumar, A. R., & Schafrik, S. (2020). Multiphase CFD modeling and laboratory testing of a Vortecone for mining and industrial dust scrubbing applications. Process Safety and Environmental Protection, 144, 330-336. https://doi.org/10.1016/j.psep.2020.07.046

32. Taylor A., Schafrik S., Kumar A.R. (2019). The Vortecone: A new maintenance-free wet scrubber device. Future Mining, Sydney, NSW.

33. Kumar, A. R., Schafrik, S., & Velasquez, O. (2020). Designing, modeling, and laboratory testing of a non-clogging impingement type filter for mining dust scrubbers. Mining, Metallurgy & Exploration, 37(6), 1911-1918. https://doi.org/10.1007/s42461-020-00311-9

34. Lu, Z., Rath, A., Amini, S. H., Noble, A., & Shahab, S. (2022). A computational fluid dynamics investigation of a novel flooded-bed dust scrubber with vibrating mesh. International Journal of Mining Science and Technology, 32/3, 525-537, https://doi.org/10.1016/j.ijmst.2022.03.002

35. Janjua, A.N., Shaefer M., Amini, S.H., Noble, C.A., Shahab, S. (under review). Vibration Energy Harvesting in Underground Continuous Mining: Dynamic Characteristics and Experimental Research of Field Data. Applied Energy. (Manuscript submitted for publication.)

36. King, R. P. (2001). Classification based on sieving–vibrating screens. Modeling and simulation of mineral processing systems. Elsevier. 81-86.

37. Chen, Z., Zhou, Z., & Peng, J. (2022). Dust Removal Mechanism of the Vibrating String Filter with Charged Water Mist. International Journal of Rotating Machinery, 2022. https://doi.org/10.1155/2022/5713983

38. Mishin, I. F., El'bert, E. I., Belikov, V. I., Tumanov, A. N., & Kachaev, V. K. (1975). Cleaning coal tar by vibrating-screen filtration, surfactant treatment, and short-term clarification. Coke Chem., USSR (Engl. Transl.);(United Kingdom), 4.

39. Yang, X., Wang, H., & Chase, G. G. (2015). Performance of hydrophilic glass fiber media to separate dispersed water drops from ultra low sulfur diesel supplemented by vibrations. Separation and Purification Technology, 156, 665-672. https://doi.org/10.1016/j.seppur.2015.10.062

40. Kim, S. C., Wang, H., Imagawa, M., Chen, D. R., & Pui, D. Y. (2006). Experimental and modeling studies of the stream-wise filter vibration effect on the filtration efficiency. Aerosol science and technology, 40(6), 389-395. https://doi.org/10.1080/02786820600640541

41. Genkin, G., Waite, T. D., Fane, A. G., & Chang, S. (2006). The effect of vibration and coagulant addition on the filtration performance of submerged hollow fibre membranes. Journal of membrane science, 281(1-2), 726-734. https://doi.org/10.1016/j.memsci.2006.04.048

42. Niţoi, D., Amza, G., Amza, Z., Radu, C., & Teodorescu, M. (2018). Practical Realisation And Finite Element Modeling Of Ultrasonic Filters Design For Air Filtration. International

Multidisciplinary Scientific GeoConference: SGEM, 18(4.2), 555-562. https://doi.org/10.1088/1757-899X/400/2/022003

43. Fuchs, E.P (1979) Coal Mining Equipment Vibration Data Report, Donaldson Company, Inc.

44. Shahab, S. (2015). Vibration energy harvesting, biomimetic actuation, and contactless acoustic energy transfer in a quiescent fluid domain (Doctoral dissertation, Georgia Institute of Technology).

45. Colinet, J., Halldin, C. N., & Schall, J. (2021). Best Practices for Dust Control in Coal Mining, Second Edition. National Institute of Occupational Safety and Health, Pittsburgh. PA; Spokane, WA. https://doi.org/10.26616/NIOSHPUB2021119

46. Chander S, Alaboyun AR, Aplan FF [1991]. On the mechanism of capture of coal dust particles by sprays. Proceedings of the 3rd Symposium on Respirable Dust in the Mineral Industries, Pittsburgh, PA, October 17–19, pp.193–202.

47. Tessum MW, Raynor PC [2017]. Effects of spray surfactant and particle charge on respirable coal dust capture. Safety and Health at Work 8(3):296–305. https://doi.org/10.1016/j.shaw.2016.12.006

48. Kost JA, Shirey GA, Ford CT [1980]. In-mine tests for wetting agent effectiveness. U.S. Department of the Interior, Bureau of Mines Open File Report 30-82, NTIS No. PB82-183344.

49. USBM [1996]. Suppression of longwall respirable dust using conventional water sprays inoculated with surfactants and polymers. By Kilau HW, Lantto OL, Olson KS, Myren TA, Voltz JI. Minneapolis, MN: U.S. Department of the Interior, Bureau of Mines, Report of Investigations 9591.

50. Noble A., Jung S., Pan L., Shahab S., Amini H., (2023) Collecting Mine Dust Particles with Liquid-Coated Vibrating Meshes, Alpha Foundation for the Improvement of Mine Safety and Health, Inc. (Final Report). https://www.alpha-foundation.org/wp-content/uploads/2023/07/AFC518SP-89_VirgTech_FinalRpt.pdf Accessed September 5, 2023.

51. John Szczap, Sunghwan Jung, Lei Pan, (2023). Understanding the Microscopic Mechanism of Clogging of both Fibrous and Mesh Filters in Flooded-bed Wet Scrubbers, Fuel, Volume 355, 2024, 129381, ISSN 0016-2361, https://doi.org/10.1016/j.fuel.2023.129381

52. Szczap, J,Pan . “Understanding Interfacial Interactions in Filter Clogging of Flooded bed Scrubbers using Experimental Approach and Modelling” {Submitting to Powder Technology}

Chapter 6

6. Scale-Up and Validation Testing of a Vibration-Enhanced Flooded Bed Dust Scrubber Design and Construction

6.1. Introduction

The system prototype was designed with the intention of demonstrating the feasibility of vibratory mesh assemblies on a full scale, including a vibration translation system. Prior small-scale laboratory testing was used during the preliminary design process to ensure that adequate airflow, waste-water egress, and mesh excitation were achieved. The unit was tested at the NIOSH dust gallery, where similar dust scrubber technologies are being tested. A full-scale unit uses a modular structure similar to the one found at NIOSH and consists of a stand and shaker assembly, an exterior tunnel structure, and an interior vibratory mesh assembly.

The novel mesh section of the scrubber was the focus of this prototype design and construction. In order to test the section, NIOSH provided equipment analogous to that found on typical flooded bed scrubbers, including a particulate feeder, water management system, demister assembly, and exhaust puller fan. This prototype has been designed and manufactured as a direct replacement for NIOSH's static-mesh scrubber section, eliminating on-site modifications.

As the vibration of an operating continuous miner could be a suitable source of vibrational energy for the filter mesh, the feasibility of an energy harvesting technique was also investigated in this chapter. As depicted in Figure 6.1, an elastic foundation of known spring constant can be used to transmit the system vibration to the mesh. The vibrational energy transmitted to the mesh can thus be controlled by proper selection of the spring constants of the elastic foundation. Using vibration data from an operating continuous miner, the proposed design has been evaluated through experimentation. A range of spring constants were identified that properly transmitted the optimal

vibrational frequencies. This vibrational translation concept was also evaluated through the high-fidelity testing campaign.

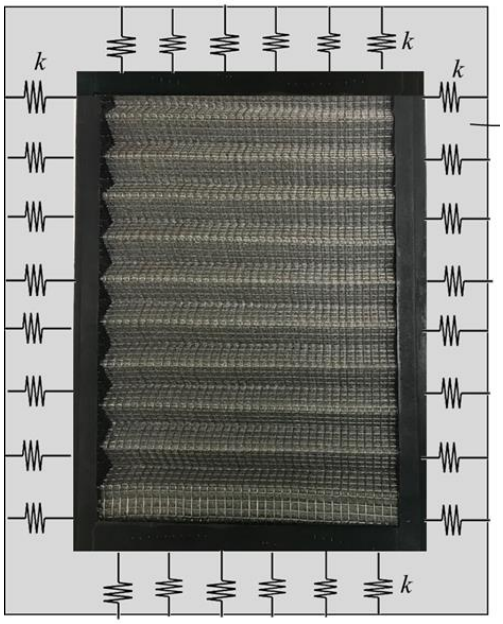

Figure 6.1: Design of a scrubber mesh attached to a spring housing

6.2. Vibrational Translation - Energy Harvesting Evaluation

As noted in the previous chapters the dust collection efficiency of the mesh scrubber system increased with the introduction of vibrations. Through this finding, a system was modeled and presented in this chapter that vibrates the mesh screen that is harvesting energy from an external source of excitation. An elastic base composed of springs is designed to be used for the mesh to move in a particular direction. This base would take the shaking of the continuous miner as the source of vibrations and transmit that to the mesh screen. The mesh screen vibrates independently of the externally generated vibration frequency. An important role here is the stiffness of the elastic base of the mesh scrubber which determines the frequency of the output vibrations.

To investigate the energy harvesting/vibrational translation system, Jung et al. conducted a series of tests on a scaled-down bench-top model (Figure 6.2) [1]. They recorded experiments with a high-speed camera by tracking them throughout testing using an image processing technique. These bench-scale experiments aimed to identify the vibration frequencies (ranging from 10-100 Hz) where more energy can be harvested from the system. Their method consisted of extracting the vertical position of each tracked point (y) and applying a Fast Fourier Transform (FFT) to them. Their findings reveal that local maximums in FFT data appear at the most dominant frequencies of oscillations.

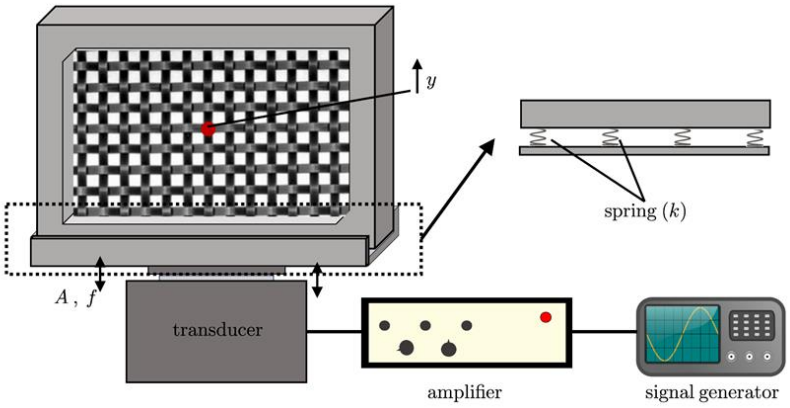

Figure 6.2: Schematic illustration of test setup[1]

They found that the energy transmitted to the mesh is the highest when the driving frequency is equal to the system natural frequency. They calculated an approximate natural frequency of the system using the relationship of natural frequency (Fn), mass (m), and stiffness (k) of the system:

$$F_n = \frac{1}{2}\sqrt{\frac{k}{m}}$$

Considering the bench-scale test setup geometry and characteristics, they identified that the natural frequency of the small-scale system, Fn yields 65 Hz. The FFT results proves that the mesh structure oscillates with the same frequency as the base oscillations when F> Fn. Hence, they neglected the effect of spring system in this limit. Alternatively, they discovered that the spring system has a significant impact on vibration modes at frequencies lower than the natural frequency.

Pairs of strong peaks are observed in FFT data shown in the subset (ii) of Figure 6.3. The first is close to the base frequency (F), and the second is close to the natural frequency (Fn).

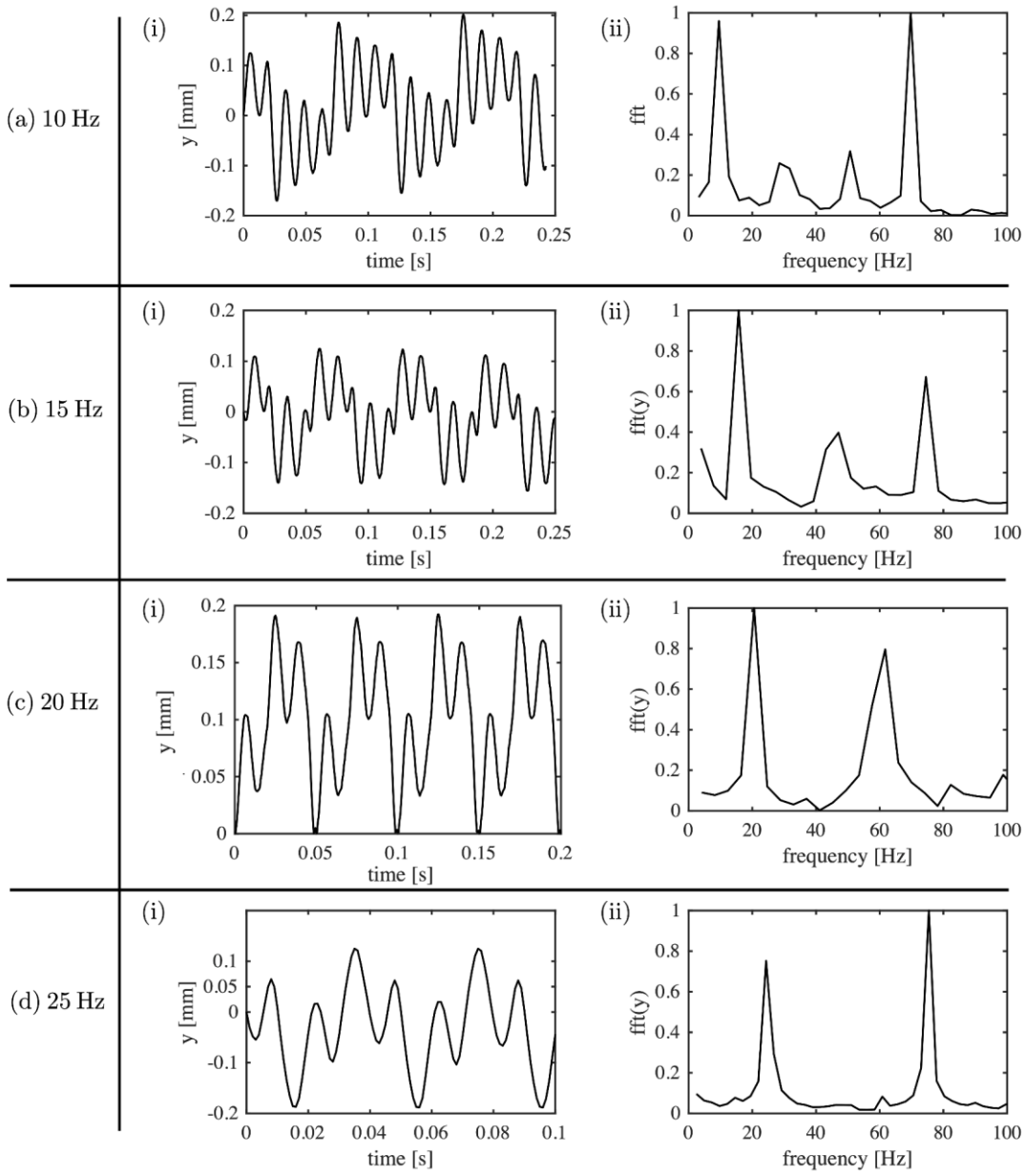

Figure 6.3: Average oscillations (i) and FFT results (ii) [1]

They concluded that it is possible to excite the natural frequency of the system in frequencies lower than the natural frequency of the system. In light of the recommended application, in order to harvest more energy from the external source to the vibratory assembly, various spring constants that provide a natural frequency larger than the range of viable external frequencies were selected in this study.

6.3. Design and Construction

6.3.1. Stand and Shaker Assembly

Stand assembly contains the scrubber mesh section and shaker assembly. This structure was assembled with bracketry made of 8020 aluminum. The shaker is positioned offset from the tunnel mounting point (Figure 6.4). This iteration of the study uses a Modal Shop 2110E shaker kit. The shaker can deliver 110 lbf pk of sine force, a frequency range of up to 6500 Hz, and a stroke distance of 1.0 inches. The specifications of this shaker make it an ideal option for testing since it meets all the operational parameters required [2].

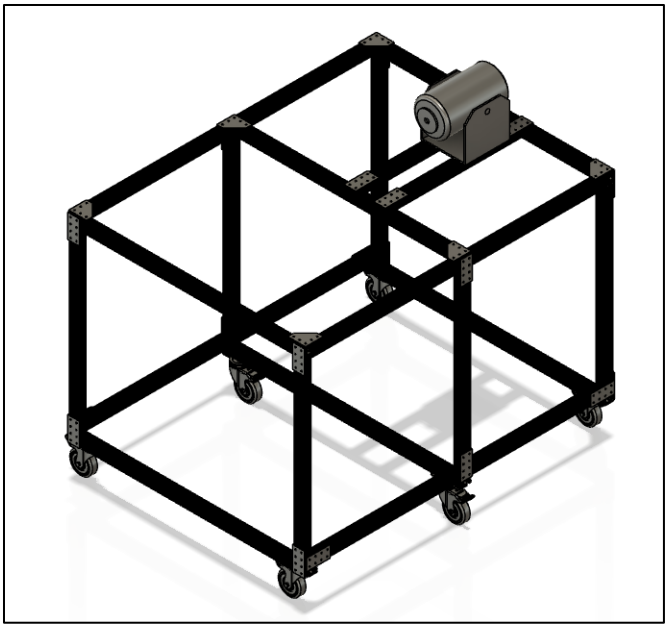

Figure 6.4: Stand and shaker assembly CAD model.

6.3.2. Tunnel Structure

To test the unit, the exterior structure was designed so that it could be modularly adapted to NIOSH's existing flooded bed dust scrubber (Figure 6.5). NIOSH's system comprises individual chambers that measure 15.50 inches x 27.00 inches and employs a static mesh that measures 15.75 inches x 25.25 inches. In order to package the vibratory mesh assembly within the confines of the NIOSH scrubber dimensions, a tapered chamber was designed. Tapering the chamber opens it up to 32.25 inches in width and yields a total increase of 5.25 inches in width.

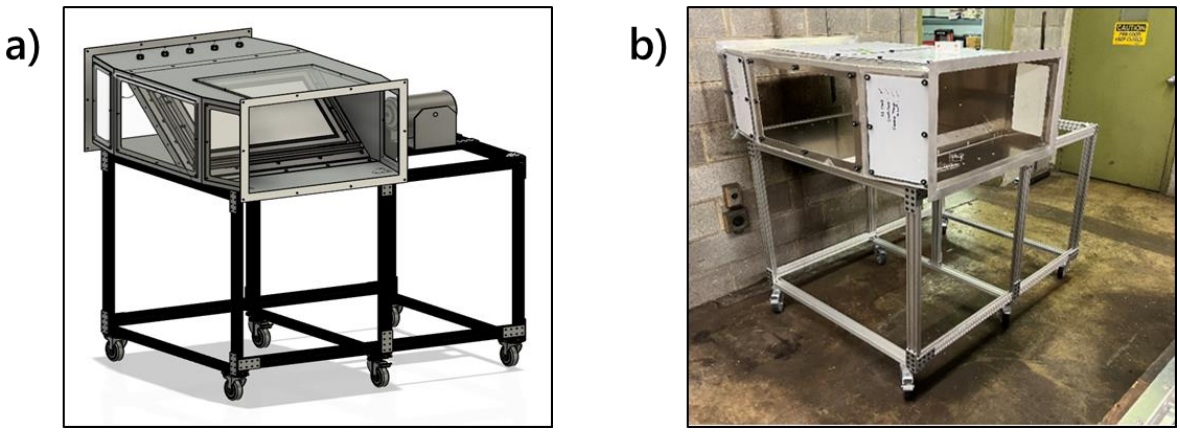

*Figure 6.5:*Full-Scale Vibrating Mesh Housing; a) CAD model, b) Prototype.

The outward taper naturally caused a marginal reduction in air velocity through this portion of the chamber. Using the same mesh and chamber section for static and dynamic testing, possible effects of the change in geometry on airspeed were negated. Eight plasma-cut flat panels were assembled and fabricated into one structure using exterior fillet-welded corner joints with a 0.125-inch 5052-H32 aluminum sheet. Unlike the NIOSH unit, which is constructed from carbon steel, aluminum was used for this unit to reduce its mass. Also, it can be formed and bent without cracking, has superior corrosion resistance, and can be welded easily.

Each viewing window in the chamber structure was constructed out of 0.25-inch-thick polycarbonate and was designed for use in testing and data collection. A mesh egress window is used to monitor the mesh upstream and downstream, as well as to install the vibratory mesh assembly.

An interior air-block plate and thick edge flanges reinforce the hollow structure of the chamber. As shown in Figure 6.6, the edge flanges are the same size on the outside as the NIOSH unit and share an identical hole pattern for ease of installation. They were made of 1.50-inch height x 0.125-inch thickness 90° aluminum angles. As shown in Figure 6.6, adding the air-block plate and its accompanying panel mounts to the structure triangulates the interior and fastens the walls, ceiling, and floor mechanically. Furthermore, this plate seals the chamber around the vibratory mesh

assembly and provides a solid mounting surface for the vibrating mesh. Similar to many industrial units, the plate is laid back at close to 45° angle within the structure [3].

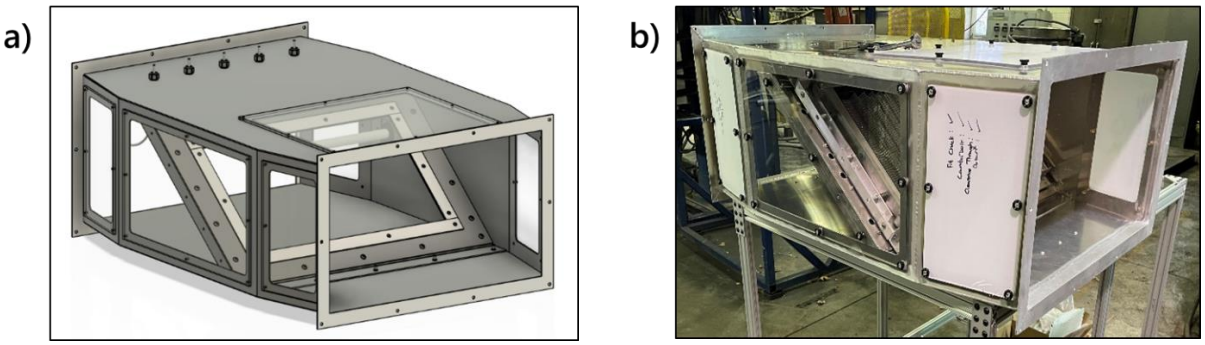

Figure 6.6: The main chamber with an air-block plate; a) CAD model, b) Prototype.

6.3.3. Vibratory Mesh Assembly

It is described in Chapter 4 that a spectrum of frequencies can be produced by several subsystems generated by the continuous miner operation. Mesh screen housings are subject to these vibrations. Based on all the possible frequencies imparted on the mesh base, the elastic foundation of mesh screens is designed so that the mesh resonates at a specific frequency. In this case, the natural frequency of the elastic system is the resonant frequency. As a result, resonance occurs when the natural frequency of the system falls within the range of frequencies produced by the continuous miner. This will result in the mesh screen vibrating at its natural frequency most of the time. This frequency has the highest force transmission between the source and the mesh screen.

The relationship between the mass (m) that needs to be moved, the stiffness (k) of the elastic base and the natural frequency (Fn) of the mesh screen system is given by:

$$k = 4\pi^2 F_n^2 m$$

An elastic base can be developed using this equivalence to stimulate the mesh screen at whatever dominant frequency is desired. In this way, the mesh screen can be designed with an elastic base capable of vibrating at a particular frequency. In other words, it is feasible to develop an operating system whose natural frequency matches the frequency range that the system experiences.

Based on the in-mine vibration data described in Fuchs' (1979) report and also in the project technical report section provided by Dr. Amini and his group [1,4], the response of a benchmark mesh screen weighing 3.52 kg was analyzed. Results showed that base stiffness influences mesh screen vibration as vibration is applied. There are also losses associated with vibrations. To simplify the analysis, a damping ratio of 5% was assumed.

In contrast to preliminary small-scale tests, the prototype system harvests and transfers machine-generated vibrations to the mesh panel. This transfer of vibration is notable because it is easy to install the novel system on existing mining equipment without significant modifications. Machine-driven transference is implemented through vibratory mesh assemblies. Figure 6.7 shows this assembly, which is composed of two separate substructures constrained by linear roller bearings.

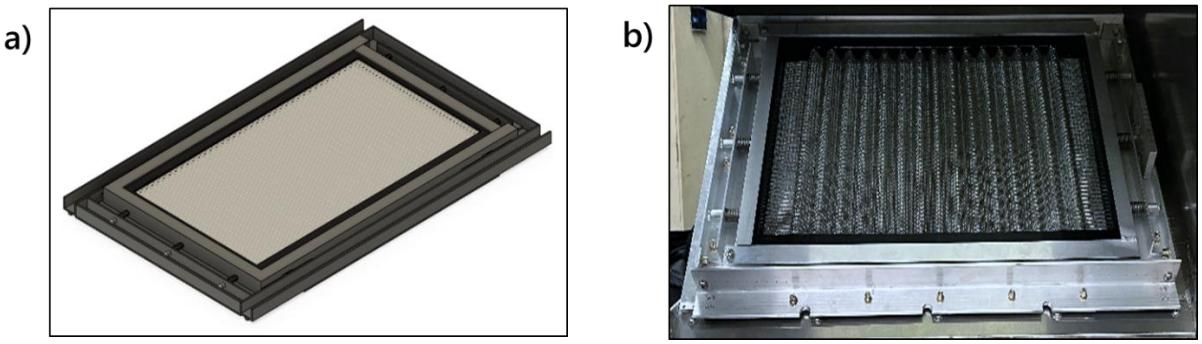

Figure 6.7: Vibrating mesh panel; a) CAD model, b) Prototype.

All components of the vibratory mesh assembly are fastened to the driven exterior panel. Through the use of four separate linear bearing carriages and rails, this panel connects directly to the air-block plate and acts as the mounting interface between the chamber and the shaker. Bearings allow the assembly to be moved laterally within the chamber to a maximum stroke of 1 inch. The mesh assembly is mounted by another set of bearings and carriages on the upward portion of the driven panel.

As seen in Figure 6.8, the mesh panel assembly consists of the filter mesh, the mounting frame, and dampening springs. Through the secondary set of linear bearings, the mounting frame is

mechanically attached to the driven panel. As a result of this dual-bearing design, the chamber and driven panel can be moved independently of each other. The driven panel is mounted to the mesh panel with compression springs. Using the coil binding of the spring as a hard stop, these springs allow the assembly to move within the stroke range of the driven panel. A further benefit of the springs is that they transfer lateral driven movement from the driven panel to the mesh panel, simulating machine-harvested vibrations.

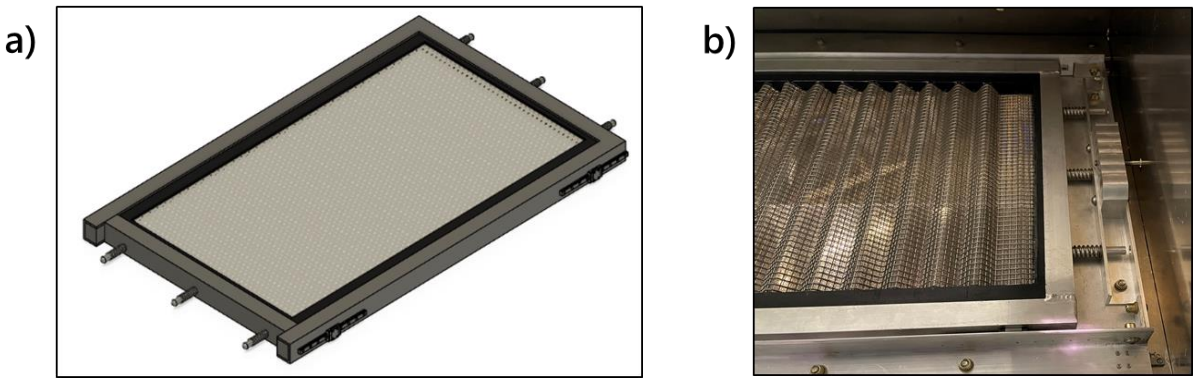

Figure 6.8: Mesh panel assembly with springs; a) CAD model, b) Prototype.

Completed interior assembly with air-block plate and vibratory mesh assembly provides adequate sealing without bypassing coal-laden upstream air. Figure 6.9a shows the completed assembly from upstream. The design ensures uniform airflow over the entire mesh surface area during the shaker's stroke. As the assembly contains two positions of linear motion, low-friction slippery polyethylene sealing surfaces were applied between both linear assemblies to mitigate strain on the shaker. Figure 6.9b shows the downstream side of the interior assembly on the opposing side. Data collection during testing is aided by the viewing windows surrounding the mesh shown in Figure 6.9b.

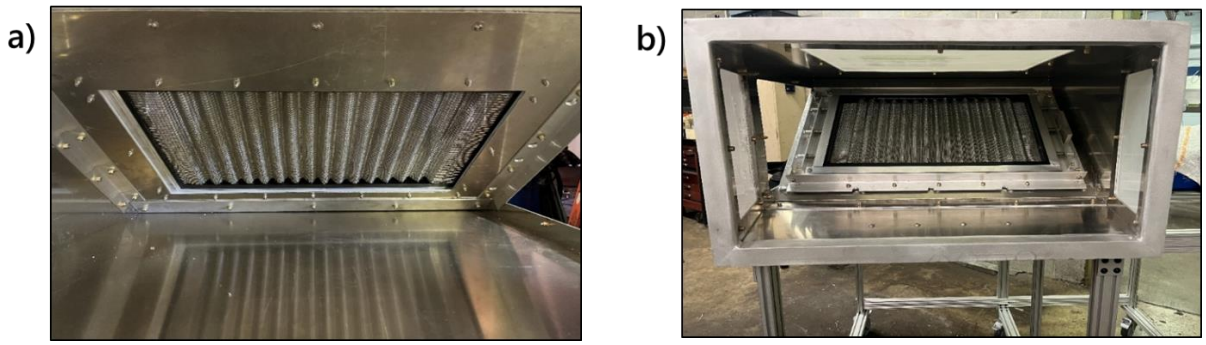

Figure 6.9: Complete prototype interior; a) upstream b) downstream.

6.4. Materials and Methods

Testing of the prototype system was conducted at the NIOSH Dust Gallery using the systems and infrastructure in place. The experimental investigation studies the influence of various operating parameters (e.g., vibrational frequency, amplitude, mesh housing design, and mesh design) on dust capture and self-cleaning potential. The primary experimental trials were conducted with the standard fine coal dust blend that is used in the NIOSH dust gallery. The apparatus for testing included the standalone dust scrubber configuration, that includes several tunnel sections as well as a discharge fan, demister, water management system, and residual dust collection system (Figure 6.10). A single custom-built tunnel section that contains the vibrating mesh configuration (Figure 6.11) and a vibratory unit (Figure 6.12) were supplied in the scope of this study. The vibratory kit includes a dual-purpose platform shaker with power amplifier and a cooling package. The electrodynamic exciter is capable of imparting 489 N (110 lbf) pk sine force and 25.4 mm (1") pk-pk stroke [2].

Figure 6.10: Standalone dust scrubber unit at the NIOSH Dust Gallery.

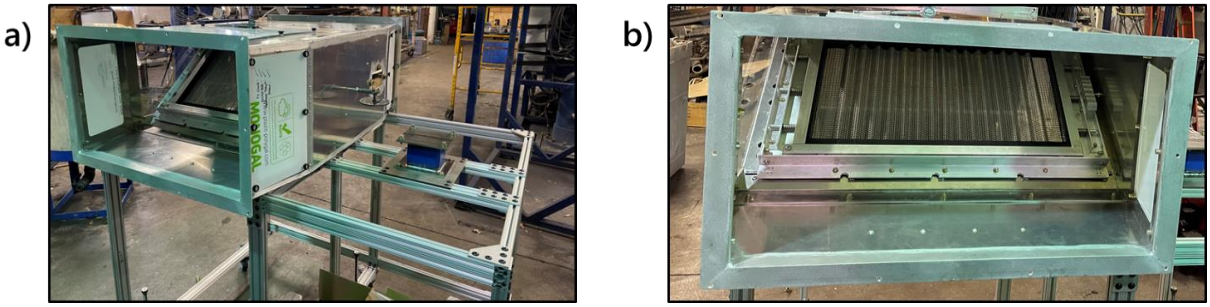

Figure 6.11: a) Custom-built mesh housing section b) The vibrating mesh configuration.

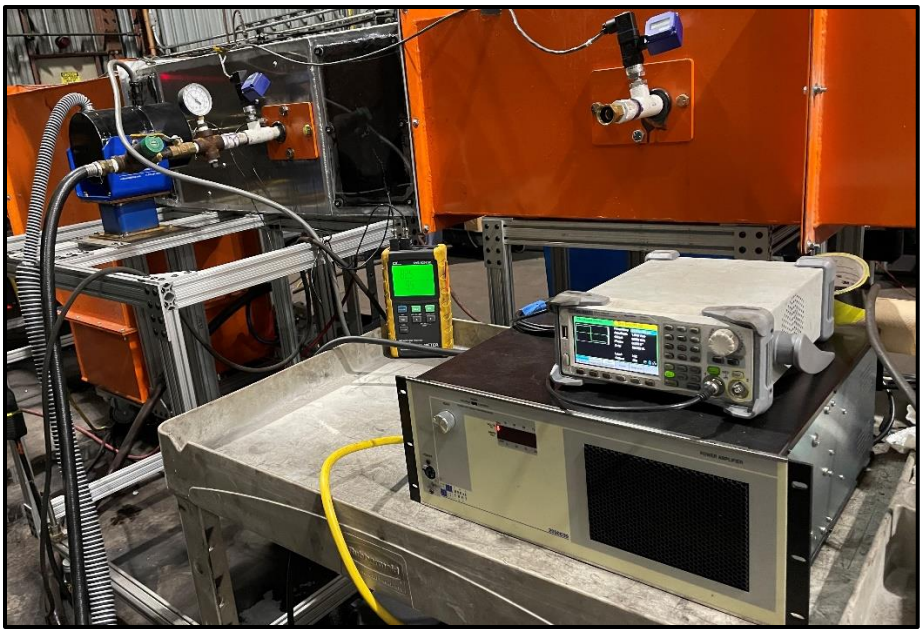

Figure 6.12: Shaker kit employed in the test.

The existing system was pretested to determine the operational and cleaning procedure for the filter and duct. Subsequent tests followed standard protocols and procedures for the dust scrubber system that have been developed by NIOSH. During each test, the fan, water sprays, mesh shaker, and dust feeding system (sequentially in that order) were initiated. Gravimetric sampling measurements were utilized using sample collection cassettes & vacuum pumps through the duration of the test (Figure 6.13). Pressure drops across mesh screen and demister and air velocity were measured using pressure gauge and pitot tube before introducing dust as well as throughout the duration of the test (Figure 6.14). The spent filters were cleaned using garden hose, the water sump was emptied when needed, and the system was prepared for a new run between tests (pre-test pressure drop was utilized as an indicator of cleanliness).

Figure 6.13: Upstream sampling configuration of the experiment.

Figure 6.14: Pressure monitoring station.

Similar to the bench-scale trials, the first block of experiments was designed using response surface methodology to empirically quantify the correlation between several independent variables and a response variable. To develop response surfaces, a 3-factor Box-Behnken-Design (BBD) was employed, and the experimental data was statistically analyzed. Surface plots were generated after data analysis. As dictated by the experimental program, 15 runs were conducted. 12 of the runs were performed using different combinations of the independent variables, and 3 repeated runs were performed at the test center point. Table 6.1 shows the factors associated with the independent

variables. The experimental program was developed using Minitab software in order to set up a reliable regression model with the least amount of error at the end of the experiment. Analyzing the experimental results from 12 different combinations of the three independent variables and 3 repeated trials with only mid-level factors illustrates the significance of the operational factors in determining mesh screen dust collection performance.

Table 6.1: Experimental factors and range values for full-scale scrubber test

Factors	**Level**		
	Low (-1)	**Medium (0)**	**High (+1)**
Spring rate (lbs/in)	10	103	-- (solid)
Amplifier gain (Vpp)	1	2	3
Frequency (Hz)	10	70	130

The constant parameters in the experimental setup are defined in Table 6.2. The duration of the test, dust feed rate/concentration in the duct, water flow rate, water spray nozzle pressure and the initial airflow rate were mainly determined by the capability of the facility's equipment capability. Test duration was determined as 25 minutes when the gravimetric sampling is employed to allow sampling cassettes to collect sufficient amount of dust concentration to evaluate the system efficiency.

Table 6.2: Fixed operating parameters for full-scale scrubber test

Property	**Unit**	**Values**
Dust feed rate	g/min	250
Nozzle pressure	PSI	37

Dust composition	--	Grounded fine coal dust
Test duration (for gravimetric sampling)	Min	25
Fan speed	Hz	60
Mesh layering	--	30-layer

After the initial experimental program, three additional runs were conducted using the mid-values of the vibrational parameters, and different mesh screens with various layering, and three more runs were conducted with the same mesh screen layering configurations but with no vibration. The six additional tests were performed to compare vibrating and non-vibrating conditions under different mesh screen layering (Table 6.3). These tests were performed using the same fixed operating parameters as shown in Table 6.2.

Table 6.3: Post experimental program testing

Run	**Vibration conditions**	**Mesh layering**
1	Vibration-free	10-layer
2	Vibrating mesh	10-layer
3	Vibration-free	20-layer
4	Vibrating mesh	20-layer
5	Vibration-free	30-layer
6	Vibrating mesh	30-layer

6.5. Results and Discussion

6.5.1. Vibrational Parameter Optimization

The tests carried out in the dust gallery of the NIOSH facility consisted of two primary campaigns. In the first part, the experimental design was applied and 15 tests were carried out with different variations of the previously determined variables shown above. Throughout the test, data was collected via gravimetric sampling, real time dust concentration monitoring with DustTrak, real time optical particle size analysis with APS, analog air velocity monitoring, analog pressure drop across the screen and demister, and analog velocity pressure monitoring of the downstream air. Response surface plots were created with the obtained results and are shown in Figure 6.15 through Figure 6.17. Each figure shows the effect of two different variables on response by keeping one of the three variables used during the experiment constant.

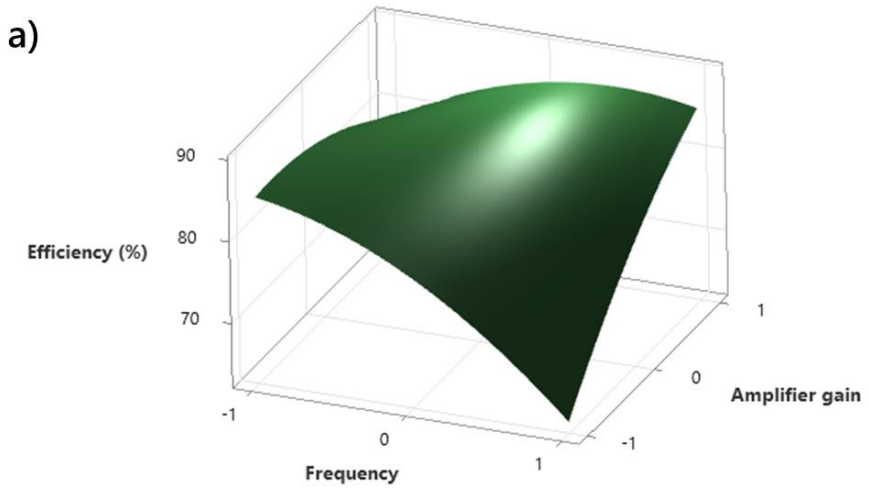

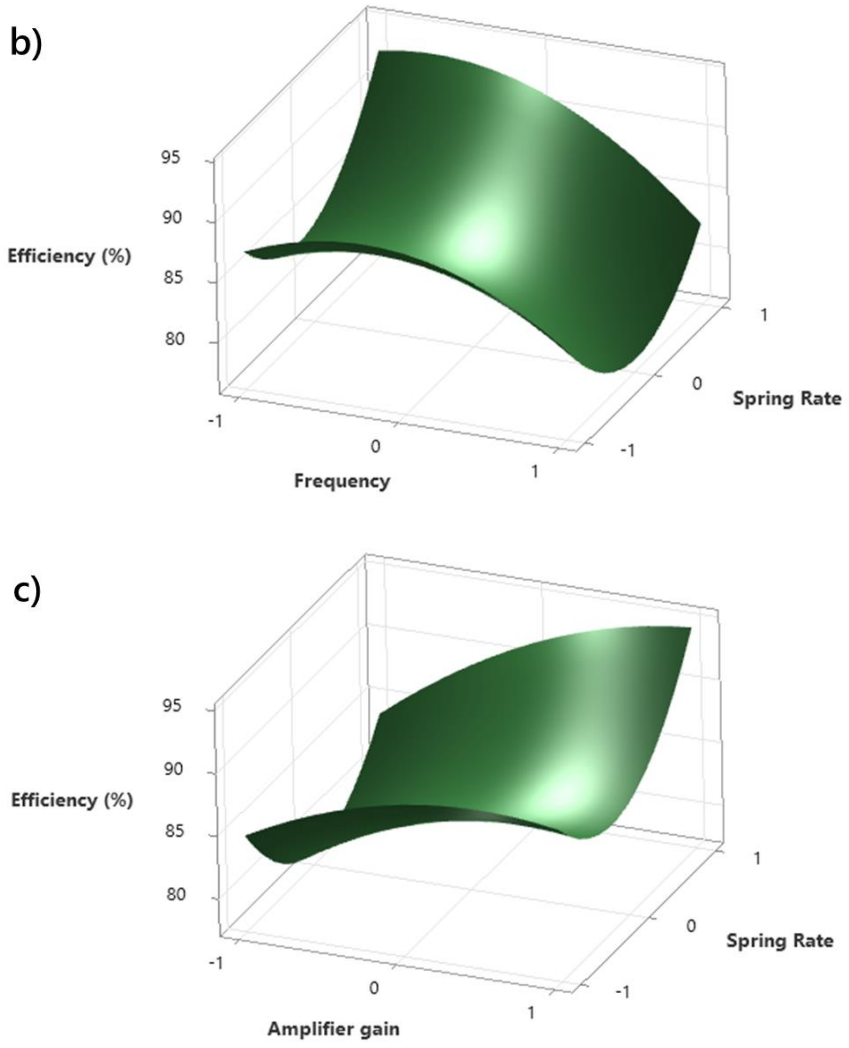

Figure 6.15: Surface Plots of Collection Efficiency (%) vs a) Amplifier gain and frequency, b) Spring rate and frequency, c) Spring rate and amplifier gain.

The collection efficiency surface (Figure 6.15) was plotted from the data obtained with the gravimetric sampling. Dust concentration data were obtained in real time with DustTrak and APS; however, they were not used in the analysis due to their inconsistency and calibration issues that were noted during testing. In Figure 6.15a, the effect of the interaction of the amplifier gain with the frequency on the efficiency is examined. The highest efficiencies (over 85%) were obtained when the frequency values were at medium and above, and at the same time the amplifier gain values were at the highest. The effect of the interaction of the spring constant with the frequency on the efficiency shown examined in Figure 6.15b. The highest efficiency values (over 92%) were

obtained when the spring constant is at the highest and the frequency is close to the medium value. However, it is worth noting that the collection efficiencies consistently approaching 90% under the conditions where the spring constant is at its lowest and the frequency is close to the medium values. As observed in Figure 6.15a and Figure 6.15c, the spring constant does not impart a significant difference in efficiency, especially under low amplifier gain conditions. In addition, higher efficiency was always achieved under test conditions with the highest application gain.

When taken together, the highest efficiency values were obtained when the frequency is at its medium value (70 Hz), the amplifier gain is at the highest (3 Vpp), and the spring constant is also at the highest (solid spacer). It should be noted, though that the effect of the spring constant used on the prototype screen will not exhibit the same behavior as the spring constant to be used in the real mine unit. The spring constant will need to be reoptimized in an operational prototype, and it is likely that a lower spring constant value will produce the desired results. The laboratory tests have shown that this lower spring constant configuration can move the screen independently and consistently from the outer frame. The slow-motion video of this movement can be found at the following link: (https://youtu.be/LRqoMVhpKoM)

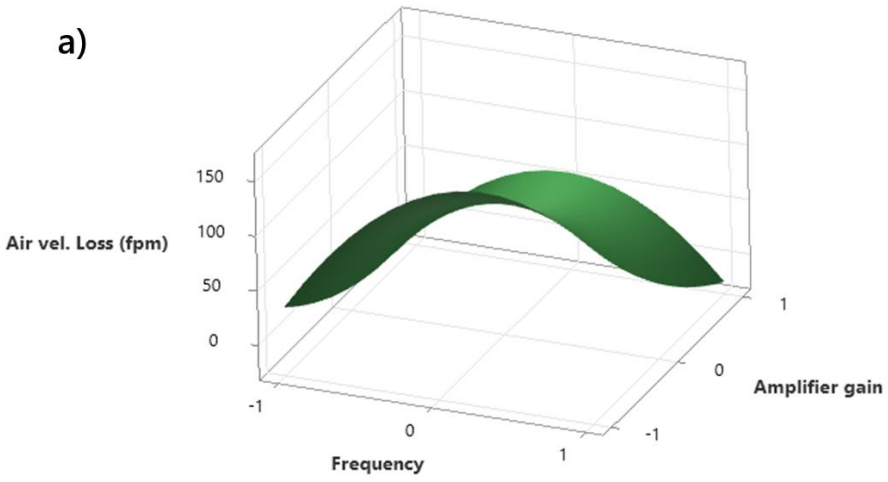

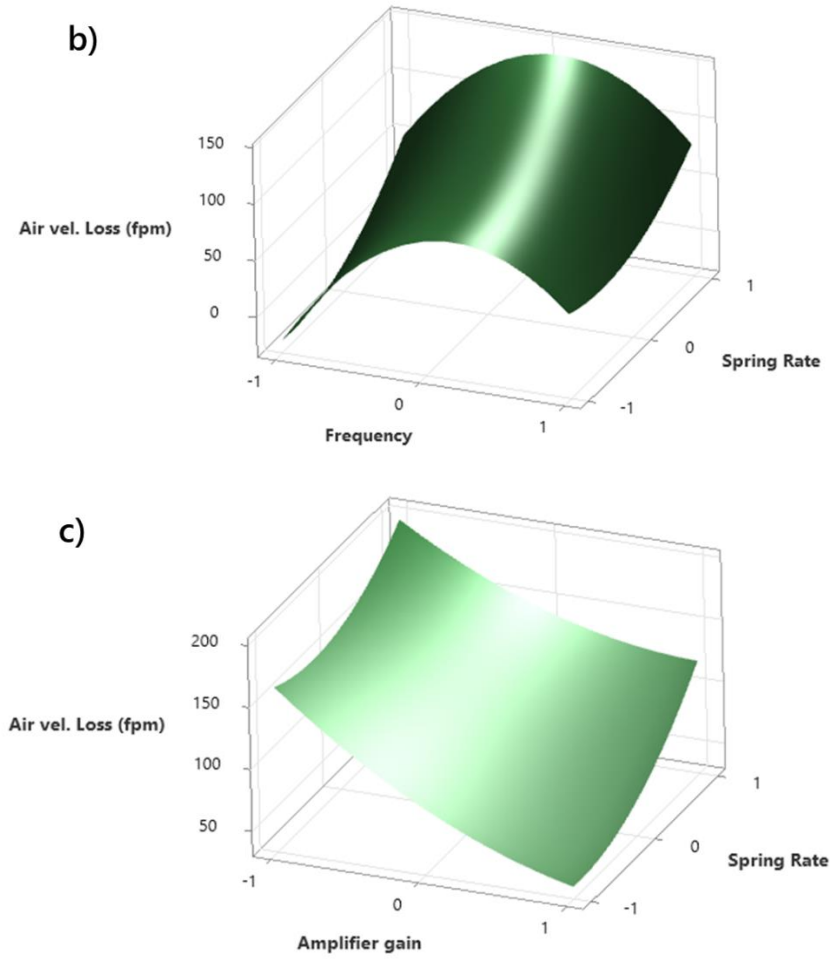

Figure 6.16: Surface Plots of Upstream Airflow Loss (fpm) vs a) Amplifier gain and frequency, b) Spring rate and frequency, c) Spring rate and amplifier gain.

In Figure 6.16, the effects of the binary interactions of the variables used in the test on the air velocity lost during the test were illustrated. In Figure 6.16a, where the effect of amplifier gain and frequency pair on air velocity loss is examined, it can be seen that the air velocity loss is most pronounced when the amplifier gain value is at its least (1 Vpp) and the frequency values are close to the medium values (70 Hz). As shown in Figure 6.16b, the air velocity loss reaches its highest (over 140 fpm) values where the spring constant is at its highest and the frequency is at its medium values. Lastly, it can be seen in Figure 6.16c that the amplifier gain is inversely proportional to the spring constant, but in an almost exact linear relationship. Accordingly, it has been observed that the air velocity loss is the most significant (over 175 fpm) when the amplifier gain is at its least

and the spring constant is at its highest. When taken together, the data show that the air velocity loss can be optimized when the amplifier gain values are at the highest, the spring constant value is at the lowest and the frequency is between medium and highest values. In addition to all these, when the air velocity pressure data in the downstream was examined, no significant change was found in any condition. Air velocity pressure drop at downstream close to fan were generally negligible throughout the test.

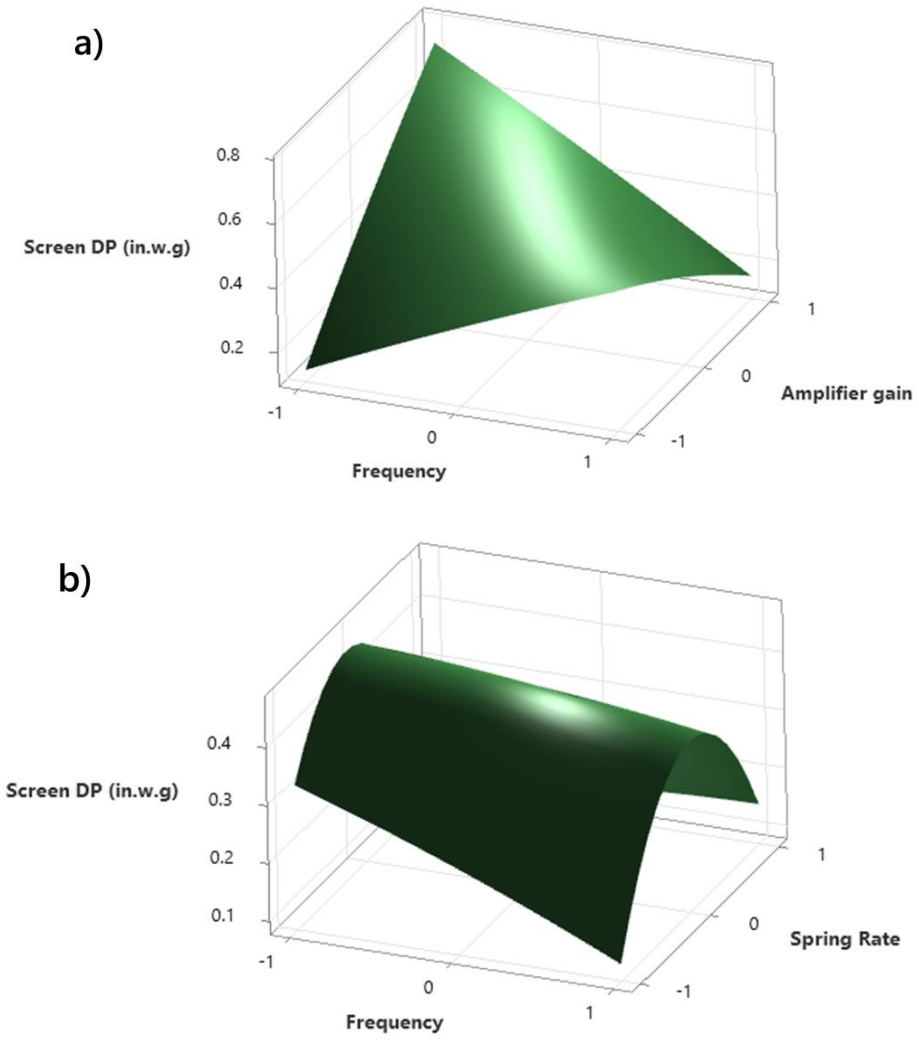

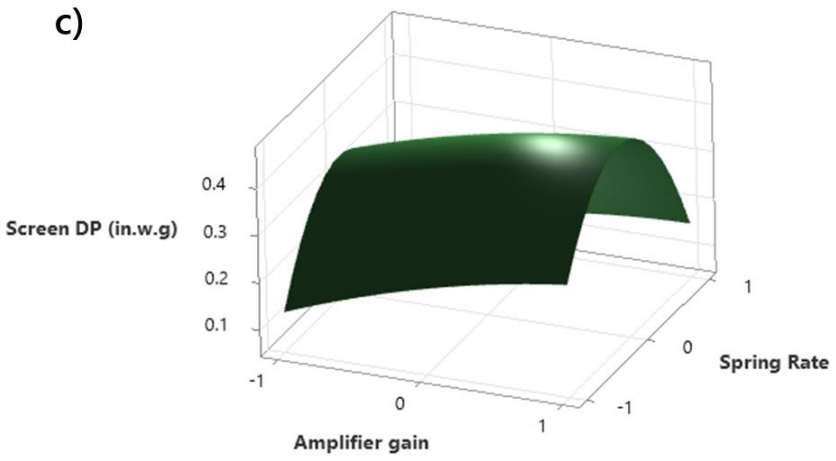

Figure 6.17: Surface plots of pressure drop across the mesh screen (in.w.g) vs a) Amplifier gain and frequency, b) Spring rate and frequency, c) Spring rate and amplifier gain.

Lastly, Figure 6.17 shows the effect of the binary interactions of the variables used in the experimental design on the pressure drops across the screen. As shown in Figure 6.17a, the interaction of frequency and amplifier gain does not have any significant effect on the increase in pressure drops across the screen. For example, in cases where there is high frequency and high amplifier gain, the lowest screen pressure drop is observed, whereas the lowest pressure drop values are also obtained at the lowest frequency value and the lowest amplifier gain. Therefore, it can be said that these two do not have a consistent effect on the related response. In addition, as shown in the Figure 6.17b, the most significant increases in the pressure drop across the screen (over 0.4 in.w.g) are observed in cases where the frequency value is between its medium and low and the spring constant is close to its medium value. Similarly, Figure 6.17c shows that when the amplifier gain value is between its medium and high and the spring constant is close to its medium value, the most significant increases in pressure drop across the screen are observed (over 0.4 in.w.g).

In addition, when the pressure drop data across the demister is examined, the data show that there is almost no increase in pressure drop in most conditions. There are even increases in the total pressure difference due to the location where the demister outlet is closest to the fan. The data show that the variables used in the experiment design do not have any significant effect on the pressure differences across the demister. When taken together, the data indicate that the pressure

drop is optimized when the spring constant is at its medium, the frequency value is between the medium and low range, and the amplifier gain is between its medium and high range.

6.5.2. Influence of Mesh Density and Vibration

The second part of the full-scale prototype tests carried out at the NIOSH facility with the full-size prototype consists of six tests with mesh screens with different steel mesh layers. These tests include vibrating and non-vibrating conditions of those mesh screen variations. The response parameters examined are the same with those examined in part 1 tests including the collection efficiency, the change in the air velocity at the system inlet during the test, and the pressure drops on the screen during the test (Figure 6.18, Figure 6.19, and Figure 6.20).

As shown in Figure 6.18, collection efficiency in the vibrating condition decreased only in the test with the 20-layer screen, however, the collection efficiency increased in the tests with the 10-layer and 30-layer screens. The effect of the difference between vibrating and non-vibrating conditions on the collection efficiency was most evident in the test with a 30-layer filter (32% increase). The collection efficiency was highest (94%) when tested with a 20-layer screen in vibration-free conditions. In addition, the test with the lowest efficiency was the test performed with a 30-layer screen in vibration-free conditions (68%). Comparing the 3 different screen types, although the highest efficiency was obtained in the vibration-free test with the 20-layer screen, it is worth noting that vibration increased the dust collection efficiency of the system in both tests using 10-layer (from 87% to 89%) and 30-layer (from 68% to 90%) screens.

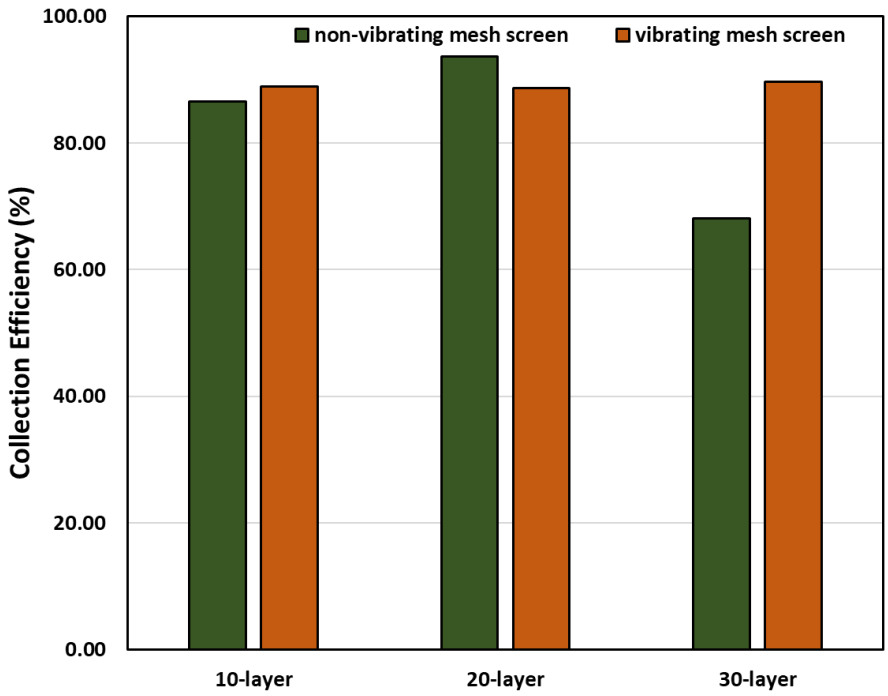

Figure 6.18: Collection efficiency by different mesh screen packages with various filter layering under vibrating and non-vibrating operational modes.

In Figure 6.19, the initial and final air velocity changes of the tests carried out in vibrating and non-vibrating conditions with screens with different steel mesh layer densities are given. Accordingly, in the 10-layer and 30-layer tests, significant air velocity losses were observed in the system (over 100 fpm), while no significant air velocity loss was observed in the tests performed with the 20-layer screen. It should be noted that the air velocity loss was greater in the tests with the vibrating 10-layer screen, and much greater in the tests with the non-vibrating 30-layer screen. These results are inconsistent and suggest that further testing and analysis of the measurement system may be needed to discern the implications of the findings.

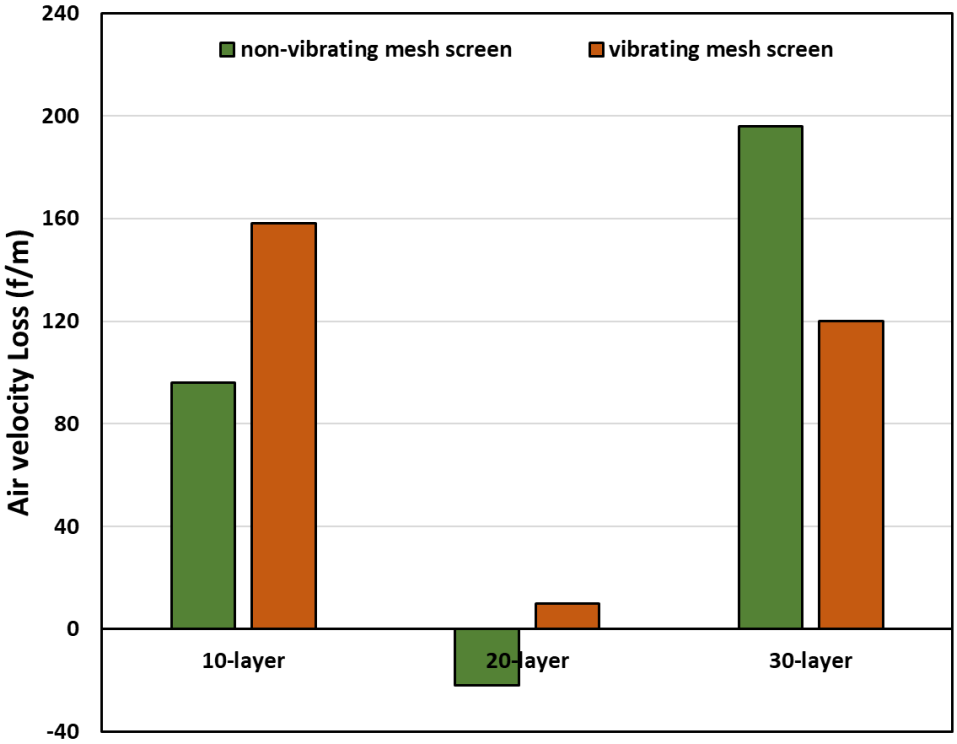

Figure 6.19: Upstream section airflow loss by different mesh screen packages with various filter layering under vibrating and non-vibrating operational modes.

Figure 6.20 shows the difference in the pressure drop detected across the screen during the tests performed. In tests with the 10-layer screen, the pressure drop decreases both in vibrating and non-vibrating conditions. It is considered that this may be due to the high air velocity upstream of the 10-layer screen. On the other hand, in the tests performed with 20- and 30-layer screens pressure drop increased throughout the tests. Less pressure drop increases were detected in the tests performed under vibrating conditions with both screen types. This finding is supporting that the presence of vibration increases the self-cleaning capacity of the screen compared to the vibration-free state.

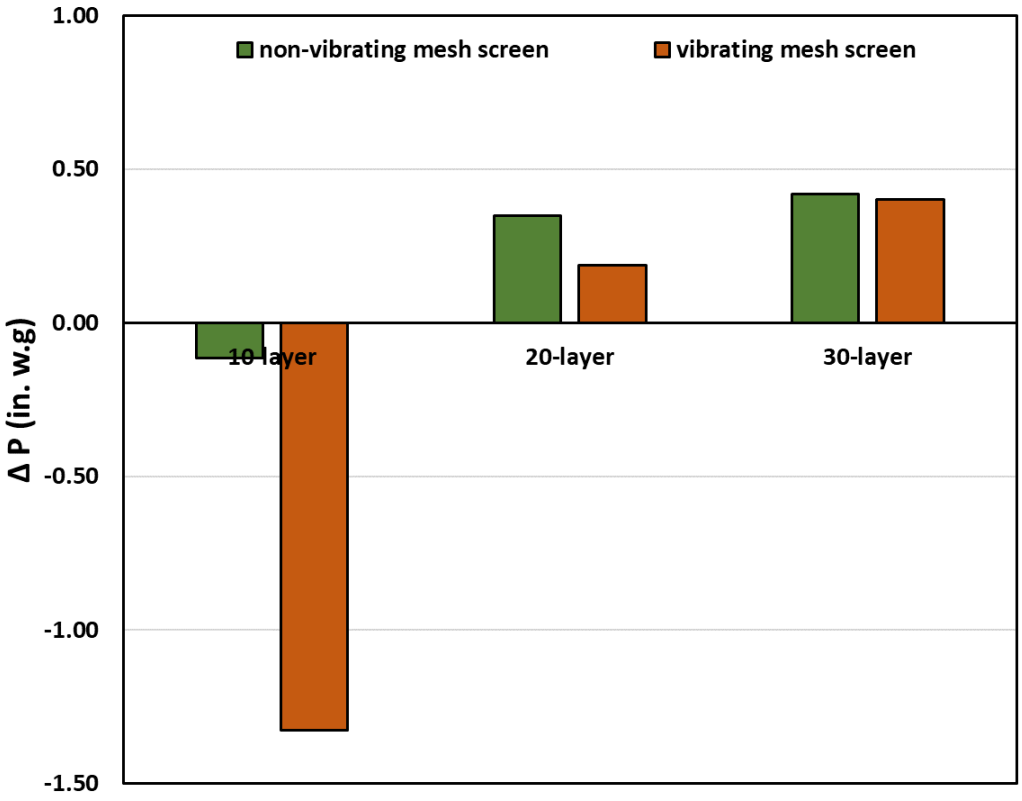

Figure 6.20: Pressure drops across the mesh screen by different mesh screen packages with various filter layering under vibrating and non-vibrating operational modes.

6.6. Conclusions

A vibration-enhanced full-scale flooded bed dust scrubber prototype was designed and manufactured in order to evaluate its capability in comparison with the traditional FBS equipped with a static mesh filter. The unit was tested at the NIOSH dust gallery. The full-scale unit employs a modular structure similar to NIOSH's and on top of that it additionally includes the stand and shaker assembly, the tunnel structure exteriorly, and the vibratory mesh assembly internally. This prototype design and construction was directed primarily at constructing and analyzing the novel section of the filter unit with a vibrating mesh panel.

Having been designed and manufactured as a direct replacement for NIOSH's static-mesh scrubber section, the prototype eliminates any on-site modifications that would have been required. NIOSH

provided the equipment that is used to test the filter unit section, which is similar to that of a typical scrubber that operates in a real mine. In the scope of the study, a single custom-built tunnel section that contains vibrating mesh, which has a specific spring configuration on its sides, was supplied along with vibratory equipment in order to perform the study.

This study provides a comprehensive analysis of the effects of vibrational parameters and mesh design on dust capture and the ability of the mesh to self-clean itself. In a similar way to the bench-scale trials, the first block of experiments was designed using response surface methodology to empirically quantify the correlation between several independent variables and a response variable simulating the entire process on a larger scale.

On the basis of the data obtained using gravimetric sampling, the collection efficiency surfaces, airflow surfaces, and pressure drop surfaces were plotted. There is a consistent trend that the collection efficiencies approach 90% when the spring constant is at its lowest and the frequency is close to the medium value. Under low amplifier gain conditions, the spring constant does not show a significant difference in efficiency. Also, the highest efficiency was always achieved under test conditions that involved the highest application gain.

As a result of these data, it is evident that the air velocity loss and pressure drop can be optimized at the highest amplifier gain values, the lowest spring constant value, and the medium to highest frequency values. Note that the effects of the spring constant on the prototype screen will not be the same as those on the real mine unit. During the development of an operational prototype, the spring constant will have to be reoptimized, and a lower spring constant value is likely to provide the desired result.

The initial experimental program was followed by additional runs using different mesh screens with varying layerings, and with mid-values of the vibrational parameters. With the same mesh screen layering configuration, more runs were conducted without vibration. The purpose of this study was to compare vibrating and non-vibrating conditions under different mesh screen layerings. When the mesh density is high (30 layers), the vibrating mesh outperforms the static mesh with superior collection efficiency and reduced airflow loss.

Based on the results of the first and second parts of the experiment with the full-size prototype, vibration-enhanced systems with 20 or less dense layered screens may have positive effects on the flooded bed dust scrubber's overall performance. Tests with the 10-layer mesh screen, however,

revealed that water droplets may pass through the demister regardless of the vibrating conditions. The fan could be damaged as a result of this, which could affect the data-generation process. For better results in the tests with a 10-layer screen, either the water or airflow rates can be decreased, or the demister's design can be modified.

Acknowledgements

The authors would like to acknowledge Matt Shigo's assistance in designing and manufacturing the test setup, as well as Tim Beckley (NIOSH) and his team's assistance in testing at their Pittsburg, PA facility.

This study was sponsored by the Alpha Foundation for the Improvement of Mine Safety and Health, Inc. (Alpha Foundation). The views, opinions, and recommendations expressed herein are solely those of the authors and do not imply any endorsement by the Alpha Foundation, its directors, and staff.

6.7. References

1. Noble A., Jung S., Pan L., Shahab S., Amini H., (2023) Collecting Mine Dust Particles with Liquid-Coated Vibrating Meshes, Alpha Foundation for the Improvement of Mine Safety and Health, Inc. (Final Report). https://www.alpha-foundation.org/wp-content/uploads/2023/07/AFC518SP-89_VirgTech_FinalRpt.pdf Accessed September 5, 2023.

2. Vibration Test Shaker Model 2110E. Data Available online at https://www.modalshop.com/vibration-test/products/vibration-test-shakers/110-lbf-exciter (accessed June 1, 2023).

3. Arya, S., Novak, T., (2020), Numerical Investigation of the Effect of a Novel Wet Scrubber on Dust Reduction in an Underground Coal Mine. Mining, Metallurgy & Exploration 37, 129–139 https://doi.org/10.1007/s42461-019-00135-2

4. Fuchs, E.P (1979) Coal Mining Equipment Vibration Data Report, Donaldson Company, Inc.

Chapter 7

7. Conclusion

7.1. Summary

Over the last 20 years, the flooded bed dust scrubber has been an integral component of dust control strategies for underground continuous mining operations. These units have been shown to be effective and robust in mining environments; however, several technical challenges and knowledge gaps limit their performance and efficiency. Most significantly, the filter mesh can easily get clogged, resulting in reduced cleaning capacity and frequent maintenance. This issue is further amplified given the natural tradeoff between mesh fineness, dust capture efficiency, and sustained air flow rate. The objective of this research was to develop, design, and test a novel flooded bed dust scrubber that mitigates these operational issues while improving overall dust capture.

A novel filter design is investigated in this study that minimizes filter clogging, achieves uniform wetting, and maintains high air flow rates. To improve particle-collecting efficiency and reduce filter clogging, the investigated design replaces static panel filters with vibrating filter mesh.

The research was mainly conducted in two phases: laboratory-scale testing with a bench-scale (6-inch x 6-inch cross-section) scrubber system and high-fidelity testing with a full-scale prototype. Both cases utilized experimental design techniques to fully investigate the parameters influencing scrubber performance. To support the development of the efficiency of the proposed design, several parallel works including modeling, laboratory-scale, and field studies were conducted by the author and the project coworkers.

Initially, a bench-scale scrubber system was manufactured by scaling down operational parameters to a lab-scale unit. This unit was then tested to evaluate how applying vibration to the filter mesh could improve the scrubber's overall efficiency. Data from bench-scale testing largely confirmed the benefits of the investigated design, with the vibrating mesh outperforming the static mesh in

every configuration tested. Additionally, further analysis revealed back the shaking effect enhances the possibility of shedding water droplet-coal dust particulate agglomerates from the filter screen, enhancing the self-cleaning capability of the demonstrated design.

Following that test, further bench-scale testing was conducted to evaluate the impact of the mesh design and surface hydrophobicity on the clogging rate of the filter in an FBS. The results revealed that making the filter surface super hydrophilic by decreasing the contact angle of the mesh screen surface improves system performance and extends the operational life of the filter panel by preventing rapid mass accumulation within the filter. On the other hand, the results showed that the mesh design manipulates significantly the filter-clogging phenomenon. The findings revealed that increasing the density of the filter media results in improving collection efficiency while it also leads to dust accumulation within the mesh screen panel, which increases the pressure drop across the mesh screen.

Lastly, the scale-up study demonstrated a way to further mature the technology, through testing a full-scale prototype in a high-fidelity simulated environment. To implement the vibrating mesh concept into a full-scale unit, the feasibility of an innovative energy harvesting approach was investigated, whereby the necessary mesh vibrations are supplied by capturing and translating the natural vibrations of the external vibration source. The full-scale prototype tests were carried out at the NIOSH facility. Collection efficiency in the vibrating condition wasn't improved only in the test with the 20-layer screen. However, vibration increased the dust collection efficiency of the system in both tests using 10-layer (from 87% to 89%) and 30-layer (from 68% to 90%) screens. Moreover, fewer pressure drop increases were detected in tests performed under vibrating conditions with all screen types. This finding supports that the presence of vibration increases the self-cleaning capacity of the screen compared to the vibration-free state.

7.2. Conclusions and Implications

Testing at various scales confirmed that the vibration-enhanced mesh screen improved particle capture while simultaneously mitigating clogging. Through this study as well as studies by other

members of the interdisciplinary project team, several mechanisms were investigated to explain this behavior. Key findings are discussed below.

Improved particle capture: The working hypothesis is that improved particle capture is primarily due to improved screen-wetted area resulting from vibration. CFD studies by Lu et al. and Nawaz et al. confirmed that vibration improves the wetted area, and the explanation is further expounded by that higher vibrating mesh velocity allows for stronger dust particle-mesh interactions, which results in a higher level of dust collection efficiency [1, 2]. To properly evaluate the performance of the scrubber unit, systematic experimental tests were conducted based on a statistically designed program to identify the role of various operational factors (i.e. water flow rate, mesh layering, surface chemistry, and mesh vibration frequency) in maximizing dust collection efficiency.

The mathematical model developed by Wang et al. (2021) identifies the acceleration of a droplet (a_f) using the parameters of where m (mass of the droplet), τ (time interval), and $E_{C\text{-}D}$ (interaction energy between liquid and surface) [3]:

$$a_f = -\frac{\tau \partial^2 z[E_{C-D}(r)]}{m \partial z(r) \partial z(t)}$$

Using this mathematical model, the researchers concluded that the interaction of liquid droplets and the surface has a positive correlation with the amplitude, vibration frequency, and contact area of the droplet surface. The current study utilized the proven phenomenon that surface-wetting characteristics can be enhanced by the existence of vibration.

Bench-scale test results showed that the vibrating mesh condition improved collection efficiencies by over 6% in wet condition and over 7% in dry condition while reducing mass accumulation in the filter by almost 10% in wet condition and over 40% in dry condition. Additionally, with the partitioning study, the system was further analyzed to investigate the size-by-size recovery of dust particles at various endpoints in the scrubber, under both vibrating and static conditions. In the wet-static case, a coarser particle size distribution was observed on the mesh screen surface. However, when vibration was imparted, this was reversed and the particle size distribution of the mass retained at the mesh screen surface got finer. This means that when the system is enhanced with vibration, the mesh screen will capture finer particles preferentially. These critical results explain how vibration is fundamentally affecting the capture mechanism of the system.

Improved clogging mitigation: The working hypothesis that informed this study was that controlled vibration induces improved liquid drainage, which in turn promotes particle shedding from the mesh. This hypothesis was initially supported by the work of Dr. Jung and his group [4]. They found that in all cases, the drop sliding speed increased with vibration frequency. Based on their experimental findings, an optimal combination of parameters can be defined that leads to the highest rate of particle collection as well as particle-laden drop drainage to ensure maximized particle collection while avoiding clogging. These findings were leveraged in the present work by establishing the optimal range of vibrational frequencies for testing. Specifically, their work showed that 150 Hz was superior to establishing the best balance for wettability of the surface, and as such a similar frequency was selected for the initial FBS tests described in this chapter.

Furthermore, this hypothesis was confirmed through studies on mesh hydrophobicity. The results of this study as well as the study of Sczap et al. showed that hydrophilic mesh surfaces (which promote improved water drainage) tended to reduce clogging, even in the absence of vibration [5]. On the other hand, hydrophobic surface modifications tended to reduce system efficiency relative to the baseline. A hydrophilic vibration-enhanced filter media provides rich wetting compared to other filter types, allowing less dust-laden air to pass through without being captured by water droplets, leading to higher collection efficiency by over 11% compared to the hydrophobic one. This study has also shown that using hydrophilic surface applications and optimized vibration, the mesh panel type commonly employed in mining applications can be reduced to a 20-layer mesh screen. By doing this, air velocity loss will be reduced by up to 79% and the overall performance of the system will be enhanced in comparison to a 30-layer hydrophobic vibration-free mesh screen.

In explaining the findings, when water contacts hydrophilic surfaces, it forms a film, whereas when it contacts hydrophobic surfaces, it beads up. Since water droplets are highly mobile, if the surface becomes hydrophobic, the area covered by water droplets is significantly reduced from the total mesh wire surface area. Besides, the hydrophilic coating increases the amount of liquid surface area on the mesh, which increases the chances of dust particles getting captured by water droplets.

Notes on scaleability: Data from bench-scale testing largely confirmed the benefits of the investigated design, with the vibrating mesh outperforming the static mesh in almost every configuration tested. The full-scale prototype testing, however, was less conclusive, with deviations between the static mesh and vibrating mesh depending on the mesh density and operating conditions. Nevertheless, at the highest mesh density (30-layer), the vibrating mesh notably outperformed the static mesh with superior collection efficiency and reduced airflow loss.

These inconsistencies in the full-scale tests can be attributed to several explanations.

Firstly, in 10-layer screen tests, pressure drops decrease both in vibrating and non-vibrating conditions. However, this is not a typical operational result for this kind of unit. Water droplets passed through the demister regardless of the vibrating conditions during the 10-layer testing and went forward to the fan. This possibly misled the data generation process. In order to eliminate this risk, the water flow rate can be decreased or as a more sophisticated solution, the demister design can be redesigned.

Secondly, these tests were short-duration experiments of only 25 minutes, and based on this, an attempt has been made to predict the general behavior of a very dynamic structure that works continuously for almost half a shift. Previous clogging studies presented in this study and the filter clogging model developed by Sczap et al. showed that as the test period gets longer, the amount of mass accumulated on the filter surface will grow and the clogging will be reached to further levels. However, in long-duration tests due to the effect of vibration, self-cleaning of the filter panel will be activated and it will help shed the mass accumulated on the dust buildup and improvement in overall efficiency will occur.

Thirdly, the small-scale unit is much more controllable and continuously monitored with environmental sensors. Data is collected in real-time, and if necessary, intervention can be made even during operation. However, in a full unit, this is not that easy. It is often possible to analyze the data after the test or even after a long process. This situation is one of the most serious handicaps in terms of productivity loss when scaling up the lab-scale unit to full scale.

Besides, these results are from only single trials. To ensure that these data are consistent for all testing campaigns, the trials should be repeated until consistency is achieved in the experimental results.

Lastly, while a small external vibration source is required in the tests performed at the lab-scale unit, as scaling the bench-scale unit to a bigger chamber the mass that needs to be moved with the help of external vibration also goes up. Therefore, the vibration source must be more powerful. In order to avoid the scaling risks that this situation may pose and to obtain optimum benefit from the vibrations currently produced by the continuous miner, spring constants, as well as other vibrational parameters, should be determined meticulously while the system is scaling up for industrial use.

Notes on implementation: There are several different subsystems that altogether produce a spectrum of frequencies generated by continuous miner operation. As the vibration of an operating continuous miner could be a suitable source of vibrational energy for the filter mesh, the feasibility of an energy harvesting technique was investigated in this research. The elastic foundation of the mesh screen is designed in such a way that the mesh resonates at a particular frequency from all the available frequencies imparted on the mesh base. This resonant frequency is the natural frequency of the elastic system designed. At this frequency, the transmissibility of force from the source to the mesh screen is the highest and the natural frequency of the system is amplified.

The relationship between the stiffness of the elastic base and the natural frequency of the mesh screen system is given by:

$$F_n = \frac{1}{2}\sqrt{\frac{k}{m}}$$

Where Fn is the natural frequency, k is the spring stiffness and m is the system mass. This equivalence can be utilized to design an elastic base that induces any desired dominant frequency on the mesh screen. The response of a benchmark mesh screen of 3.52 kg was computed using the in-mine vibration data described in Fuchs' (1979) report and also in a technical report section provided by Amini and his group [6, 7]. The results showed the effect of the stiffness of the base on mesh screen vibration as it is subjected to input excitation. The incurring of vibration also entails losses in the system, so, for simplicity, a 5% damping ratio in the system was assumed.

Through the use of four separate linear bearing carriages and spring configurations around the sides of the interior mesh screen panel, the chamber and driven panel can be moved independently of each other. Laboratory testing successfully showed how these vibrations could be translated to the filter mesh through the design of an elastic housing with a controlled spring constant. This

vibration transfer is notable because it is easy to install the novel system on existing mining equipment without significant modifications. Full-scale prototype testing provides a valuable initial design as to how external vibrations could be translated to the filter mesh through the design of an elastic housing with a controlled spring constant.

7.3. Recommendations for Future Work

The results of the laboratory and prototype testing campaigns have confirmed that the vibrating mesh system can improve operational outcomes over a static mesh system, and fundamental modeling efforts have provided insight into particle clogging within porous mesh materials. The final test prototype integrated several design features derived from fundamental testing, notably including the use of a hydrophilic mesh and the use of a flexible housing to translate external vibration. Based on the work of this research, the vibrating mesh technology has been validated in a relevant environment. In the next step, a fully integrated prototype should be validated on an operational system. A mine-worthy system must be designed and rigorously tested using either a retrofit or custom-built add-on to a continuous miner. Successful demonstration of a mine-worthy unit would facilitate broader commercialization within the industry.

Additional in-mine vibrational studies should be conducted to better understand the variability of characteristic vibrational frequencies as a function of the following variables: continuous miner machine, mining height, geologic factors, operator factors, and others. The energy harvesting system should be evaluated in an operating mine environment. For this research, most of the major design components were fully integrated into the test prototype; however, owing to practical constraints, the vibration was still supplied by a unidirectional external source with a fixed frequency and amplitude. Future testing of the dust scrubber should be conducted with a hydrophilic mesh that has been subject to the heat treatment process. Several construction materials/design approaches for elastic housing should be evaluated to determine the most operationally robust and cost-effective option. While most scrubber testing is conducted with a standalone unit, more information is needed to determine how these results will be translated into overall dust mitigation system performance. Future studies should not only focus on the factors

local to the continuous miner (e.g. dust capture, pressure drop) but also on the global factors at the mining face and throughout the mine environment.

7.4. References

1. Lu, Z., Rath, A., Amini, S. H., Noble, A., & Shahab, S. (2022) A computational fluid dynamics investigation of a novel flooded-bed dust scrubber with vibrating mesh. International Journal of Mining Science and Technology, 32/3, 525-537, https://doi.org/10.1016/j.ijmst.2022.03.002.

2. Janjua, A.N., Shaefer M., Amini, S.H., Noble, C.A., Shahab, S. (2023). Vibration Energy Harvesting in Underground Continuous Mining: Dynamic Characteristics and Experimental Research of Field Data. Applied Energy. (Manuscript submitted for publication.)

3. Pengyu W., Xiaokun S., Hongqing L., Shang M., Zhenqing W., (2021) Investigation of surface wettability and their influencing mechanisms under vibration field: A molecular dynamics simulation study. Computational Materials Science, Vol 197, https://doi.org/10.1016/j.commatsci.2021.110615.

4. Jung S., Noble A., Pan L., Shahab S. (2017) Collecting Mine Dust Particles with Liquid-Coated Vibrating Meshes, Alpha Foundation for the Improvement of Mine Safety and Health, Inc. (Technical Report). https://www.alpha-foundation.org/wp-content/uploads/2019/03/AFC518-25_VirgTech_FinalRpt.pdf Accessed January 5, 2023.

5. John Szczap, Sunghwan Jung, Lei Pan, (2023). Understanding the Microscopic Mechanism of Clogging of both Fibrous and Mesh Filters in Flooded-bed Wet Scrubbers, Fuel, Volume 355, 2024, 129381, ISSN 0016-2361, https://doi.org/10.1016/j.fuel.2023.129381

6. Fuchs, E.P (1979) Coal Mining Equipment Vibration Data Report, Donaldson Company, Inc.

7. Noble A., Jung S., Pan L., Shahab S., Amini H., (2023) Collecting Mine Dust Particles with Liquid-Coated Vibrating Meshes, Alpha Foundation for the Improvement of Mine Safety and Health, Inc. (Final Report). https://www.alpha-foundation.org/wp-content/uploads/2023/07/AFC518SP-89_VirgTech_FinalRpt.pdf Accessed September 5, 2023.

Appendices

Appendix A: Vibration Analysis

Table A1. Bench-Scale Filter Panel - Modal Analysis

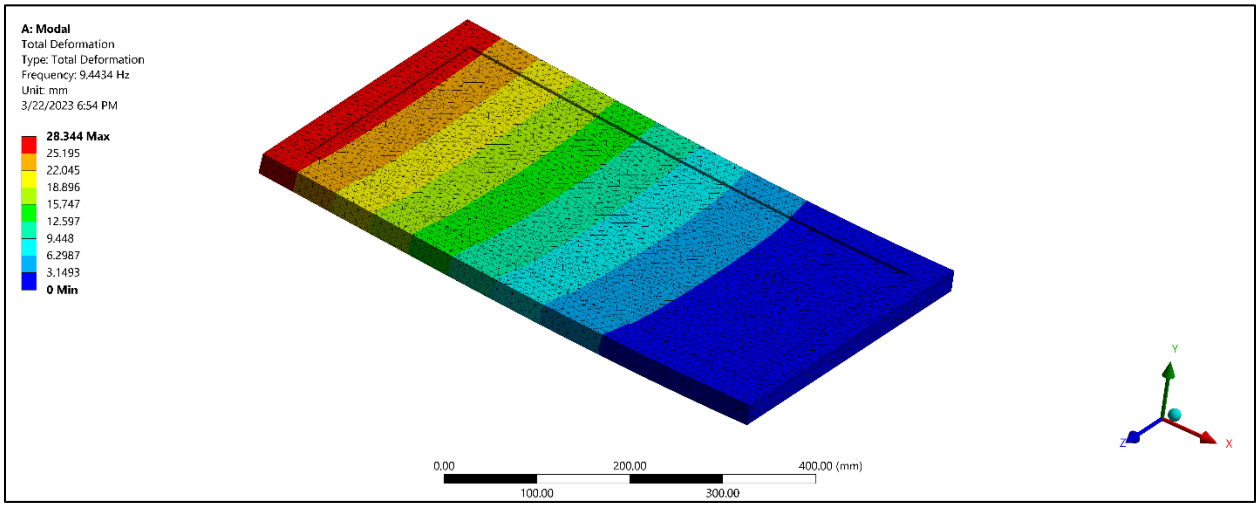

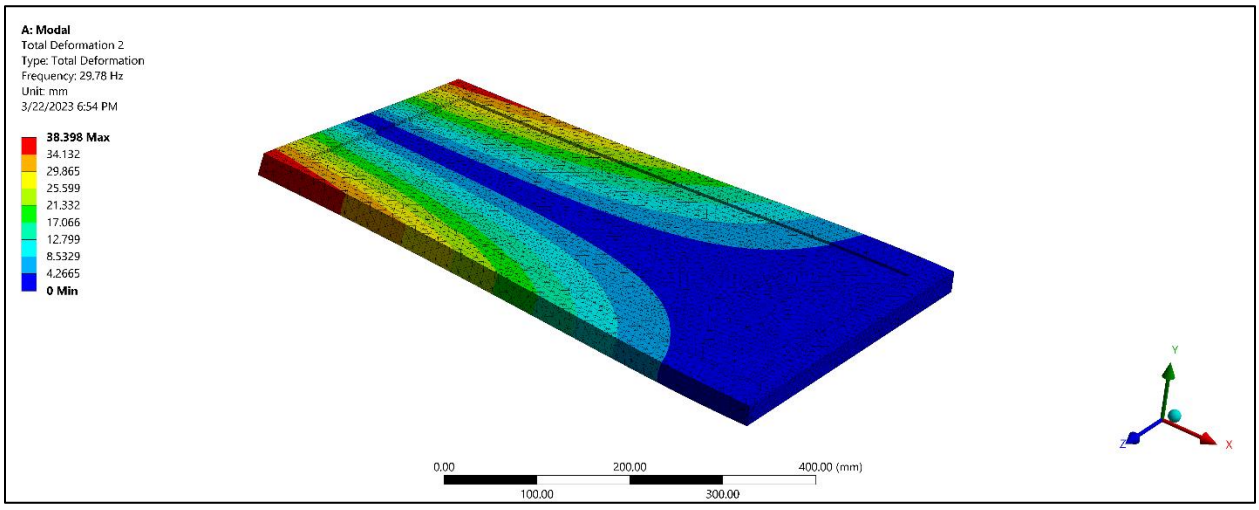

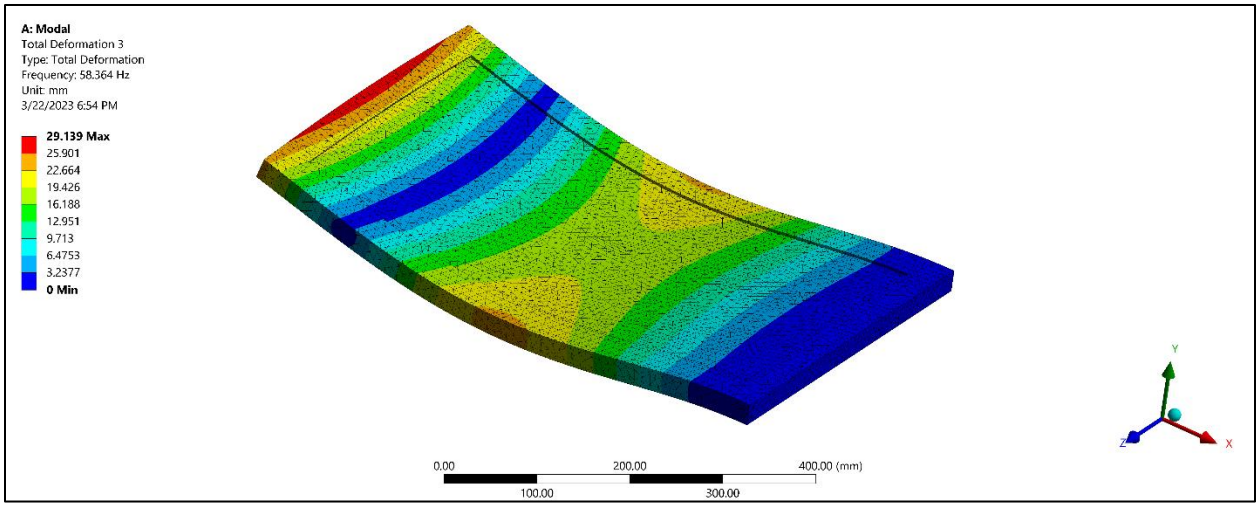
A: Modal
Total Deformation 3
Type: Total Deformation
Frequency: 58.364 Hz
Unit: mm
3/22/2023 6:54 PM
29.139 Max
25.901
22.664
19.426
16.188
12.951
9.713
6.4753
3.2377
0 Min
0.00
200.00
400.00 (mm)
100.00
300.00
Y
Z
X

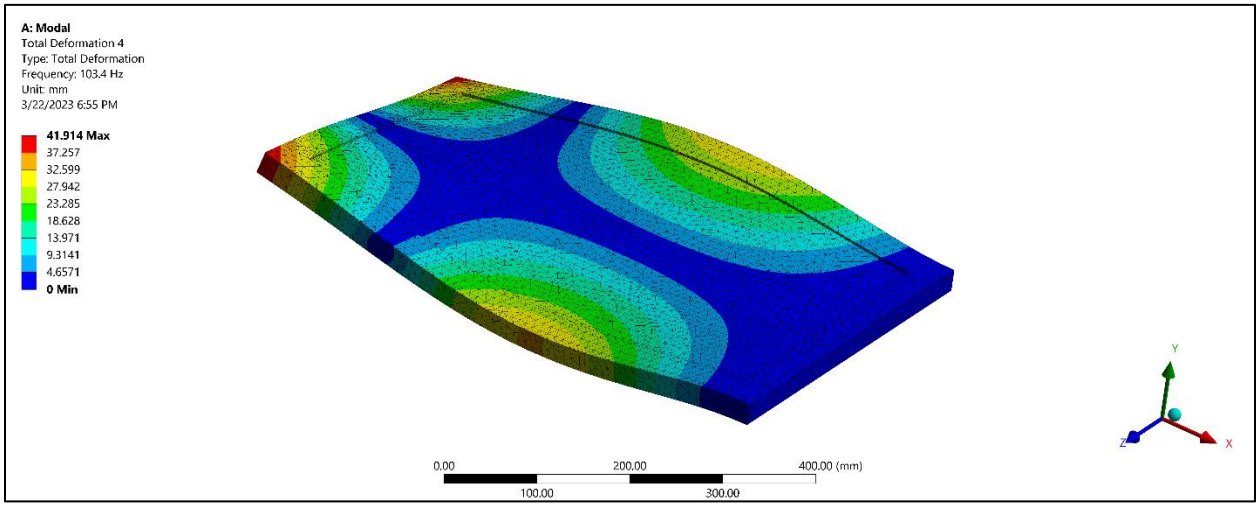
A: Modal
Total Deformation 4
Type: Total Deformation
Frequency: 103.4 Hz
Unit: mm
3/22/2023 6:55 PM
41.914 Max
37.257
32.599
27.942
23.285
18.628
13.971
9.3141
4.6571
0 Min
0.00
200.00
400.00 (mm)
100.00
300.00
Y
Z
X

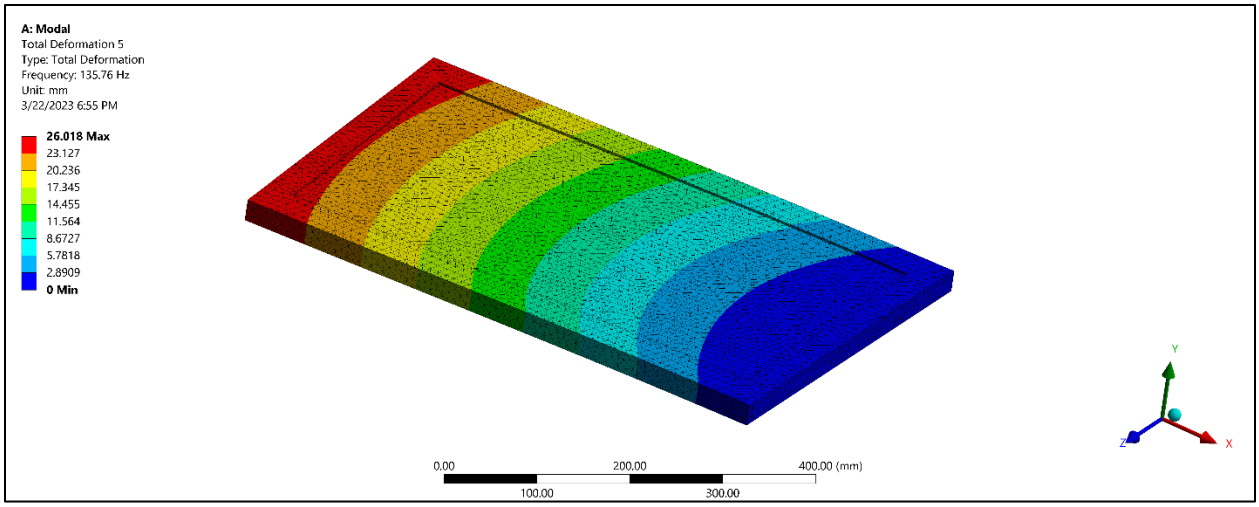
A: Modal
Total Deformation 5
Type: Total Deformation
Frequency: 135.76 Hz
Unit: mm
3/22/2023 6:55 PM
26.018 Max
23.127
20.236
17.345
14.455
11.564
8.6727
5.7818
2.8909
0 Min
0.00
200.00
400.00 (mm)
100.00
300.00
Y
Z
X

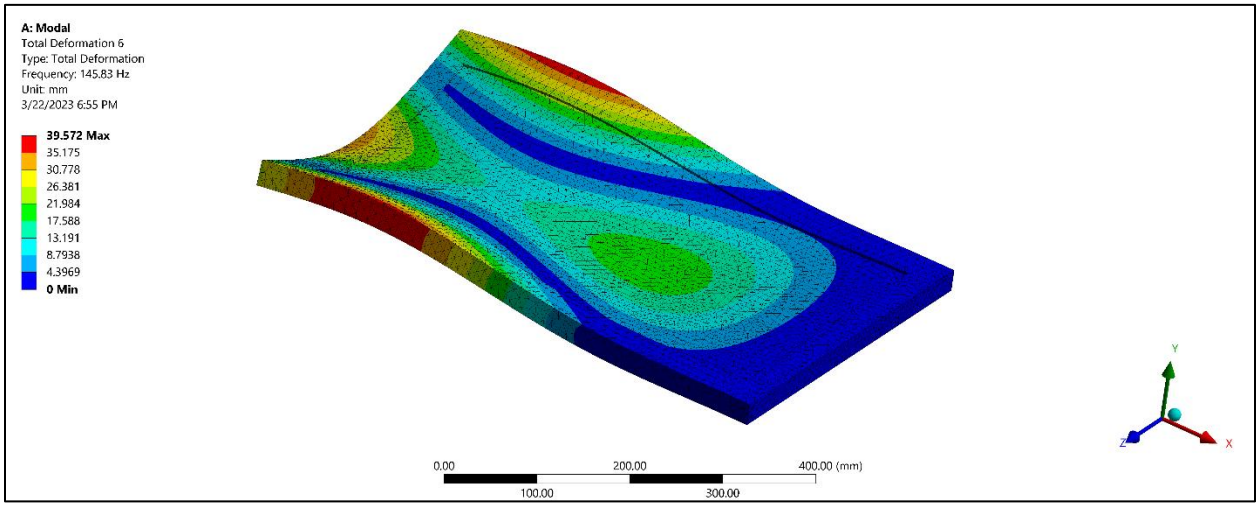
A: Modal
Total Deformation 6
Type: Total Deformation
Frequency: 145.83 Hz
Unit: mm
3/22/2023 6:55 PM
39.572 Max
35.175
30.778
26.381
21.984
17.588
13.191
8.7938
4.3969
0 Min
0.00
200.00
400.00 (mm)
100.00
300.00
Y
Z
X

Appendix B: Size-by-size material balance

Table B1. Flowsheets under various operational conditions

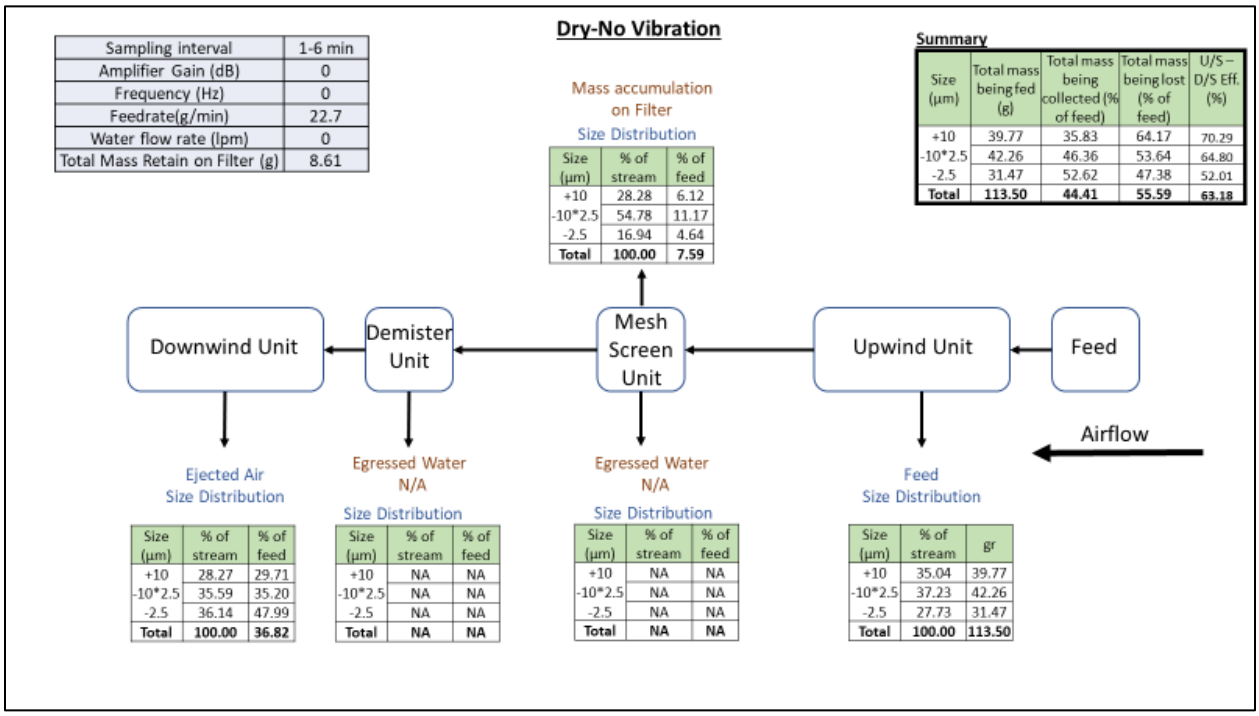

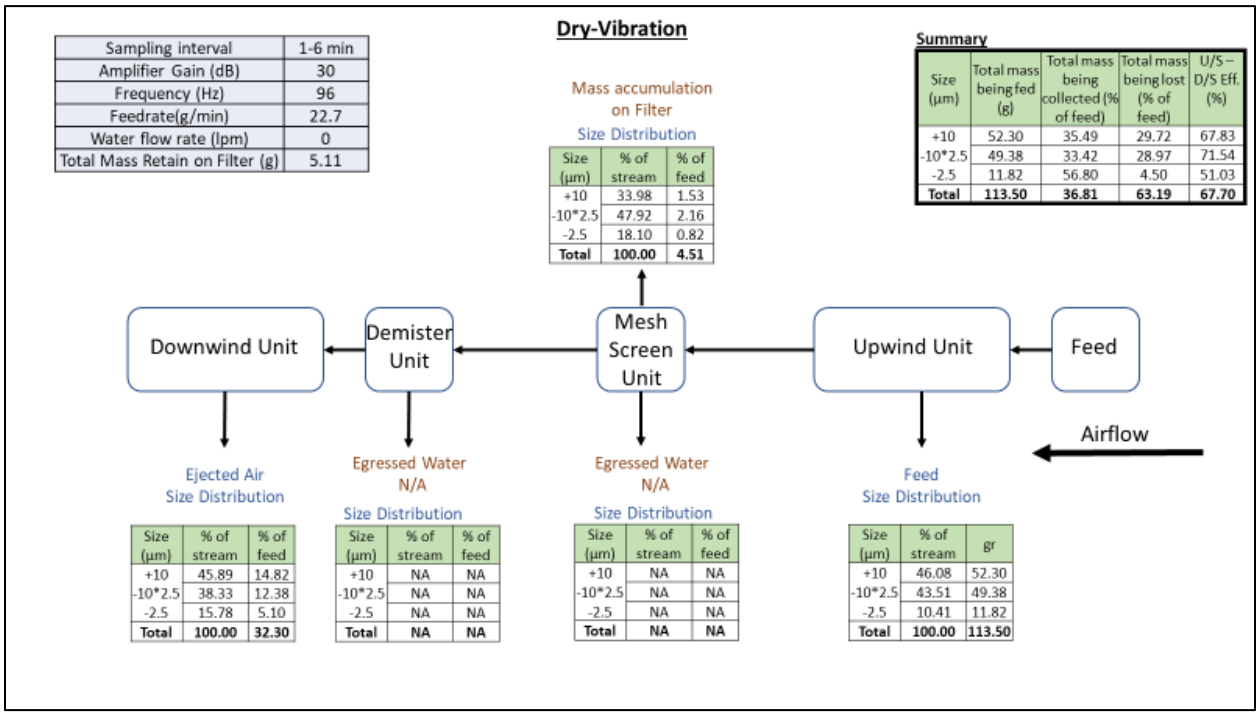

Wet-No Vibration

Sampling interval	1-6 min
Amplifier Gain (dB)	0
Frequency (Hz)	0
Feedrate(g/min)	22.7
Water flow rate (lpm)	3
Total Mass Retain on Filter (g)	3.60

Summary

Size (μm)	Total mass being fed (g)	Total mass being collected (% of feed)	Total mass being lost (% of feed)	U/S – D/S Eff. (%)
+10	19.96	14.17	3.42	95.30
-10*2.5	62.19	51.86	2.93	87.23
-2.5	31.35	25.81	1.81	81.88
Total	**113.50**	**91.83**	**8.17**	**87.17**

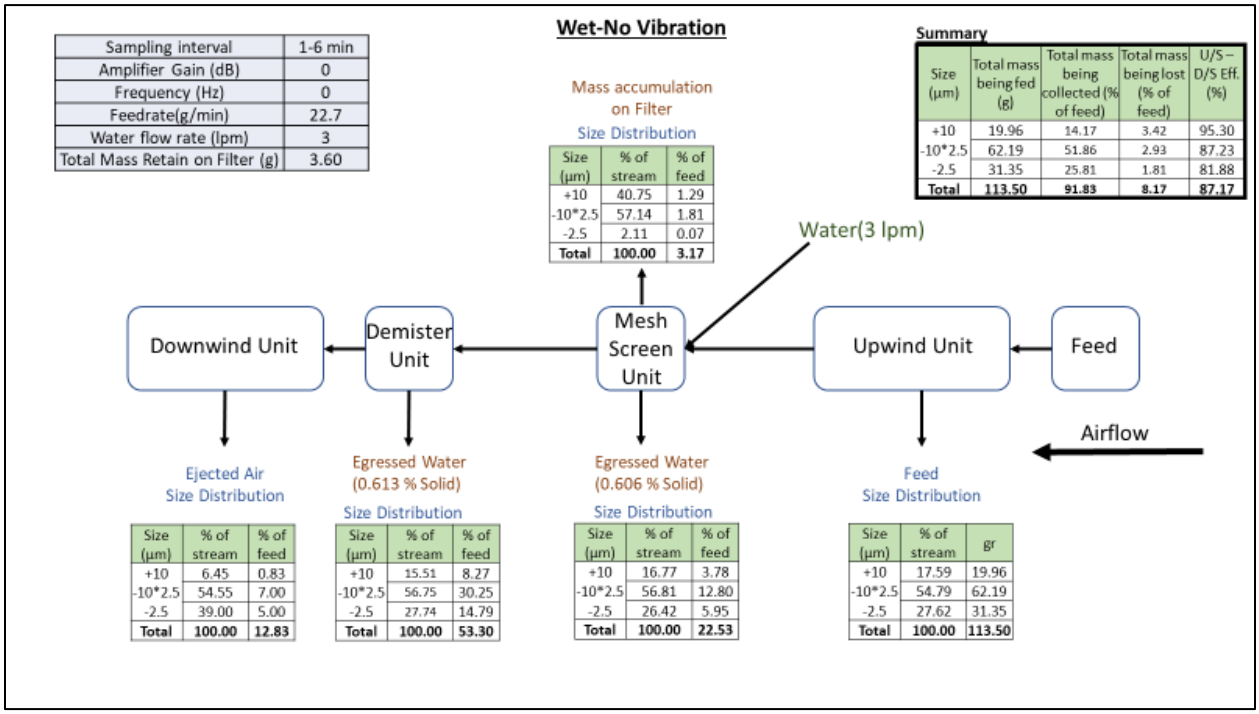

Size (μm)	% of stream	% of feed
+10	40.75	1.29
-10*2.5	57.14	1.81
-2.5	2.11	0.07
Total	**100.00**	**3.17**

Size (μm)	% of stream	% of feed
+10	6.45	0.83
-10*2.5	54.55	7.00
-2.5	39.00	5.00
Total	**100.00**	**12.83**

Size (μm)	% of stream	% of feed
+10	15.51	8.27
-10*2.5	56.75	30.25
-2.5	27.74	14.79
Total	**100.00**	**53.30**

Size (μm)	% of stream	% of feed
+10	16.77	3.78
-10*2.5	56.81	12.80
-2.5	26.42	5.95
Total	**100.00**	**22.53**

Size (μm)	% of stream	gr
+10	17.59	19.96
-10*2.5	54.79	62.19
-2.5	27.62	31.35
Total	**100.00**	**113.50**

Wet - Vibration

Sampling interval	1-6 min
Amplifier Gain (dB)	30
Frequency (Hz)	96
Feedrate(g/min)	22.7
Water flow rate (lpm)	3
Total Mass Retain on Filter (g)	3.25

Summary

Size (μm)	Total mass being fed (g)	Total mass being collected (% of feed)	Total mass being lost (% of feed)	U/S – D/S Eff. (%)
+10	34.42	28.70	1.63	94.73
-10*2.5	55.55	46.91	2.03	94.11
-2.5	23.53	18.51	2.22	86.00
Total	**113.50**	**94.12**	**5.88**	**92.62**

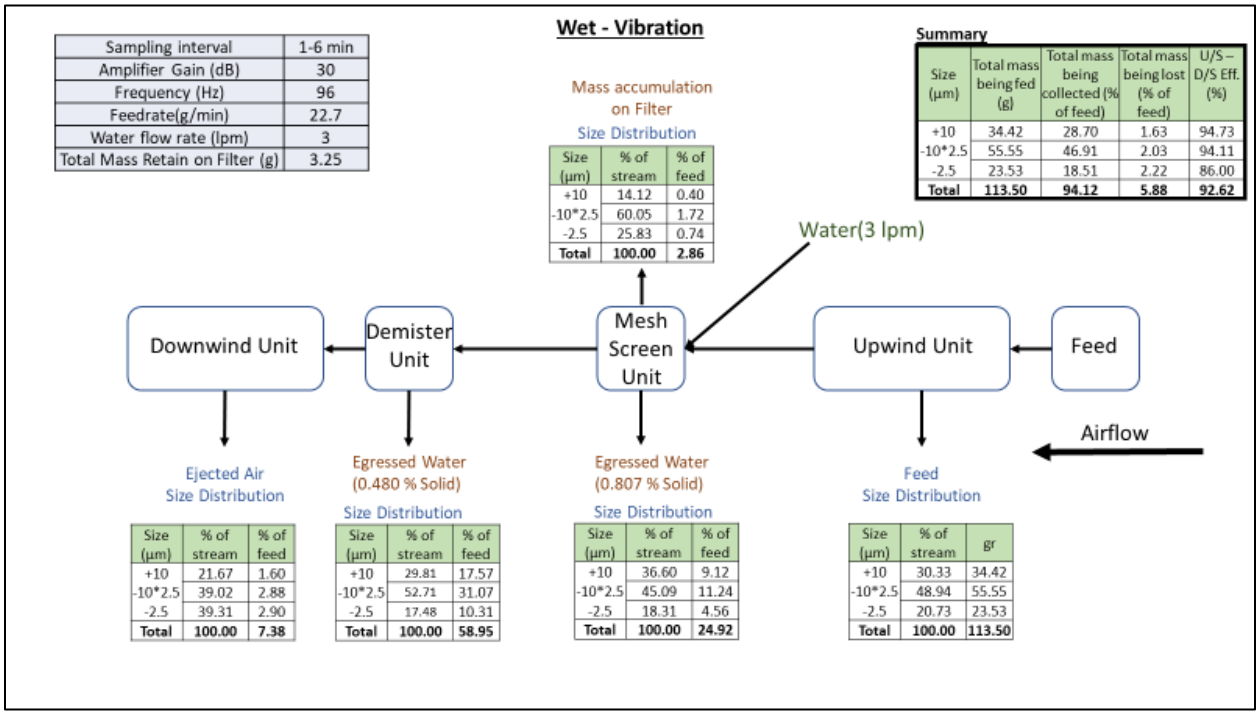

Size (μm)	% of stream	% of feed
+10	14.12	0.40
-10*2.5	60.05	1.72
-2.5	25.83	0.74
Total	**100.00**	**2.86**

Size (μm)	% of stream	% of feed
+10	21.67	1.60
-10*2.5	39.02	2.88
-2.5	39.31	2.90
Total	**100.00**	**7.38**

Size (μm)	% of stream	% of feed
+10	29.81	17.57
-10*2.5	52.71	31.07
-2.5	17.48	10.31
Total	**100.00**	**58.95**

Size (μm)	% of stream	% of feed
+10	36.60	9.12
-10*2.5	45.09	11.24
-2.5	18.31	4.56
Total	**100.00**	**24.92**

Size (μm)	% of stream	gr
+10	30.33	34.42
-10*2.5	48.94	55.55
-2.5	20.73	23.53
Total	**100.00**	**113.50**

Appendix C: Full-scale prototype setting

Table C1. Data summary

Test Number	Date	Time Start	Time End	Vibration	Spring	Amp Gain	Screen	Fan Speed, Hz	Spray	Dust Feed, g/m	Upstream Filter 1 [mg/m3]	Upstream Filter 2 [mg/m3]	Upstream DT 1 avg [mg/m3]	Upstream DT 2 avg [mg/m3]	Downstream Filter 3 [mg/m3]	Downstream Filter 4 [mg/m3]	Downstream DT 3 avg [mg/m3]	Downstream DT 4 avg [mg/m3]
1	4/3/2023	13:25	13:50	70	103	2	30	60	Max	250	21.40	58.18	9.5	33.7	6.20	8.26	19.6	8.8
2	4/3/2023	15:13	15:38	130	103	1	30	60	Max	250	26.40	67.06	6.0	44.8	11.04	4.16	27.5	10.6
3	4/4/2023	11:24	11:49	10	103	3	30B	60	Max	250	42.72	92.80	27.9	54.0	10.22	11.68	24.8	21.1
4	4/4/2023	12:29	12:44	130	103	3	30	60	Max	250	37.42	129.78	47.2	63.6	13.26	11.58	28.2	23.9
5	4/4/2023	13:38	14:03	10	103	1	30	60	Max	250		118.96	56.5	67.7	17.52		41.5	34.4
6	4/4/2023	14:35	15:00	70	103	2	30B	60	Max	250	55.12	103.36	52.2	78.0	18.54	23.30	41.4	22.5
7	4/4/2023	15:47	16:12	70	103	2	30	60	Max	250	46.18	134.58	53.7	72.1	14.10	16.72	35.7	29.1
8	4/4/2023	16:46	17:11	10	10	2	30	60	Max	250	44.24	121.20	53.4	71.5	15.78	16.30	35.5	33.0
9	4/5/2023	8:44	9:09	130	10	2	30	60	Max	250	11.34	46.34	15.6	15.1	6.40	3.40	6.2	9.2
10	4/5/2023	9:40	10:05	70	10	1	30B	60	Max	250	39.98	77.94	39.4	68.6	10.84		18.4	31.4
11	4/5/2023	10:32	10:57	70	10	3	30	60	Max	250	49.70	87.28	56.8	67.5	7.64	6.22	21.0	25.6
12	4/5/2023	11:28	11:53	70	Solid	1	30	60	Max	250	12.28	46.08	65.1	58.4	7.14	2.82	28.8	33.0
13	4/5/2023	12:29	12:54	70	Solid	3	30	60	Max	250	35.88	38.08	48.6	58.6	4.98	3.58	33.0	35.1
14	4/5/2023	13:21	13:46	130	Solid	2	30	60	Max	250	33.96	45.78	28.7	67.4	8.76		39.7	36.6
15	4/5/2023	14:11	14:36	10	Solid	2	30	60	Max	250	24.48	87.32	2.3	30.1	2.00	5.86	7.2	8.6
16	4/5/2023	15:00	15:25	130	103	1	30	60	Max	250		41.14	2.0	63.5	3.76	13.64	10.0	11.5
17	4/5/2023	15:51	16:16	70	103	2	30	60	Max	250	24.48	42.54	4.1	63.3		2.90	16.6	20.6
18	4/6/2023	10:53	11:18	NA	NA	NA	20	60	Max	250	14.98	41.18	10.0	13.5	3.52		4.4	5.4
19	4/6/2023	12:05	12:30	70	10	3	20	60	Max	250	23.36	21.52	28.2	50.5		5.06	7.0	9.3
20	4/6/2023	12:54	13:19	70	10	3	10	60	Max	250	24.94	46.06	7.7	17.3	2.18	5.66	4.5	13.3
21	4/6/2023	14:09	14:34	70	10	3	30	60	Max	250	18.76	41.36	28.7	53.4	1.92	4.26	9.3	13.3
22	4/6/2023	15:10	15:35	NA	NA	NA	10	60	Max	250	20.24	26.20	34.7	71.5	2.40	3.86	16.4	23.1
23	4/7/2023	8:38	9:03	NA	NA	NA	30	60	Max	250	12.02	12.14	19.6	11.6	3.64	4.06	4.6	11.7

Test Number	Date	Time Start	Time End	Vibration	Spring	Amp Gain	Screen	Air Velocity1, fpm	Air Velocity2, fpm	Dust Fed, g	Spray Pressure t0, psi	Spray Pressure t1, psi	Spray Pressure Avg psi
1	4/3/2023	13:25	13:50	70	103	2	30	2706	2672	NA	38.398	38.786	38.552
2	4/3/2023	15:13	15:38	130	103	1	30	2944	2726	NA	38.351	38.361	38.500
3	4/4/2023	11:24	11:49	10	103	3	30B	1490	1495	6392.2	36.617	36.577	36.446
4	4/4/2023	12:29	12:44	130	103	3	30	2786	2792	6494.5	36.445	36.214	36.301
5	4/4/2023	13:38	14:03	10	103	1	30	2716	2700	6488.1	36.567	36.689	36.380
6	4/4/2023	14:35	15:00	70	103	2	30B	1562	1505	5445.7	36.533	36.436	36.407
7	4/4/2023	15:47	16:12	70	103	2	30	2880	2866	6337.7	35.732	37.397	36.315
8	4/4/2023	16:46	17:11	10	10	2	30	2814	2860	5724.1	36.173	37.191	36.696
9	4/5/2023	8:44	9:09	130	10	2	30	2716	2701	6173.8	37.897	37.479	37.721
10	4/5/2023	9:40	10:05	70	10	1	30B	1636	1437	6148.7	36.862	37.174	36.773
11	4/5/2023	10:32	10:57	70	10	3	30	2847	2798	5988.3	36.097	37.087	36.463
12	4/5/2023	11:28	11:53	70	Solid	1	30	3008	2821	6561.4	36.883	37.741	37.228
13	4/5/2023	12:29	12:54	70	Solid	3	30	2774	2690	6342.3	36.956	37.591	36.951
14	4/5/2023	13:21	13:46	130	Solid	2	30	2716	2613	6130.9	36.362	36.788	36.959
15	4/5/2023	14:11	14:36	10	Solid	2	30	2886	2813	5732.3	36.309	37.024	36.708
16	4/5/2023	15:00	15:25	130	103	1	30	3006	2887	6125.4	36.830	36.221	36.367
17	4/5/2023	15:51	16:16	70	103	2	30	2864	2667	6183.7	36.225	38.061	36.217
18	4/6/2023	10:53	11:18	NA	NA	NA	20	3018	3040	5987.0	36.042	36.507	36.324
19	4/6/2023	12:05	12:30	70	10	3	20	3075	3065	6700.5	36.474	36.577	36.464
20	4/6/2023	12:54	13:19	70	10	3	10	3530	3372	6612.3	36.152	36.949	36.331
21	4/6/2023	14:09	14:34	70	10	3	30	3000	2880	5701.3	35.831	35.991	36.256
22	4/6/2023	15:10	15:35	NA	NA	NA	10	3555	3459	6903.8	37.617	36.664	36.542
23	4/7/2023	8:38	9:03	NA	NA	NA	30	2836	2640	6059.1	36.546	36.103	36.179

Test Number	Date	Time Start	Time End	Vibration	Spring	Amp Gain	Screen	Dp Screen t0, in. w.g.	Dp Screen t1, in. w.g.	Dp Screen Avg, in. w.g.	Dp Demister t0, in. w.g.	Dp Demister t1, in. w.g.	Dp Demister Avg, in. w.g.	Pitot t0, in. w.g.	Pitot t1, in. w.g.	Pitot Avg, in. w.g.
1	4/3/2023	13:25	13:50	70	103	2	30	4.354	4.426	4.433	2.231	2.044	2.067	0.207	0.162	0.182
2	4/3/2023	15:13	15:38	130	103	1	30	4.081	4.270	4.264	2.592	2.281	2.238	0.208	0.179	0.186
3	4/4/2023	11:24	11:49	10	103	3	30B	4.068	5.120	4.876	1.064	1.343	1.405	0.066	0.066	0.066
4	4/4/2023	12:29	12:44	130	103	3	30	4.144	4.301	4.304	2.359	2.092	2.136	0.220	0.205	0.203
5	4/4/2023	13:38	14:03	10	103	1	30	4.063	4.204	4.189	2.466	2.073	2.135	0.217	0.205	0.199
6	4/4/2023	14:35	15:00	70	103	2	30B	4.405	5.095	4.951	1.305	1.688	1.453	0.078	0.059	0.070
7	4/4/2023	15:47	16:12	70	103	2	30	3.961	4.218	4.142	2.506	2.242	2.289	0.244	0.210	0.223
8	4/4/2023	16:46	17:11	10	10	2	30	3.848	3.987	3.939	2.540	2.218	2.317	0.246	0.241	0.241
9	4/5/2023	8:44	9:09	130	10	2	30	3.677	3.920	3.902	2.403	1.979	2.163	0.223	0.199	0.208
10	4/5/2023	9:40	10:05	70	10	1	30B	4.082	4.390	4.347	0.992	1.544	1.451	0.098	0.062	0.070
11	4/5/2023	10:32	10:57	70	10	3	30	3.420	3.576	3.577	2.360	2.065	2.253	0.229	0.198	0.211
12	4/5/2023	11:28	11:53	70	Solid	1	30	3.068	3.263	3.282	2.591	2.226	2.368	0.240	0.224	0.232
13	4/5/2023	12:29	12:54	70	Solid	3	30	3.349	3.327	3.295	2.340	2.055	2.196	0.219	0.202	0.212
14	4/5/2023	13:21	13:46	130	Solid	2	30	3.128	3.462	3.293	2.357	2.065	2.122	0.187	0.146	0.162
15	4/5/2023	14:11	14:36	10	Solid	2	30	3.235	3.198	3.232	2.202	2.273	2.251	0.185	0.187	0.187
16	4/5/2023	15:00	15:25	130	103	1	30	2.978	3.190	3.157	2.762	2.347	2.436	0.229	0.194	0.207
17	4/5/2023	15:51	16:16	70	103	2	30	3.987	4.304	4.243	2.553	1.949	2.141	0.184	0.185	0.183
18	4/6/2023	10:53	11:18	NA	NA	NA	20	3.910	4.257	4.146	2.720	2.491	2.637	0.263	0.261	0.268
19	4/6/2023	12:05	12:30	70	10	3	20	3.594	3.782	3.673	3.099	2.698	2.850	0.322	0.015	0.126
20	4/6/2023	12:54	13:19	70	10	3	10	5.346	4.018	4.915	3.742	3.370	3.512	0.356	-0.112	0.006
21	4/6/2023	14:09	14:34	70	10	3	30	3.815	4.215	4.099	2.646	2.645	2.561	0.418	0.277	0.287
22	4/6/2023	15:10	15:35	NA	NA	NA	10	3.495	3.379	3.422	3.720	3.594	3.634	0.333	0.395	0.411
23	4/7/2023	8:38	9:03	NA	NA	NA	30	4.122	4.541	4.356	2.687	2.253	2.350	0.243	0.289	0.255

Table C2. Dust Concentration (Gravimetric Sampling)

Test Number	Date	Time Start	Time End	U/S Pump1	U/S Filter1	Filter1 Pre [mg]	Filter1 Post [mg]	Filter1 Conc [mg/m3]	U/S Pump2	U/S Filter2	Filter2 Pre [mg]	Filter2 Post [mg]	Filter2 Conc [mg/m3]	D/S Pump3	D/S Filter3	Filter3 Pre [mg]	Filter3 Post [mg]	Filter3 Conc [mg/m3]
1	4/3/2023	13:25	13:50	2302	1	11.246	12.316	21.4	2305	3	10.993	13.902	58.18	2301	4	13.374	13.684	6.2
2	4/3/2023	15:13	15:38	2302	7	11.507	12.827	26.4	2305	8	12.873	16.226	67.06	2301	14	13.264	13.816	11.04
3	4/4/2023	11:24	11:49	2302	25	10.95	13.086	42.72	2305	24	11.17	15.81	92.8	2301	19	11.17	11.681	10.22
4	4/4/2023	12:29	12:44	2302	17	11.135	13.006	37.42	2305	23	11.039	17.528	129.78	2301	21	12.398	13.061	13.26
5	4/4/2023	13:38	14:03	2302	28	11.4	NA	#VALUE!	2305	29	11.11	17.058	118.96	2301	10	11.243	12.119	17.52
6	4/4/2023	14:35	15:00	2302	27	13.32	16.076	55.12	2305	30	11.016	16.184	103.36	2301	6	10.815	11.742	18.54
7	4/4/2023	15:47	16:12	2302	40	12.635	14.944	46.18	2305	39	12.137	18.866	134.58	2301	35	11.26	11.965	14.1
8	4/4/2023	16:46	17:11	2302	49	11.337	13.549	44.24	2305	53	11.889	17.949	121.2	2301	45	13.189	13.978	15.78
9	4/5/2023	8:44	9:09	2302	42	10.972	11.539	11.34	2305	37	11.208	13.525	46.34	2301	47	12.166	12.486	6.4
10	4/5/2023	9:40	10:05	2302	32	11.353	13.352	39.98	2305	43	11.098	14.995	77.94	2301	31	12.279	12.821	10.84
11	4/5/2023	10:32	10:57	2302	51	11.177	13.662	49.7	2305	52	11.049	15.413	87.28	2301	46	12.297	12.679	7.64
12	4/5/2023	11:28	11:53	2302	80	10.616	11.23	12.28	2305	61	11.001	13.305	46.08	2301	62	11.629	11.986	7.14
13	4/5/2023	12:29	12:54	2302	57	10.562	12.356	35.88	2305	63	11.097	13.001	38.08	2301	88	12.172	12.421	4.98
14	4/5/2023	13:21	13:46	2302	70	12.153	13.851	33.96	2305	75	11.401	13.69	45.78	2301	72	12.207	12.645	8.76
15	4/5/2023	14:11	14:36	2302	81	12.742	13.966	24.48	2305	94	11.236	15.602	87.32	2301	67	12.206	12.306	2
16	4/5/2023	15:00	15:25	2302	92	14.375	NA	#VALUE!	2305	58	11.131	13.188	41.14	2301	68	10.412	10.6	3.76
17	4/5/2023	15:51	16:16	2302	73	11.408	12.632	24.48	2305	60	11.777	13.904	42.54	2301	69	10.458	NA	#VALUE!
18	4/6/2023	10:53	11:18	2302	78	13.267	14.016	14.98	2305	59	11.844	13.903	41.18	2301	82	10.932	11.108	3.52
19	4/6/2023	12:05	12:30	2302	79	13.362	14.53	23.36	2305	135	11.708	12.784	21.52	2301	84	12.637	NA	#VALUE!
20	4/6/2023	12:54	13:19	2302	134	10.833	12.08	24.94	2305	139	11.365	13.668	46.06	2301	140	11.377	11.486	2.18
21	4/6/2023	14:09	14:34	2302	127	11.913	12.851	18.76	2305	131	11.428	13.496	41.36	2301	124	10.789	10.885	1.92
22	4/6/2023	15:10	15:35	2302	133	11.888	12.9	20.24	2305	137	13.616	14.926	26.2	2301	123	12.723	12.843	2.4
23	4/7/2023	8:38	9:03	2301	138	10.844	11.445	12.02	2302	147	12.633	13.24	12.14	0043	132	10.691	10.873	3.64

Test Number	Date	Time Start	Time End	D/S Pump4	DS Filter4	Filter4 Pre [mg]	Filter4 Post [mg]	Filter4 Conc [mg/m3]	Blank	Blank Pre [mg]	Blank Post [mg]	Blank Var [mg]
1	4/3/2023	13:25	13:50	0043	5	11.262	11.675	8.26	18	11.284	11.293	0.009
2	4/3/2023	15:13	15:38	0043	13	10.819	11.027	4.16	12	11.475	11.481	0.006
3	4/4/2023	11:24	11:49	0043	20	13.387	13.971	11.68	2	12.3	12.309	0.009
4	4/4/2023	12:29	12:44	0043	22	11.314	11.893	11.58	15	12.244	12.254	0.010
5	4/4/2023	13:38	14:03	0043	9	11.516	NA	#VALUE!	16	10.552	10.559	0.007
6	4/4/2023	14:35	15:00	0043	34	12.036	13.201	23.3	11	12.161	12.169	0.008
7	4/4/2023	15:47	16:12	0043	38	11.298	12.134	16.72	33	12.885	12.905	0.020
8	4/4/2023	16:46	17:11	0043	50	11.815	12.63	16.3	55	11.67	11.674	0.004
9	4/5/2023	8:44	9:09	0043	36	11.033	11.203	3.4	44	11.306	11.312	0.006
10	4/5/2023	9:40	10:05	0043	54	10.931	NA	#VALUE!	56	11.297	11.304	0.007
11	4/5/2023	10:32	10:57	0043	48	11.68	11.991	6.22	41	11.344	11.357	0.013
12	4/5/2023	11:28	11:53	0043	95	11.96	12.101	2.82	96	11.5	11.491	-0.009
13	4/5/2023	12:29	12:54	0043	71	11.293	11.472	3.58	86	13.237	13.239	0.002
14	4/5/2023	13:21	13:46	0043	90	11.818	NA	#VALUE!	76	10.933	10.878	-0.055
15	4/5/2023	14:11	14:36	0043	87	12.496	12.789	5.86	66	11.644	11.647	0.003
16	4/5/2023	15:00	15:25	0043	93	11.615	12.297	13.64	74	11.869	11.857	-0.012
17	4/5/2023	15:51	16:16	0043	89	12.74	12.885	2.9	85	13.144	13.143	-0.001
18	4/6/2023	10:53	11:18	0043	85	13.144	NA	#VALUE!	77	12.626	12.629	0.003
19	4/6/2023	12:05	12:30	0043	129	10.93	11.183	5.06	130	11.47	11.459	-0.011
20	4/6/2023	12:54	13:19	0043	141	11.561	11.844	5.66	136	11.62	11.619	-0.001
21	4/6/2023	14:09	14:34	0043	125	11.813	12.026	4.26	126	11.539	11.535	-0.004
22	4/6/2023	15:10	15:35	0043	128	11.317	11.51	3.86				
23	4/7/2023	8:38	9:03	2305	142	11.385	11.588	4.06				